AFRL-VA-WP-TR-2003-3063

RAPID FATIGUE LIFE PROJECTION FOR THERMAL AND ACOUSTIC LOADS

P.C. Chen
Dr. Xiaowei Gao
D.D. Liu

Zona Technology, Inc.
7430 E. Stetson Drive
Suite 205
Scottsdale, AZ 85251-3540

M.P. Mignolet

Arizona State University
Department of Mechanical & Aerospace Engineering
Tempe, AZ 85287

JULY 2003

Final Report for 30 May 2002 – 30 May 2003

THIS IS A SMALL BUSINESS INNOVATION RESEARCH (SBIR) PHASE I REPORT

AIR VEHICLES DIRECTORATE
AIR FORCE MATERIEL COMMAND
AIR FORCE RESEARCH LABORATORY
WRIGHT-PATTERSON AIR FORCE BASE, OH 45433-7542

NOTICE

Using Government drawings, specifications, or other data included in this document for any purpose other than Government procurement does not in any way obligate the U.S. Government. The fact that the Government formulated or supplied the drawings, specifications, or other data does not license the holder or any other person or corporation; or convey any rights or permission to manufacture, use, or sell any patented invention that may relate to them.

This report has been reviewed by the Office of Public Affairs (ASC/PA) and is releasable to the National Technical Information Service (NTIS). At NTIS, it will be available to the general public, including foreign nations.

This technical report has been reviewed and is approved for publication.

/s/

S. MICHAEL SPOTTSWOOD
Aerospace Engineer
Structural Mechanics Branch

/s/

DAVID J. LAIRD, Captain, USAF
Deputy Chief, Structural Mechanics Branch
Structures Division

/s/

MICHAEL P. CAMDEN, USAF
Deputy Chief, Structures Division
Air Vehicles Directorate

This report is published in the interest of scientific and technical information exchange and does not constitute approval or disapproval of its ideas or findings

Do not return copies of this report unless contractual obligations or notice on a specific document requires its return.

REPORT DOCUMENTATION PAGE

Form Approved
OMB No. 0704-0188

1. REPORT DATE *(DD-MM-YY)*	2. REPORT TYPE	3. DATES COVERED *(From - To)*
July 2003	Final	05/30/2002 – 05/30/2003

4. TITLE AND SUBTITLE
RAPID FATIGUE LIFE PROJECTION FOR THERMAL AND ACOUSTIC LOADS

5a. CONTRACT NUMBER
F33615-02-M-3244

5b. GRANT NUMBER

5c. PROGRAM ELEMENT NUMBER
65502F

6. AUTHOR(S)
P.C. Chen, Dr. Xiaowei Gao, and D.D. Liu (Zona Technology, Inc.)
M.P. Mignolet (Arizona State University)

5d. PROJECT NUMBER
3005

5e. TASK NUMBER
42

5f. WORK UNIT NUMBER
2T

7. PERFORMING ORGANIZATION NAME(S) AND ADDRESS(ES)

Zona Technology, Inc.
7430 E. Stetson Drive
Suite 205
Scottsdale, AZ 85251-3540

Arizona State University
Department of Mechanical & Aerospace Engineering
Tempe, AZ 85287

8. PERFORMING ORGANIZATION REPORT NUMBER
ZONA 03-36

9. SPONSORING/MONITORING AGENCY NAME(S) AND ADDRESS(ES)
Air Vehicles Directorate
Air Force Research Laboratory
Air Force Materiel Command
Wright-Patterson AFB, OH 45433-7542

10. SPONSORING/MONITORING AGENCY ACRONYM(S)
AFRL/VASM

11. SPONSORING/MONITORING AGENCY REPORT NUMBER(S)
AFRL-VA-WP-TR-2003-3063

12. DISTRIBUTION/AVAILABILITY STATEMENT
Approved for public release; distribution is unlimited.

13. SUPPLEMENTARY NOTES
This is a Small Business Innovation Research (SBIR) Phase I report. Report contains color.

14. ABSTRACT

Report developed under an SBIR Phase I contract for topic AF02-244. The focus of this investigation is on the prediction of the fatigue life of aircraft panels subjected to the combination of a strong random acoustic excitation and to steady thermal effects. A novel parametric model for the probability density function of the ranges (displacement or stress) is proposed and is validated using a set of 57 time histories of displacement and stresses. These time histories correspond to the response of a single well Duffing oscillator, the displacements and stresses of a NASTRAN plate model that is either buckled or unbuckled and subjected to an acoustic excitation at either normal or grazing incidence. The matching of the exact distribution of ranges and its model is at least very good in all 57 cases studied. The dependency of the five parameters of the model on the spectral moments of the response is clarified to enable a direct prediction of the fatigue life. A reliable approximation of three of the five parameters of the stress distribution model is obtained that involves the mean and spectral moments of the stress process.

15. SUBJECT TERMS
SBIR Report, Panel, Acoustic, Thermal, Buckled, Stress, Strain, Displacement, Nastran, Vibration, Random Excitation, Grazing Incidence, Probability Density Function

16. SECURITY CLASSIFICATION OF:			17. LIMITATION OF ABSTRACT:	18. NUMBER OF PAGES	19a. NAME OF RESPONSIBLE PERSON (Monitor)
a. REPORT	b. ABSTRACT	c. THIS PAGE			S. Michael Spottswood
Unclassified	Unclassified	Unclassified	SAR	106	19b. TELEPHONE NUMBER *(Include Area Code)* (937) 255-5200 x457

Standard Form 298 (Rev. 8-98)
Prescribed by ANSI Std. Z39-18

TABLE OF CONTENTS

Page

LIST OF FIGURES

LIST OF FIGURES (continued)

LIST OF FIGURES (continued)

LIST OF FIGURES (continued)

LIST OF FIGURES (continued)

LIST OF FIGURES (continued)

LIST OF FIGURES (continued)

LIST OF FIGURES (continued)

LIST OF FIGURES (continued)

LIST OF FIGURES (continued)

LIST OF FIGURES (continued)

ABSTRACT

The focus of this investigation is on the prediction of the fatigue life of aircraft panels subjected to the combination of a strong random acoustic excitation and to steady thermal effects. More specifically, a novel parametric model for the probability density function of the ranges (displacement or stress) is proposed and is validated using a set of 57 time histories of displacement and stresses. These time histories correspond to the response of a single well Duffing oscillator, the displacements and stresses of a NASTRAN plate model that is either buckled or unbuckled and subjected to an acoustic excitation at either normal or grazing incidence. Finally, strain gauge data recorded during testing of an unbuckled panel at the Air Force Research Laboratory is also considered. The matching of the exact distribution of ranges and its model is at least very good in all 57 cases. Finally, the dependency of the 5 parameters of the model on the spectral moments of the response is clarified to enable a direct prediction of the fatigue life. In fact, a reliable approximation of 3 of the 5 parameters of the stress distribution model is obtained that involves the mean and spectral moments of the stress process. Further, it is found that the remaining two parameters exhibit a definite scatter around approximations based on either the mean, spectral moments, skewness, and kurtosis of the stress process and/or combinations of these characteristics. Continuing work in this area is suggested to fine tune this component of the model.

FOREWORD

This final report is submitted in fulfillment of Item 0001AE, Title: Final Report of a Small Business Innovative Research (SBIR) program Phase I contract No. F33615-02-M-3244 entitled, "Rapid Fatigue Life Projection for Thermal and Acoustic Loads," covering the performance period from May 30, 2002 to May 30, 2003.

This work was performed by ZONA Technology, Inc. (ZONA) and its subcontractor: Arizona State University (Dr. Marc P. Mignolet). This work is supported by the United States Air Force, Air Force Research Laboratory (AFRL) Wright-Patterson AFB, OH 45433-7801. This SBIR Phase I contract was performed by Mr. P.C. Chen (P.I.) and Dr. Xiaowei Gao of ZONA Technology Inc.; and Dr. Marc P. Mignolet of Arizona State University.

At AFRL/Wright-Patterson AFB, Capt. S. Michael Spottswood was the technical contract monitor. During the course of the present phase on the investigation of the VSS technology, the technical advice and assistance received from Capt. Spottswood, Dr. Stephen Rizzi of NASA Langley Research Center and others from AFRL are gratefully acknowledged.

NOMENCLATURE

a, b, c, d	Parameters of the model for the probability density function of the peaks and ranges, Eq. (6)-(8), and (18).
$\bar{a}$, $\bar{b}$	Dimensionless parameters of the probability density function of the ranges, Eq. (19).
a_1 , a_2 , ..., a_m , b_0	Autoregressive coefficients, Eq. (17).
B, $\overline{B}$, B' , $\hat{B}$, $\overline{B'}$	Normalization constants in the probability density function models.
$f(.)$	Component of the probability density function of ranges, see Eq. (5), (14), and (15).
m	Autoregressive order, Eq. (17).
$p_P(.)$	Probability density function of the displacements/stress peaks.
$p_S(.)$	Probability density function of the displacements/stress ranges.
$\bar{p}_0$	Constant term in the one mode model of the panel (Duffing eq.) representing the effects of a non-uniformity of the panel temperature (thermal moments), Eq. (1)-(3).
p_n	Autoregressive process, Eq. (17).
s	Ratio of the uniform panel temperature to the temperature required to induce buckling, Eq. (1)-(3).
S, s	Displacements/stress range, Eq. (4) onward.
$S_{\bar{p}\bar{p}}$	Power spectral density of the acoustic pressure on the panel (white noise), Eq. (2).
S_{XX}	Power spectral density of the stress process.
w_n	White noise sequence in autoregressive model, Eq. (17).
α, β	Parameters of the model for the probability density function of the ranges, see Eq. (14)-(15), and (18).
$\bar{\alpha}$	Dimensionless parameter in the probability density function of the ranges, see Eq. (19).
α_p	Dimensionless spectral moment of the stress process, Eq. (20).
γ	Nonlinear stiffness coefficient of the one mode model of the panel (Duffing eq.), Eq. (1)-(3).
$\Phi(.)$	Error function, Eq. (1), (6).
λ_p	Spectral moment of the stress process, Eq. (16).
μ	Mean of the stress process, Eq. (21) and (23).
σ_*^2	Variance of the acoustic pressure on the panel, Eq. (1).
ω_0	Linear natural frequency of the one mode model of the unbuckled panel (Duffing eq.), Eq. (1)-(3).
ζ	Damping ratio of the one mode model of the unbuckled panel (Duffing eq.), Eq. (1)-(2).

1.0 MODEL FORMULATION

Relying on a single mode model approximation of the panel response, it was shown (Yang et al., 2002, ZONA, 2002) that the probability density function of the peaks of the response of a panel exhibiting a nonlinear response can be modeled as

$$p_P(u) = B\, p_q(u)\left[\sigma_* \exp\left[-\frac{g^2(u)}{2\,\sigma_*^2}\right] - \sqrt{2\pi}\; g(u)\,\Phi\left(-\frac{g(u)}{\sigma_*}\right)\right] \tag{1}$$

where

$$p_q(u) = \exp\left[-\frac{2\,\zeta\,\omega_0}{\pi\, S_{\bar{p}\bar{p}}}\left(-\bar{p}_0\, u + \frac{1}{2}\,\omega_0^2\,(1-s)\,u^2 + \frac{1}{4}\,\gamma\, u^4\right)\right] \tag{2}$$

and

$$g(u) = \bar{p}_0 - \omega_0^2\,(1-s)\,u - \gamma\, u^3 . \tag{3}$$

In the above equations, the parameters $\omega_0^2\,(1-s)$ and γ denote the "effective" linear and nonlinear stiffness exhibited by the panel while $\bar{p}_0$ is a measure of the asymmetry in the temperature distribution or a constant transverse loading on the panel. Further, the excitation, assumed above to be a white noise process in time but fully correlated in space, is characterized by its power spectral density $S_{\bar{p}\bar{p}}$ and its variance σ_*^2. Finally, the term $2\,\zeta\,\omega_0$ represents the damping on the panel and Φ denotes the error function.

Assuming that the panel response is fairly narrowband, it is found that the range of response S is twice the peak value, i.e. $S = 2\,P$, so that the probability density of the response ranges could be modeled as

$$p_S(s) = \frac{1}{2}\, p_P(s/2). \tag{4}$$

An inspection of the few results presented in Yang et al. (2002) immediately demonstrates that Eq. (4) alone could not produce a successful model of the probability density function of the ranges. Indeed, the function $p_S(s)$ of Eq. (4) achieves very low values for $s \approx 0$ while the distribution of the ranges typically exhibits a sharp peak at that location. On this basis, it was proposed to develop a new model of the distribution of the response ranges in the form of a mixture, i.e.

$$p_S(s) = \frac{1}{2}\, p_P(s/2) + f(s) \tag{5}$$

where the first term would model the "high-range" behavior while the function *f*(*s*) would be selected to match the "small-range" peak. In this context, it is particularly interesting to note that the form of Eq. (5) is consistent with the Dirlik formula (see Bouyssy et al., 1993) which was developed for Gaussian processes and expresses the distribution of the ranges as a mixture of two Rayleigh distributions (characterizing exactly the peaks of a narrowband Gaussian process) and an exponential probability density function.

Before moving on to the selection of a possible function *f*(*s*), it is however convenient to reformulate Eq. (1)-(3) in the smallest possible number of coefficients and to discuss simpler approximations of Eq. (1) and (2). Specifically, it is found that

$$p_P(u) = \overline{B}\; p_q(u)\left[\exp\left[-\frac{d}{2}\,\bar{g}^2(u)\right] - \sqrt{2\pi}\; d\; \bar{g}(u)\,\Phi\left(-d\;\bar{g}(u)\right)\right] \tag{6}$$

where

$$p_q(u) = \exp\left[- b \left(c\, u + \frac{1}{2}\, a\, u^2 + \frac{1}{4}\, u^4 \right) \right] \tag{7}$$

and

$$\bar{g}(u) = - c - a\, u - u^3 . \tag{8}$$

In the above form, the distribution of the response ranges is found to involve 5 distinct parameters, *a*, *b*, *c*, *d*, and $\overline{B}$. If the function *f*(*s*) was neglected in Eq. (5), the last of these parameters ($\overline{B}$) would actually have a well defined value in terms of the other by enforcing that the total probability be equal to 1. In the context of Eq. (5), however, the constant $\overline{B}$ represents a measure of the probability associated with the corresponding part of the mixture and thus it is a bonafide, independent parameter. The preliminary work accomplished in Yang et al. (2002) and ZONA (2002) has suggested that Eq. (6) could be simplified with the assumption $- d\ \bar{g}(u) >> 1$. In this case, Eq. (6) becomes

$$p_P(u) = B'\, \bar{g}(u)\ p_q(u) \tag{9}$$

where B' is a new constant.

Next, in the absence of anisotropy through the panel, it is readily shown that *c* = 0 and thus Eq. (7) and (8) reduce to

$$p_q(u) = \exp\left[- b \left(\frac{1}{2}\, a\, u^2 + \frac{1}{4}\, u^4 \right) \right] \tag{10}$$

and

$$\bar{g}(u) = - a\, u - u^3 . \tag{11}$$

Finally, it has been argued in the presence of a very strong acoustic excitation that the quadratic terms in Eq. (10) and the linear ones in Eq. (11) would be negligible and thus it was proposed that the parameter *a* could be taken as 0 in these situations. Equations (10) and (11) then further reduce to

$$p_q(u) = \exp\left[-\frac{b}{4}u^4\right] \tag{12}$$

and

$$\bar{g}(u) = -u^3 \tag{13}$$

leaving only one shape parameter (*b*) and the probability factor B'.

For convenience of discussions, the following terminology will be used in the remainder of this report:

Model A: Eq. (6)-(8); 5 parameters present for fitting purpose.

Model B: Eq. (7)-(9); referred to as the "Model" in ZONA (2002), 4 parameters present for fitting purpose.

Model C: Eq. (6)-(8) with $a = 0$; 4 parameters present for fitting purpose.

Model D: Eq. (9) and (12)-(13); referred to as "Model - s =1" in ZONA (2002), 3 parameters present for fitting purpose.

In regard to the selection of an appropriate function $f(s)$, note that the Dirlik formula which was developed for Gaussian processes is of the same form as Eq. (5) and utilizes an exponential probability density function for $f(s)$. But, is this an appropriate model here as well?

Before specifically answering this question, it is necessary to investigate the physics which may be associated with this term. To this end, it is useful to reiterate that Eq. (5) is obtained under the narrowband assumption that the peaks and valleys of the process considered are fully correlated and equal in magnitude but opposite in sign to each other. Thus, $f(s)$ could be viewed as a correction associated with the lack of a perfect narrowbandedness of the response process but could also potentially arise from perturbations to the model that are associated with measurement noise/computational inaccuracies, the influence of other modes (in the frequency band associated with the Nyquist frequency and/or aliased modes), etc. Such perturbations will often manifest themselves as high frequency fluctuations appended to the dominant narrowband signal and thus will alter only slightly the large ranges but will produce an additional component to the distribution that is centered around very small ranges. It is this secondary component that is to be modeled by the function $f(s)$.

To substantiate the above expectations, a series of experiments were conducted with a signal composed of multiple harmonics, one of low frequency and largely dominant and one or several small amplitude higher frequency perturbations. As expected, it was noted that the high range part of the distribution of the ranges was almost unaffected by the perturbations while a significant low range component of the distribution appeared that was highly dependent on the high frequency harmonics.

One clear difficulty in the selection of $f(s)$ is the lack of knowledge of which of the above mechanisms have actually generated the small range part of the distribution. Fortunately, since only small ranges are involved in this modeling, their effect on the fatigue life may be quite small

with one notable exception: *since the total probability associated with the distribution of ranges must remain 1, the existence of a small range component reduces the probability of the other, dominant (high-range) component.* That is, the presence of a nonzero $f(s)$ implies a decrease of the scaling constant of the model, $\overline{B}$ or B'.

These various comments demonstrate that the most important feature of the $f(s)$ modeling may be the capture of its total probability. Accordingly, the functional form of $f(s)$ can be assumed with enough free parameters as to provide an appropriate fit of the true distribution. Given the behavior of the probability density function of the ranges, the following expressions were considered

$$f(s) = \hat{B} \exp(-\alpha s), \tag{14}$$

as already considered by Dirlik, and

$$f(s) = \hat{B} \exp\left(-\alpha s^{\beta}\right). \tag{15}$$

2.0 FINAL MODEL SELECTION

2.1 High-Range Component of the Model

Since the high-range component of the model is most critical in predicting the fatigue life, its modeling will be considered first. More specifically, it is desired to assess the relative merits of the models A-D in modeling the high range values of the distribution. This analysis will be carried out on the displacement generated from a one-mode structural model, a set of experimental data, and some initial finite element results.

2.2 One-Mode Structural Model

The first validation effort focused on the structural model from which Eq. (1)-(3) were derived. This test was accomplished on both unbuckled ($s = 0$) and buckled ($s = 1.8$) panels using first the original values of the parameters, i.e. without curve fitting (models A, B, C, and D). However, the models C and D were also tested with a value of b determined from the response statistics, these models are henceforth referred to as C' and D'.

The validation focused first on the distribution of the peaks, for which the model of Eq. (1)-(3) should be most relevant, and on the buckled panel data. It is clearly seen from Fig. 1-4 that the matching of the simulation data by the models A and B is excellent through the entire domain of sound pressure levels. In fact, it appears that model B is as good as model A except in regions where the probability density function of the peaks is nearly zero. In those areas, model B tends

to yield a negative values. The models C' and D', however, are only accurate in the high sound pressure regime where the response levels are high enough so that the nonlinear restoring term is significantly larger than the linear one, compare Fig. 1-4.

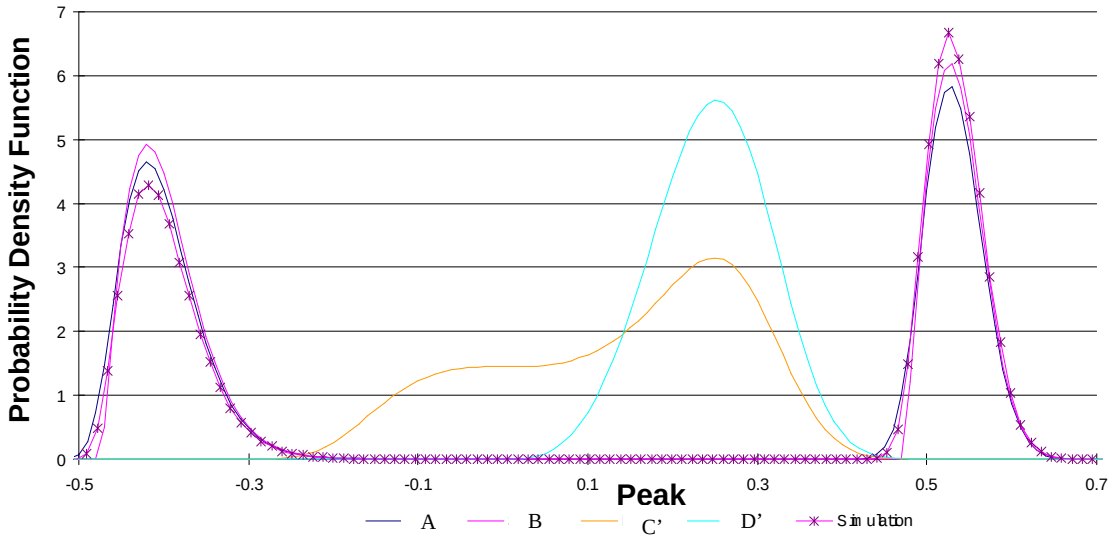

Figure 1. Comparison of Probability Density Functions of Peak Displacements One-Mode Model, Buckled Panel, s = 1.8, SPL =114 dB.

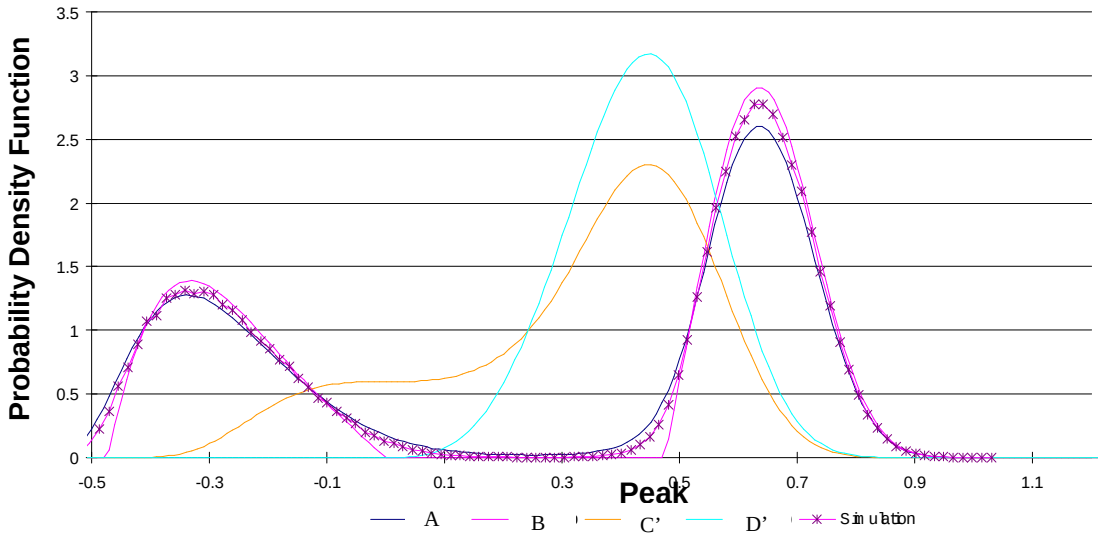

Figure 2. Comparison of Probability Density Functions of Peak Displacements One-Mode Model, Buckled Panel, s = 1.8, SPL =124 dB.

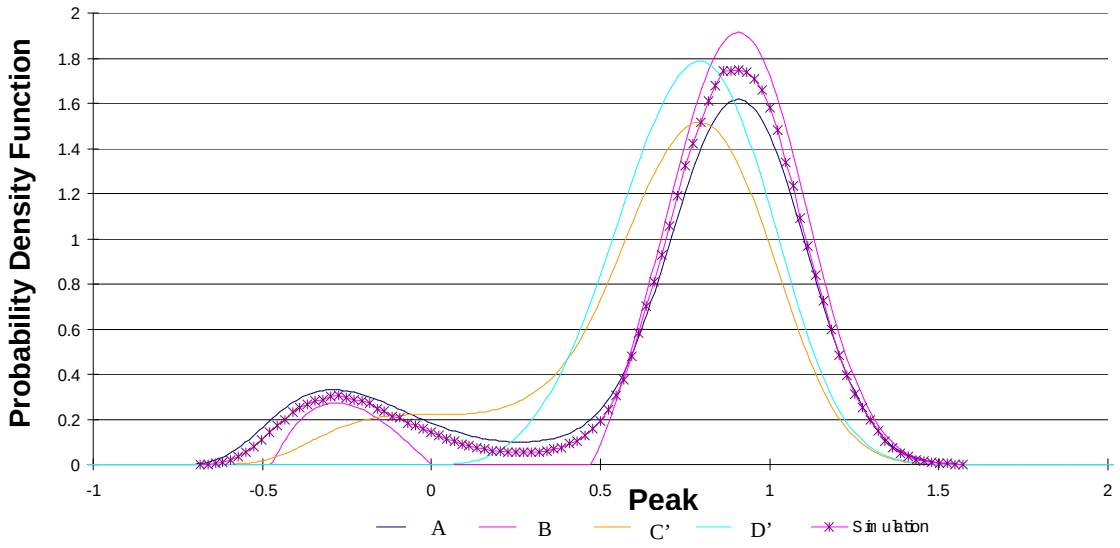

Figure 3. Comparison of Probability Density Functions of Peak Displacements One-Mode Model, Buckled Panel, *s* = 1.8, *SPL* =134 dB.

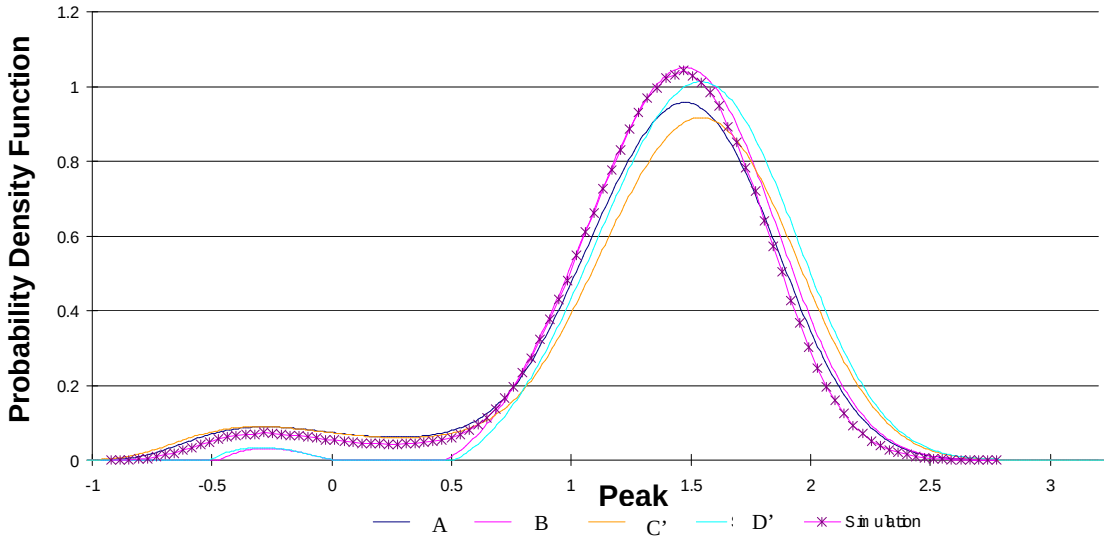

Figure 4. Comparison of Probability Density Functions of Peak Displacements One-Mode Model, Buckled Panel, *s* = 1.8, *SPL* =144 dB.

Having established the accuracy of the approximation given by Eq. (1)-(3) in modeling the peak response distribution, it is next necessary to assess its adequacy for the modeling of the ranges, following the narrowband approximation of Eq. (4). Shown in Fig. 5-8 are the distributions of response ranges corresponding to Fig. 1-4. Note from these figures that the model B yields again an excellent matching and is fully appropriate for the two highest *SPL* values (134 dB and 144 dB). At the other two, lowest sound pressure levels, the various models do not account for the existence of a second peak in the distribution. In fact, this peak is associated with motions taking place around one buckled state as opposed to snap-throughs. The mixture of these two types of events cannot be accounted for because of the narrowband assumption and is most dramatic for sound pressure levels in the transition range, see Fig. 5.

In the case of an unbuckled panel, see Fig. 9-12, no such situation occur and an excellent matching by model B is obtained for all sound pressure levels. Note again the improved accuracy of models D and D' as the sound pressure increases.

Finally, the presence of the aforementioned sharp peak of the range distribution near zero range should be observed in Fig. 5-12.

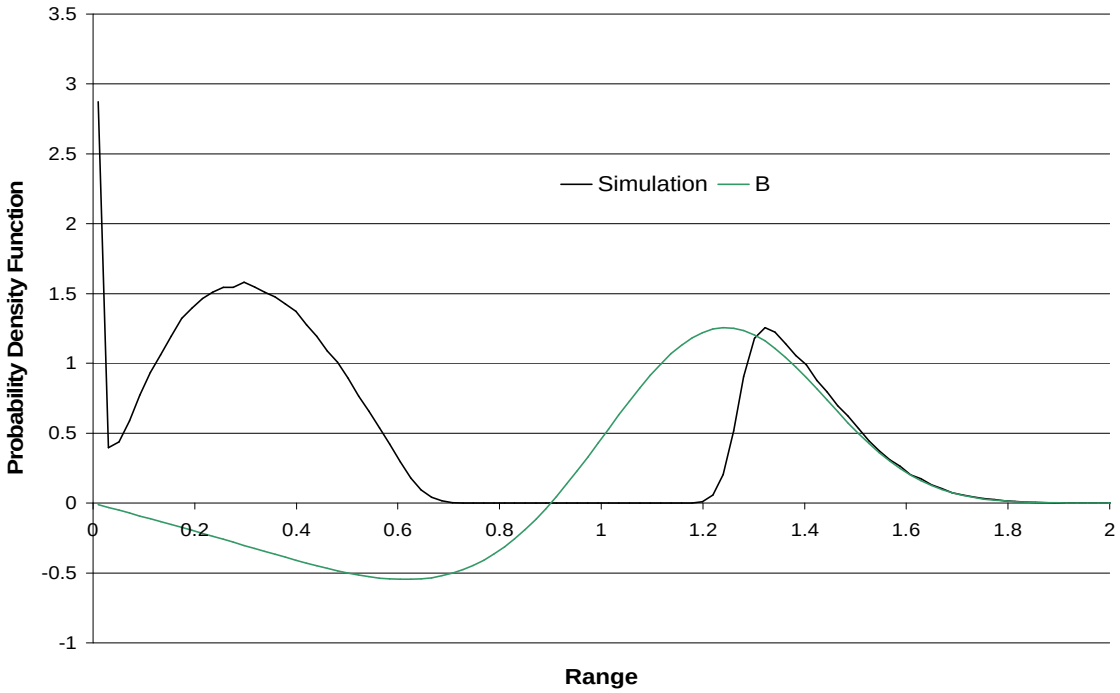

Figure 5. Comparison of Probability Density Functions of Displacement Ranges One-Mode Model, Buckled Panel, *s* = 1.8, *SPL* =114 dB.

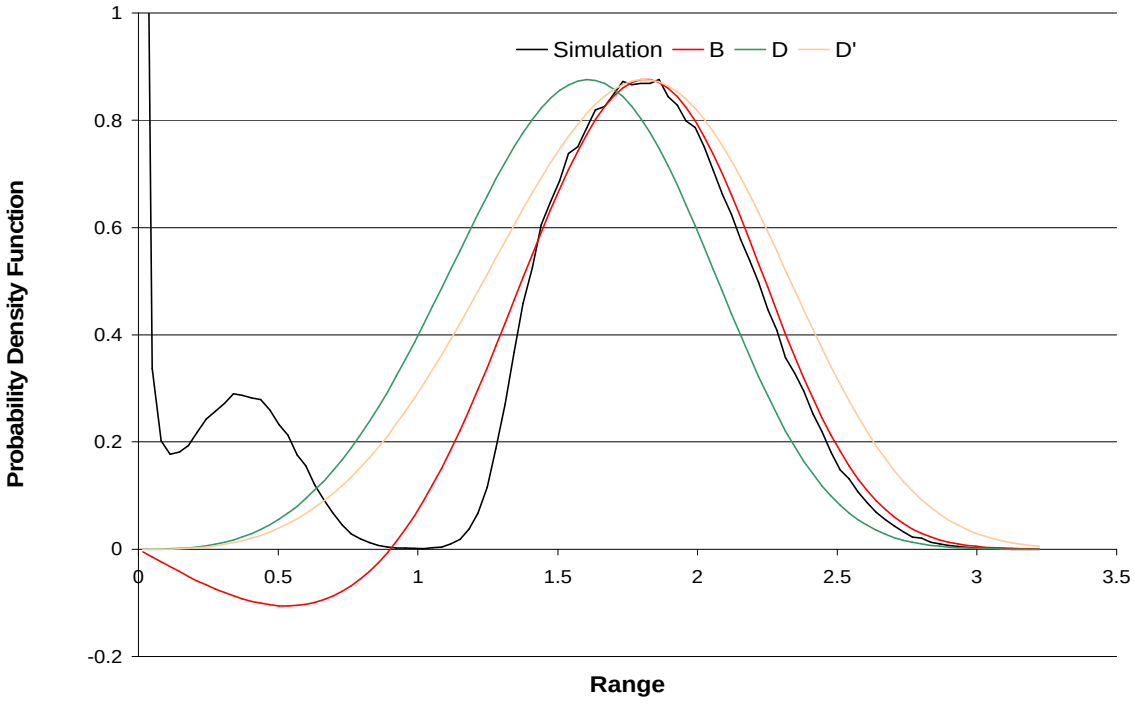

Figure 6. Comparison of Probability Density Functions of Displacement Ranges One-Mode Model, Buckled Panel, *s* = 1.8, *SPL* =124 dB.

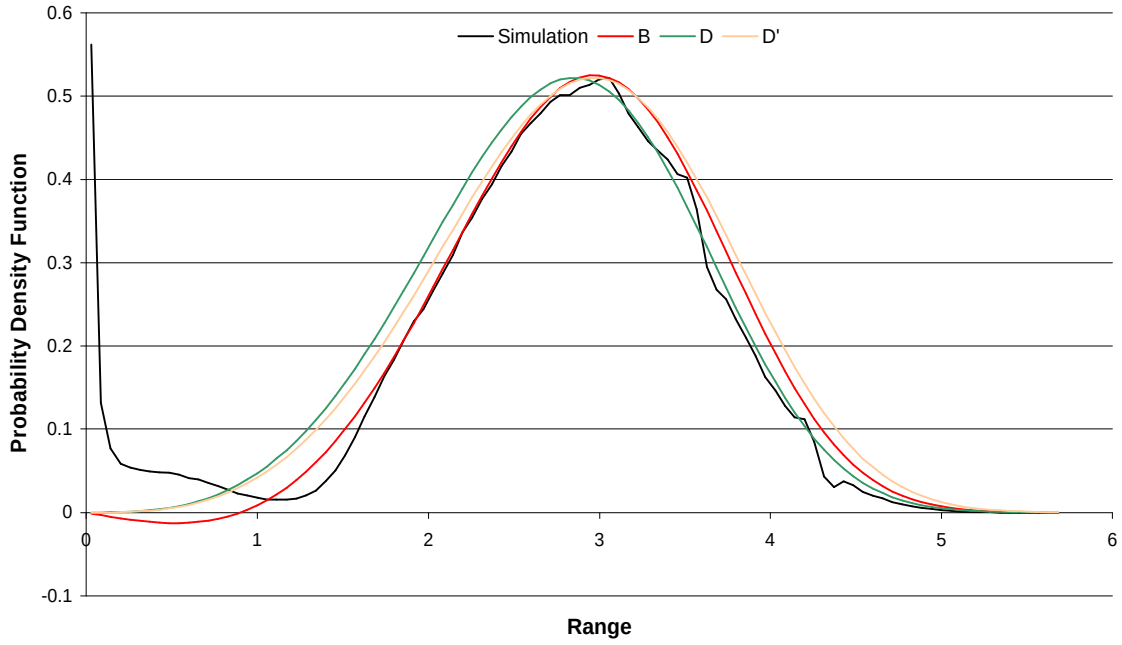

Figure 7. Comparison of Probability Density Functions of Displacement Ranges One-Mode Model, Buckled Panel, s = 1.8, SPL =134 dB.

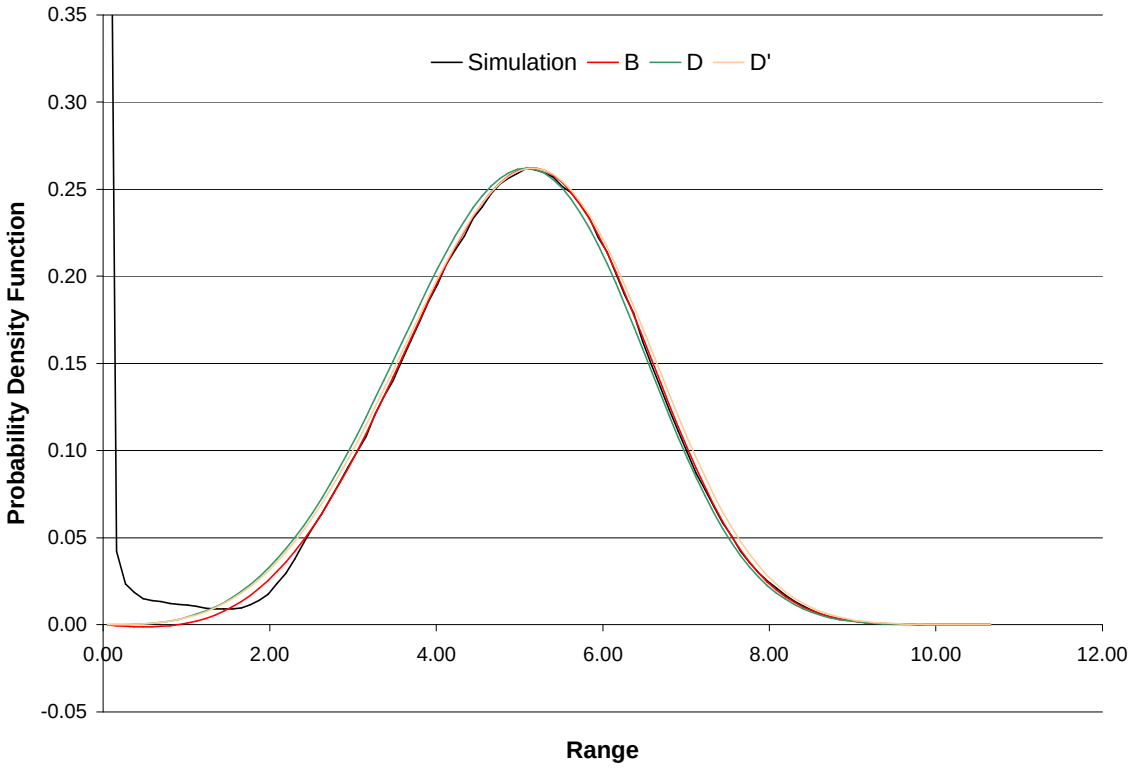

Figure 8. Comparison of Probability Density Functions of Displacement Ranges One-Mode Model, Buckled Panel, s = 1.8, SPL =144 dB.

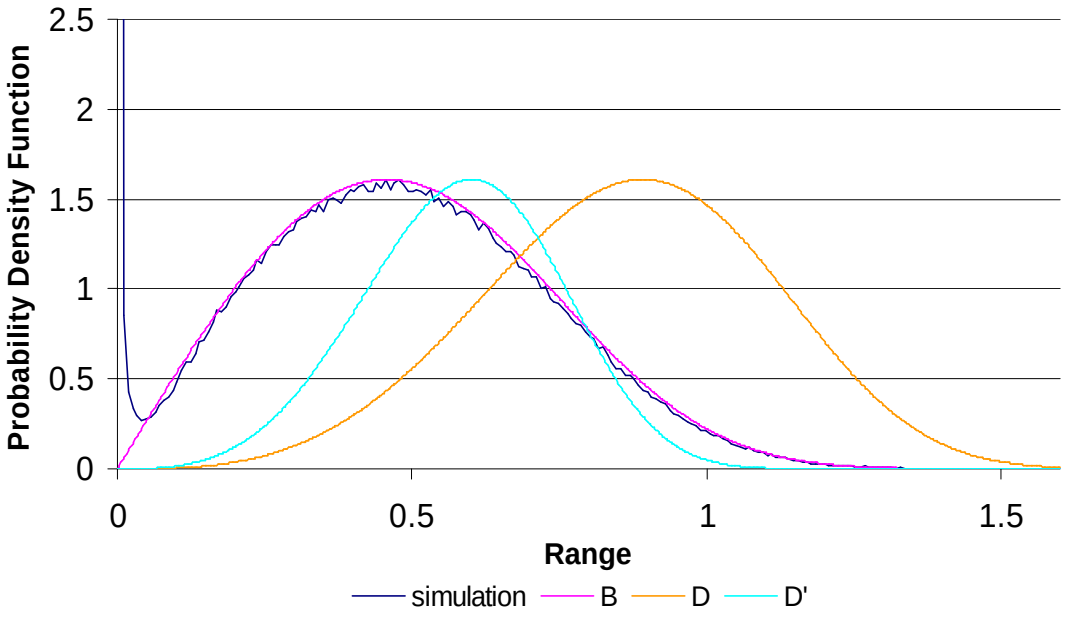

Figure 9. Comparison of Probability Density Functions of Ddisplacement Ranges One-Mode Model, Unbuckled Panel, *s* = 0, *SPL* =114 dB.

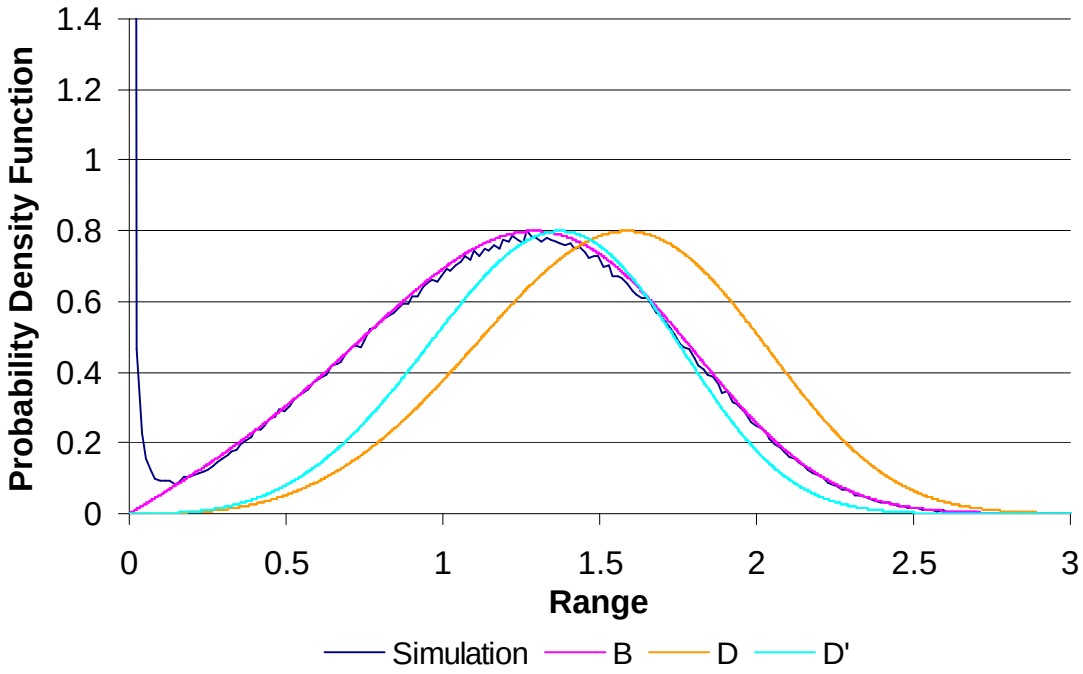

Figure 10. Comparison of Probability Density Functions of Displacement Ranges One-Mode Model, Unbuckled Panel, *s* = 0, *SPL* =124 dB.

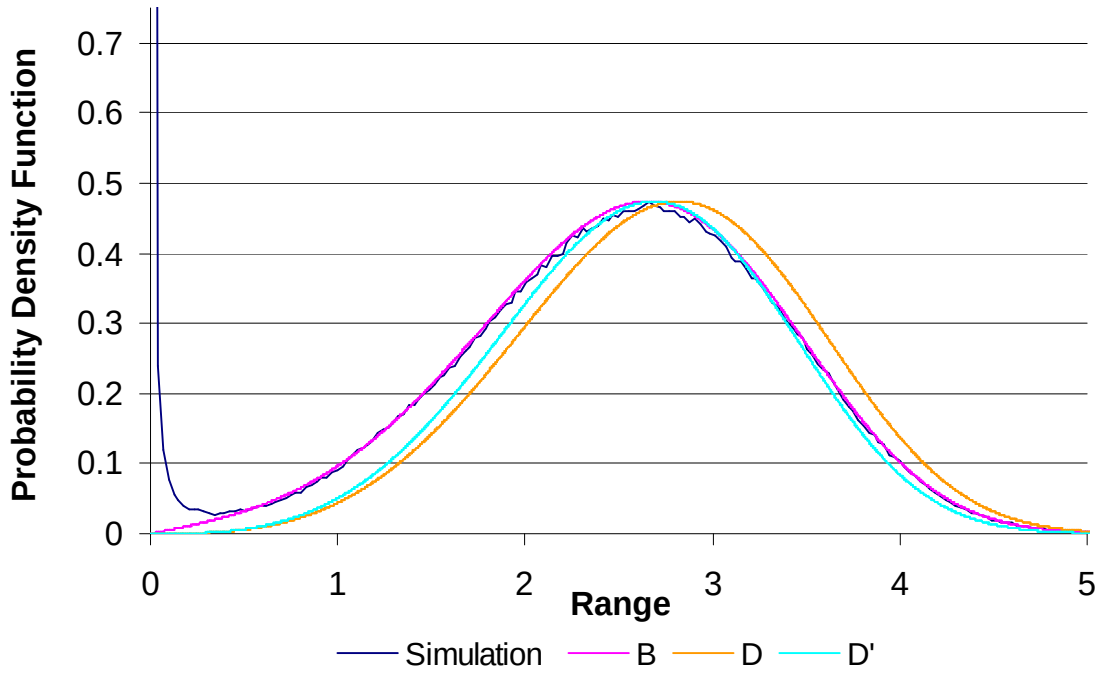

Figure 11. Comparison of Probability Density Functions of Displacement Ranges One-Mode model, Unbuckled Panel, *s* = 0, *SPL* =134 dB.

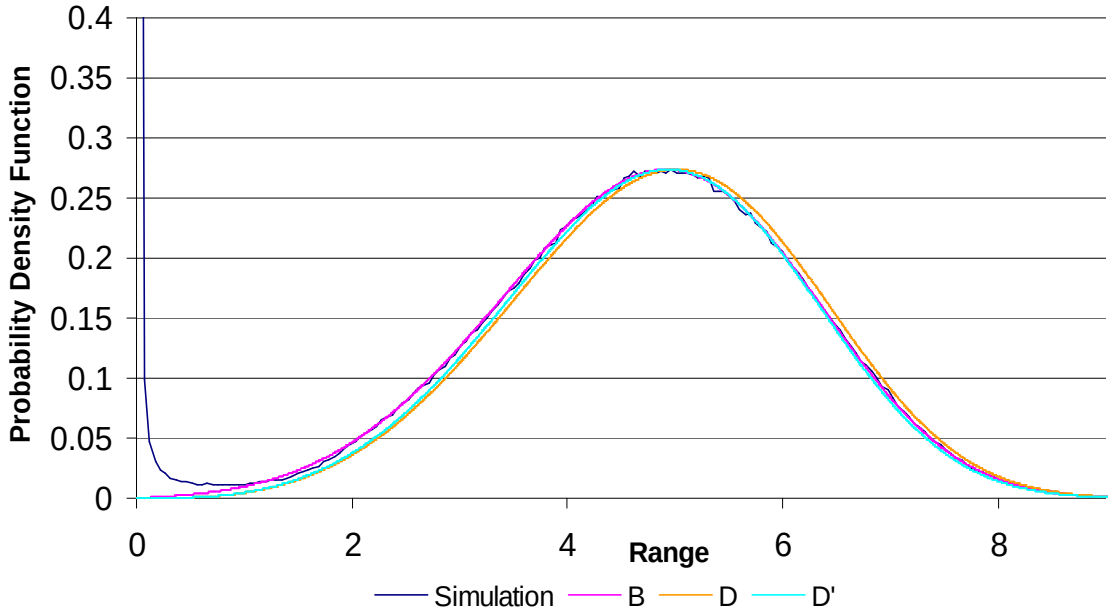

Figure 12. Comparison of Probability Density Functions of Displacement Ranges One-Mode Model, Unbuckled Panel, *s* = 0, *SPL* =144 dB.

2.3 Finite Element Data

The excellent results presented in the previous section might have been expected as the proposed model is consistent with the one mode formulation. Accordingly, it was desired to obtain a more in-depth validation by using full finite element data. To this end, an aluminum panel of dimensions 10 in. x 14 in. x 0.04 in. was discretized in MSC.Nastran with 140 1”x1” elements. The response of this panel to a uniform pressure, white noise in time but fully correlated in space, was then obtained at the sound pressure levels of 110 dB, 120 dB, 130 dB, and 140 dB in both buckled (s = 1.8) and unbuckled (s = 0) scenarios. Only the matching of model B was considered as the other models did not exhibit the same generality of application in the connection with the one mode model data.

The validation effort focused first on the distribution of the peaks and shown in Fig. 13 and 14 are the corresponding probability density functions for s = 0 and s =1.8, respectively. Clearly, the curve fitted model B provides a very good match of the right tail of the peak distribution but cannot account for the sometime very long left tails shown on these figures. This result is in fact not surprising as both negative and small positive values of peaks do not correspond to the dominant response of the panel, rather they are associated with small contributions of secondary modes that are superposed on the large amplitude motions. In this light, it might be expected that the distribution of the ranges would be better matched than the probability density functions of the peaks. This is indeed the case, as shown in Fig. 15 and 16. In fact, the agreement between the model B results and the simulation data is excellent for both unbuckled and buckled panels at all sound pressure levels. In this regard, it should be noted that it is the ranges that are associated

with fatigue, not the peaks. Thus, the results of Fig. 15 and 16 demonstrate the definite validity of the model for the displacements. Note again in Fig. 15 and 16 the presence of the sharp peak of the distribution near zero ranges. This component is not accounted for in Eq. (9)-(11) and thus will be represented by $f(s)$, see Eq. (5).

To conclude the validation effort on the finite element data, it remains to assess the validity of Eq. (9)-(11) to the *stress* ranges. Since stresses are nonlinearly related to displacements, the good fit of one does not guarantee the appropriateness for the other. This is however not the case here as the excellent matching of the stress ranges of Fig. 17 and 18 clearly demonstrates, at the exception again of the near zero ranges.

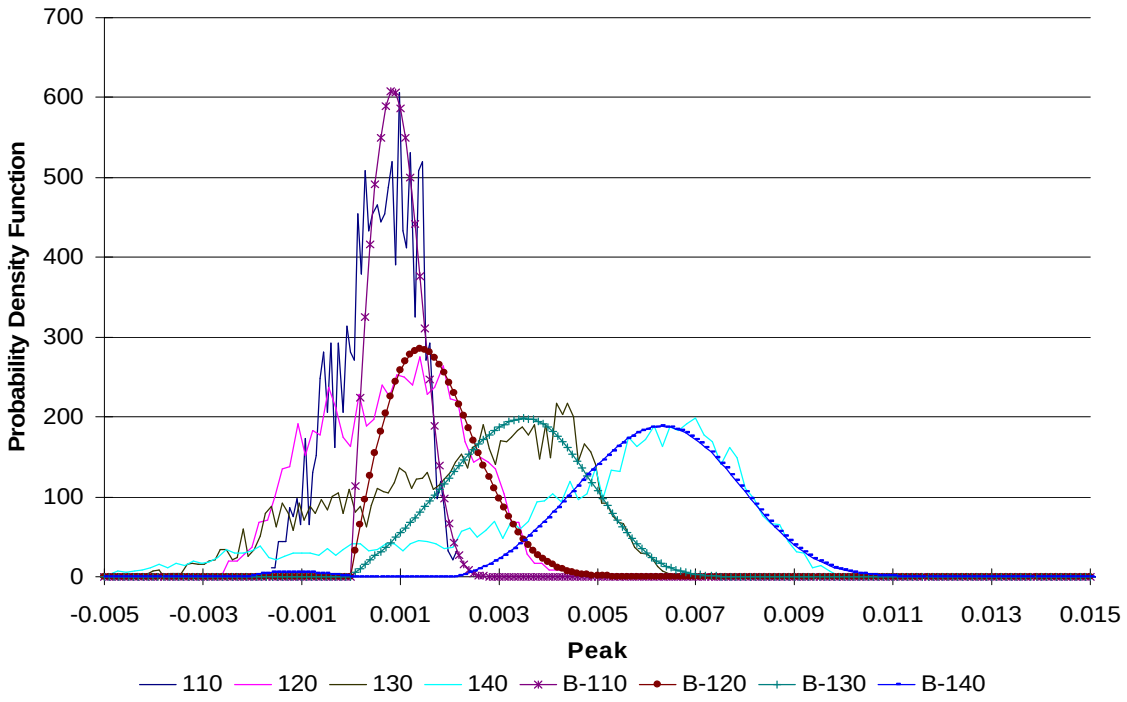

Figure 13. Comparison of Probability Density Functions of Peak Displacements Finite Element Data, Unbuckled Panel, s = 0, SPL = 110 dB-140 dB.

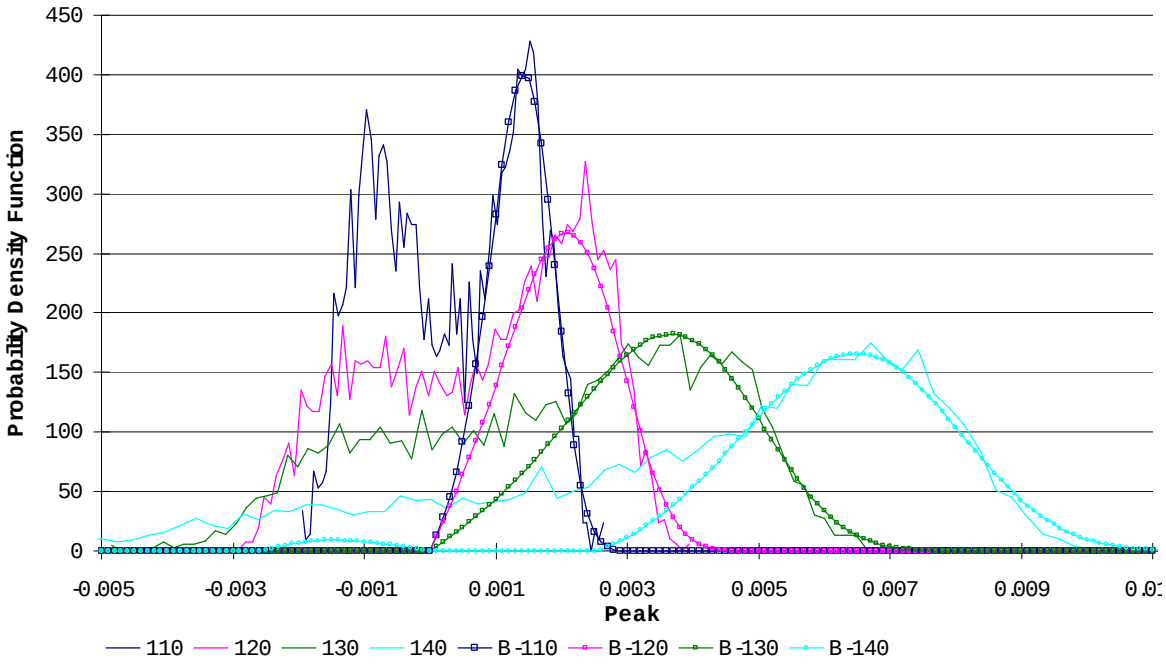

Figure 14. Comparison of Probability Density Functions of Peak Displacements Finite Element Data, Buckled Panel, *s* = 1.8, *SPL* =110 dB-140 dB.

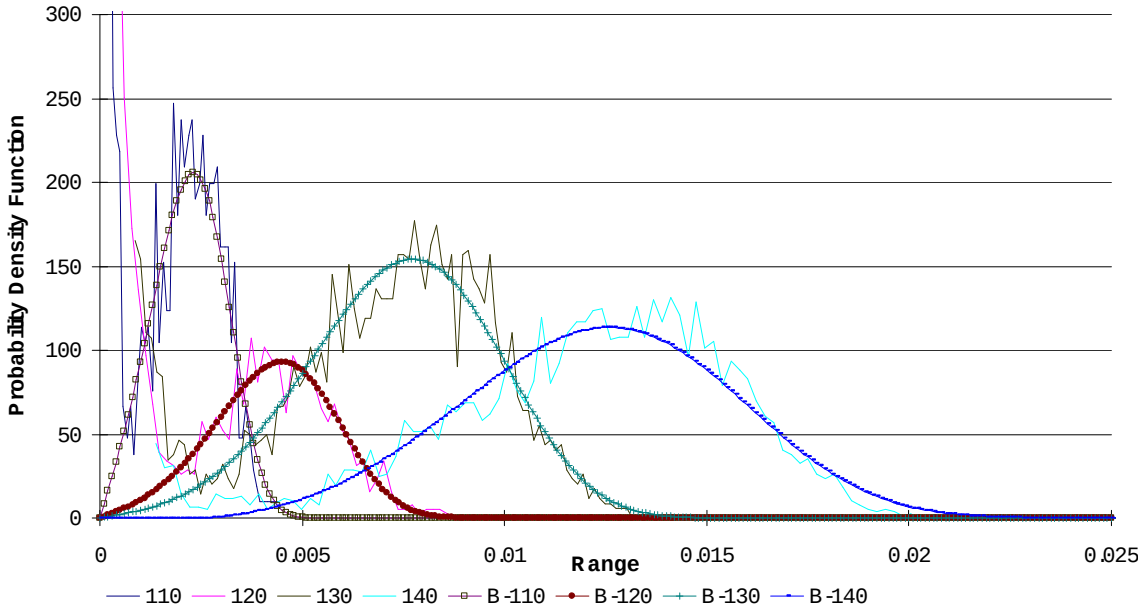

Figure 15. Comparison of Probability Density Functions of Displacement Ranges Finite Element Data, Buckled Panel, *s* = 0, *SPL* =110 dB-140 dB.

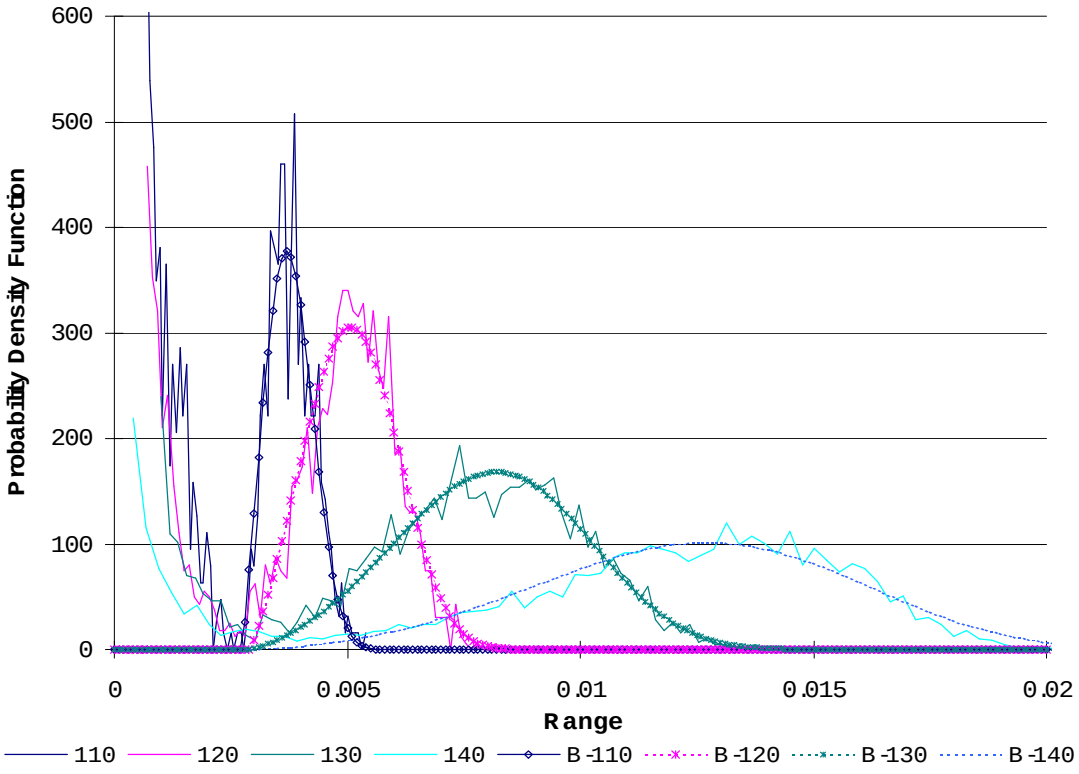

Figure 16. Comparison of Probability Density Functions of Displacement Ranges Finite Element Data, Buckled Panel, *s* = 1.8, *SPL* =110 dB-140 dB.

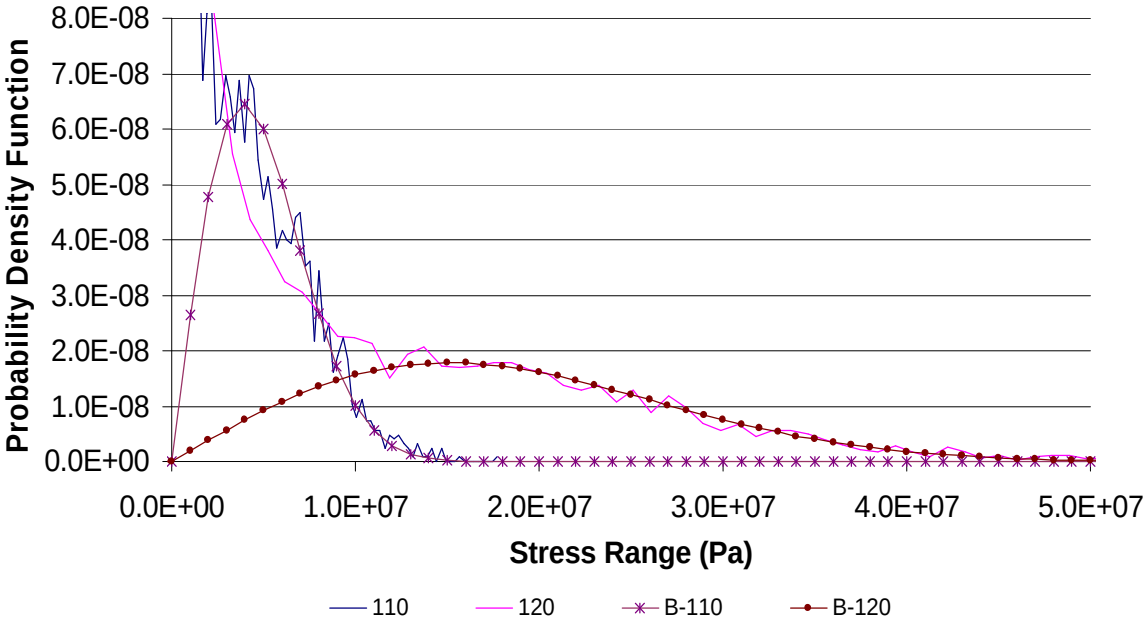

Figure 17. Comparison of Probability Density Functions of Stress Ranges Finite Element Data, Unbuckled Panel, *s* = 0, *SPL* =110 dB and 120 dB.

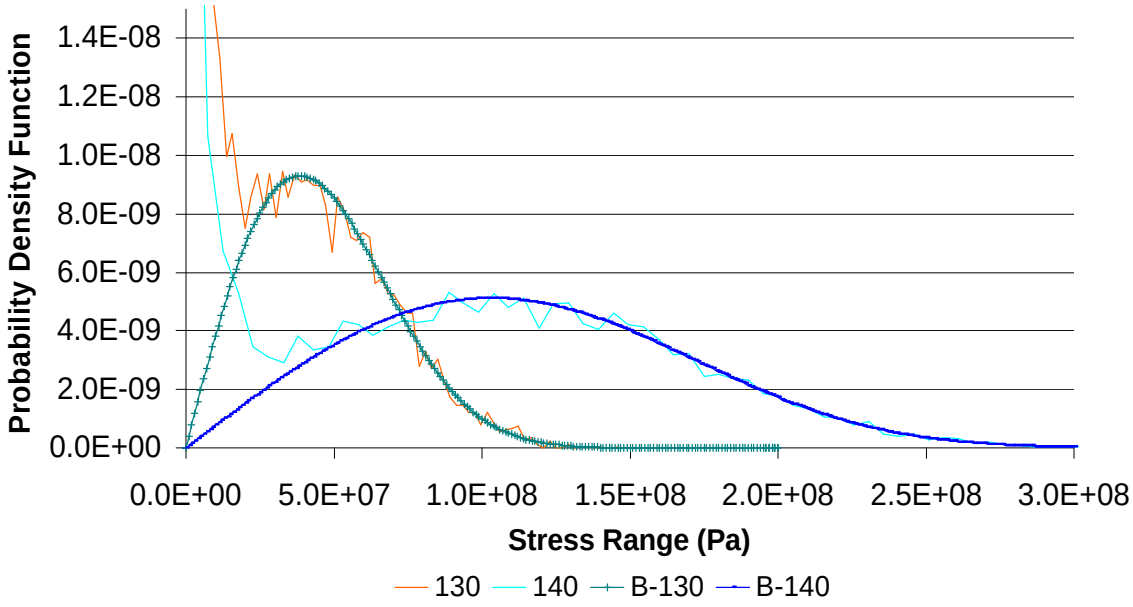

Figure 18. Comparison of Probability Density Functions of Stress Ranges Finite Element Data, Unbuckled Panel, s = 0, SPL =130 dB and 140 dB.

2.4 Experimental Data

The next validation effort focused on a set of experimental data obtained from Capt. S.M. Spottswood of the USAF/AFRL and relating to an unbuckled panel subjected to an acoustic excitation of sound pressure level from 152 dB to 172 dB. The measurements are strain measurements and the ranges were curved fitted to the model of Eq. (9)-(11). The results of this fitting are shown in Fig. 19-22 for the 152 dB, 158 dB, 167 dB, and 172 dB excitations. It is again seen that the model B, Eq. (9)-(11), provides an excellent matching of the strain ranges, except near the zero strain range as observed before.

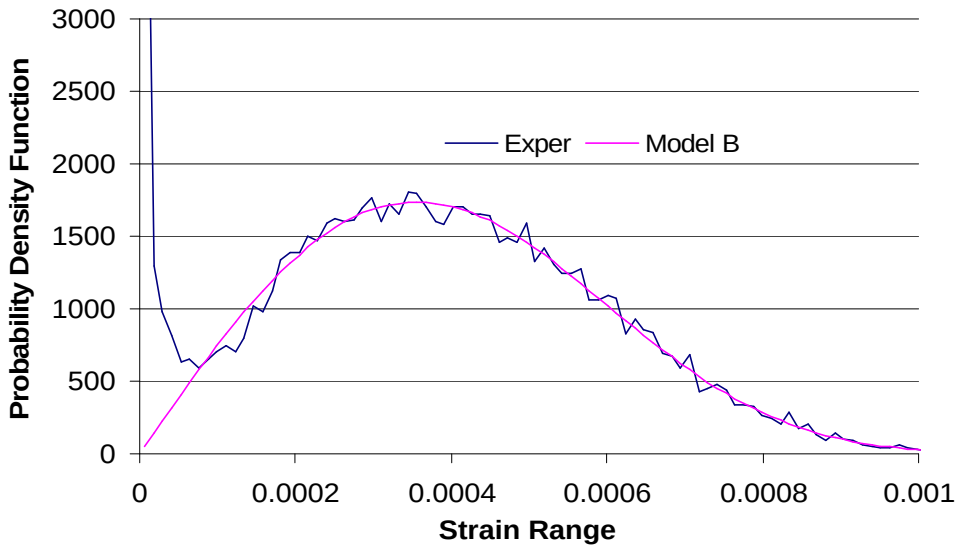

Figure 19. Comparison of Probability Density Functions of Strain Ranges Experimental Data, Unbuckled Panel, s = 0, SPL =152 dB.

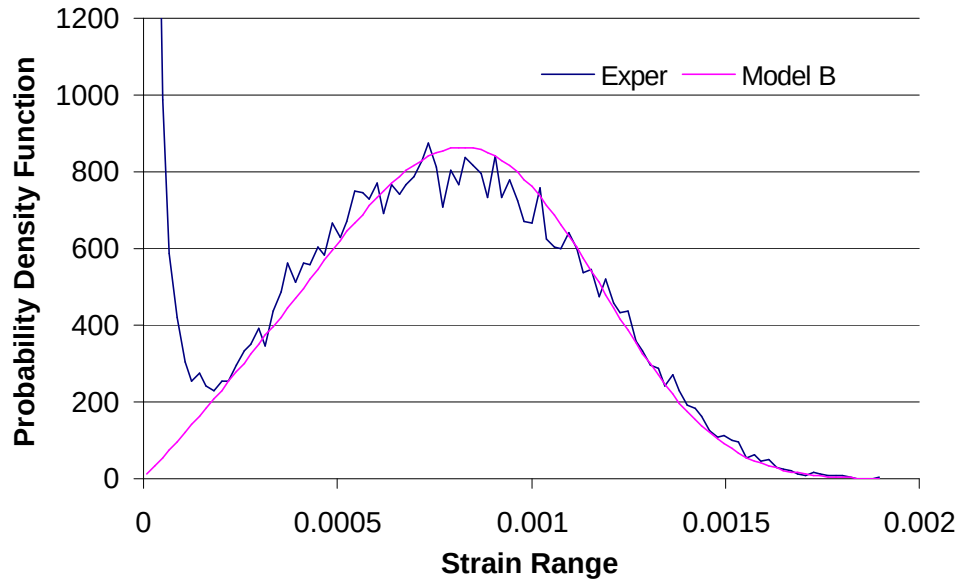

Figure 20. Comparison of Probability Density Functions of Strain Ranges Experimental Data, Unbuckled Panel, s = 0, SPL =158 dB.

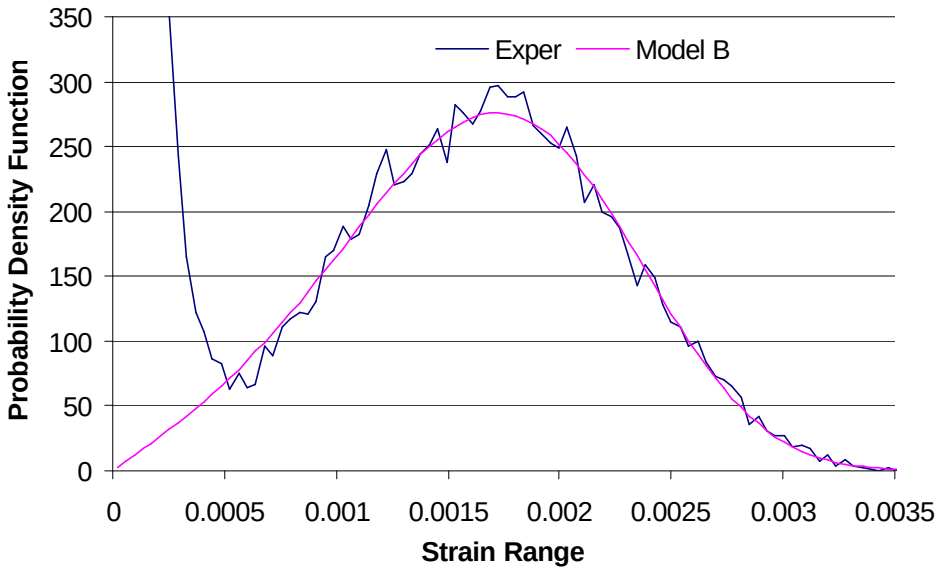

Figure 21. Comparison of Probability Density Functions of Strain Ranges Experimental Data, Unbuckled Panel, *s* = 0, *SPL* =167 dB.

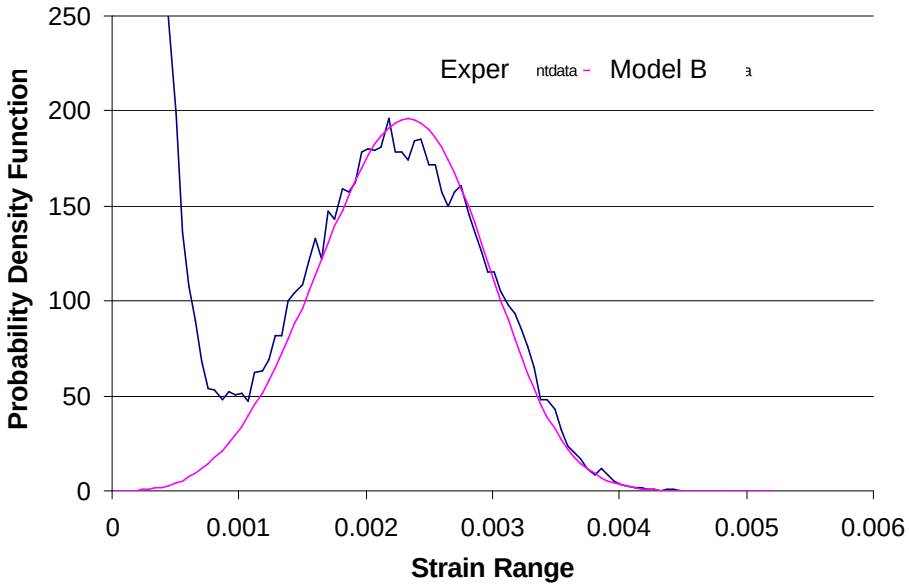

Figure 22. Comparison of Probability Density Functions of Strain Ranges Experimental Data, Unbuckled Panel, *s* = 0, *SPL* =172 dB.

2.5 Low-Range Component of the Model

The modeling of the high-range component of the model has been successfully addressed in the previous section with Model B being found to be reliable/the most reliable on a broad validation set. The present section aims similarly at the selection of the low-range component of the model, i.e. the function $f(s)$, to complete the model formulation.

Before proceeding with a comparative assessment of Eq. (14) and (15), it was desired to further confirm that computational issues can affect the low-range part of the model. Specifically, the effect of the frequency span/Nyquist frequency on the probability density function of the ranges was investigated. In all cases considered, the tolerance was set to be very low so that the responses would not significantly change at times that were common to different time histories. Thus, only the Nyquist frequency would vary from one case to the next. As suggested earlier, the shape of the distribution of ranges stayed the same except near the zero range limit, see Fig. 23 and 24 and the probability of small ranges is increased by increasing the frequency span/Nyquist frequency (i.e. decreasing the time step), that is increasing the high frequency content of the response. While this effect is very localized, the increase in occurrence of near zero ranges implies that the probability density function must be decreased everywhere else to maintain a total probability of one. This effect is definitely noticeable in Fig. 23 where the probability density function of the ranges for the time step Δt is indeed everywhere below the one corresponding to the time step $2\,\Delta t$. This observation confirms the definite role of the small range component of the distribution on the fatigue life through the normalization constant B' of Eq. (9) and thus demonstrates the need to introduce a model such as Eq. (14) or (15).

In regards to the number of parameters in the model, it should be noted that the combination of Eq. (9) and (14) leads, in the absence of asymmetry, to 4 unknown coefficients, a, b, α, and B', since the value of $\hat{B}$ is then evaluated so that the total probability equals 1. The selection of Eq. (15) instead leads similarly to a 5 parameter model with a, b, α, β, and B'. For comparison, note that the Dirlik model involves 4 independent coefficients. Here, however, the probability density function of the response is not characterized by a single parameter, i.e. the variance as in the Gaussian case (only the fluctuations around the mean deformation are analyzed), but requires two separate coefficients, e.g. a and b. A 5-parameter model can thus be considered to be on equal footing as the Dirlik formula. Note additionally, as recognized above, that only the three parameters a, b, and B' are expected to have a significant effect on the predicted fatigue life.

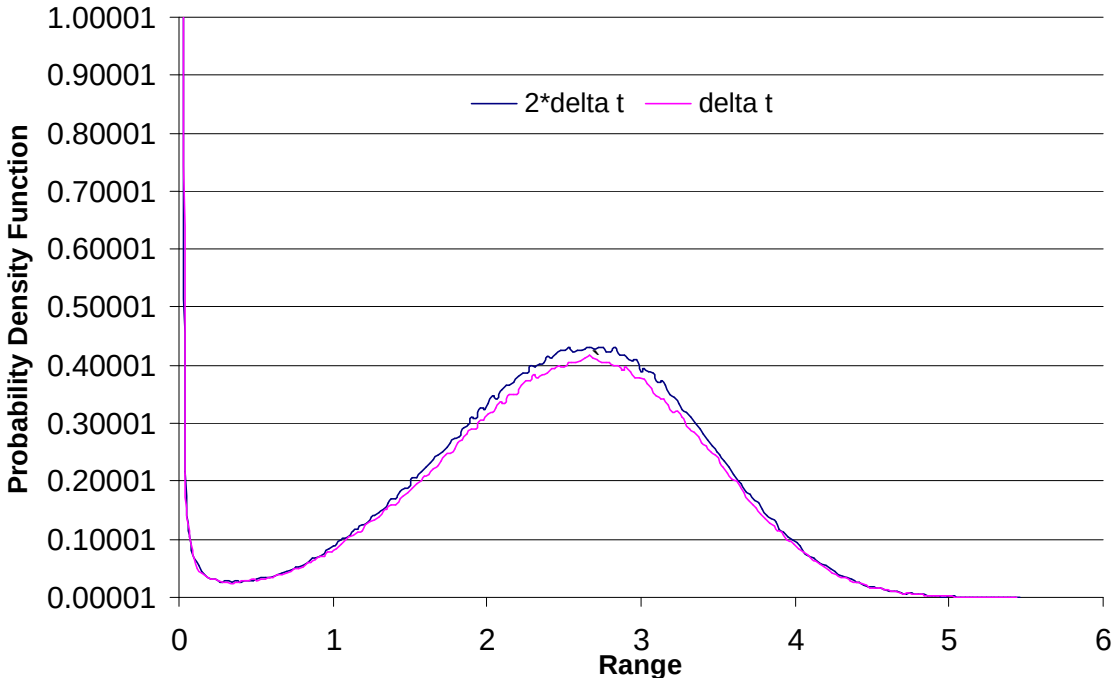

Figure 23. Comparison of the Distributions of Ranges Corresponding to Two Different Integration Time Steps/Nyquist Frequency.

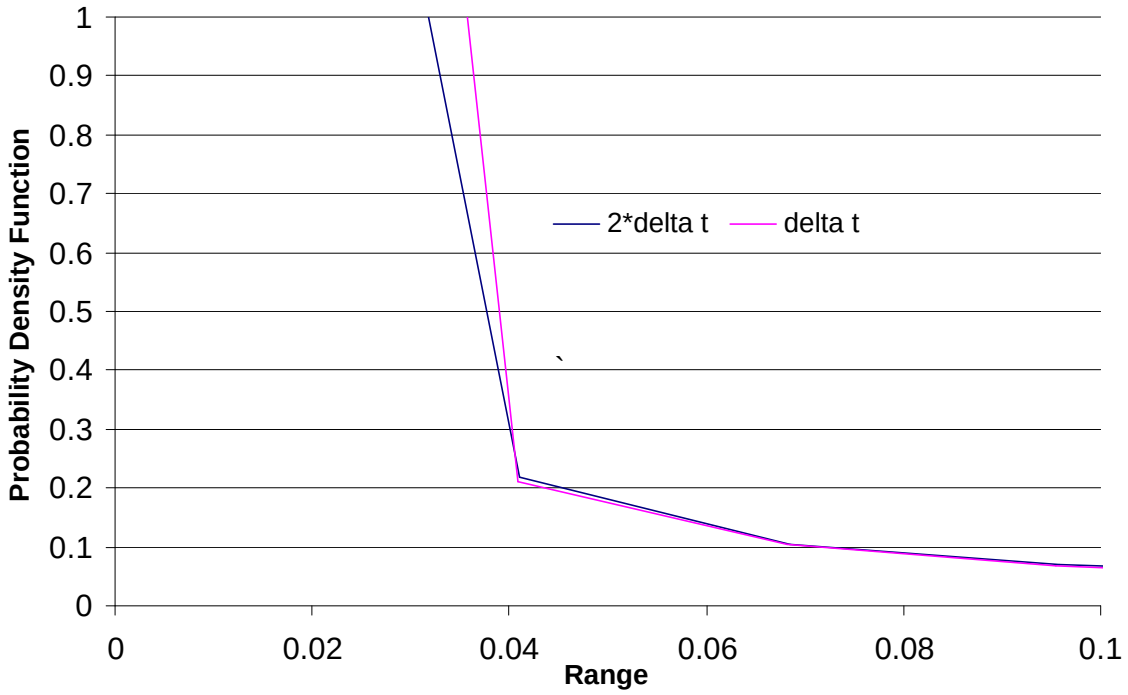

Figure 24. Comparison of the Distributions of Ranges Corresponding to Two Different Integration Time Steps/Nyquist Frequency (zoomed-in small range domain).

The assessment of the comparative merits of Eq. (14) and (15) to model the low range domain of the probability density function was achieved in consort with the adopted high range model, i.e. Eq. (9)-(11) and on the data considered above, i.e. from the single mode model, the MSC.Nastran runs on unbuckled and unbuckled panels (displacements and stresses), and on the AFRL strain measurements, see Fig. 25-48. In all of these plots, note that the vertical axis is shown logarithmically as to highlight the matching obtained both near the zero range (high values of the probability density function) and away from that zone.

The comparison of the two models, i.e. Eq. (9)-(11), and (14) (referred to as "Model with pure exponential" in the figures) and Eq. (9)-(11), and (15) (referred to as "Model" in the figures)

must reflect the use of the probability density function, i.e. the determination of the fatigue life which involves the moment $E\lfloor s^m \rfloor$ with m in the range [1,8] say. Accordingly, the best of the two models should be the one that provides the closest agreement at medium to high values of the range. Although the matching near zero ranges directly affects only very little the estimates of the fatigue life, it may have a larger impact implicitly through the coefficient B'.

Considering first the one mode model data, Fig. 25-28, it is seen that the two models yield very similar curves except near the zero range limit where the model of Eq. (15) appears to yield a slightly improved matching (see Fig. 28). When analyzing the ranges of displacements obtained from the finite element model without temperature, it would appear that the model of Eq. (15) provides a slightly better matching at the two highest sound pressure levels (see Fig. 31 and 32) but this trend is more pronounced for the buckled case, see Fig. 33 and 36. A slight improvement is also noticed for the stress ranges of Fig. 37 and 40 and for the experimental data, see Fig. 45-48.

On the basis of these 24 figures, it is suggested that the model of Eq. (15)

(1) leads to a better fit of the probability density function of the ranges, and

(2) provides a very good to excellent match of the distribution of ranges in all cases.

Accordingly, the functional form of Eq. (15) will be retained in all future work.

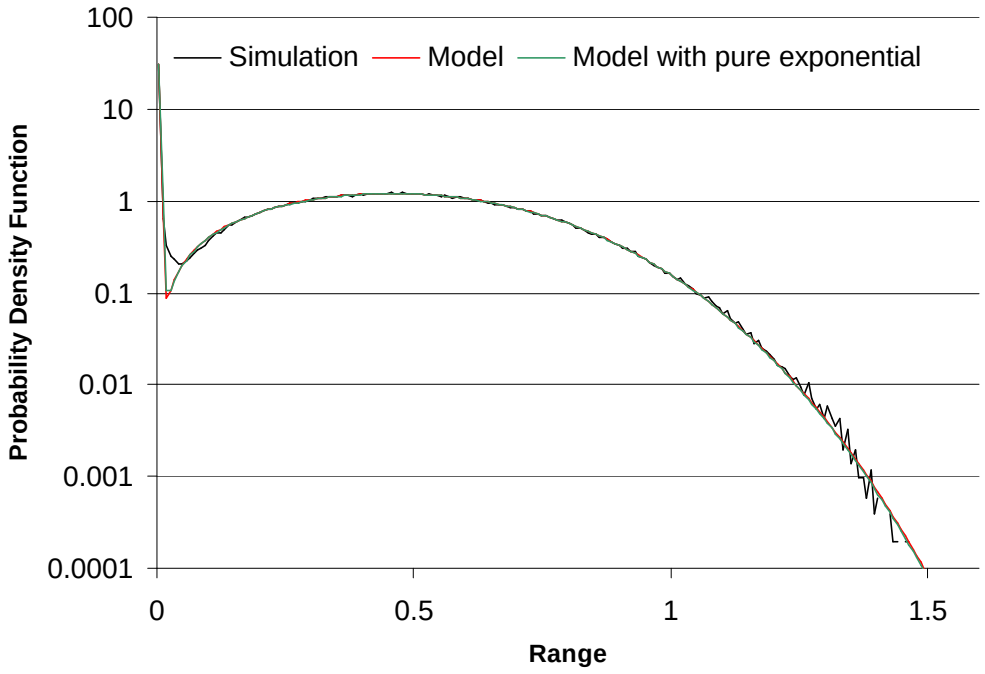

Figure 25. Comparison of Probability Density Functions of Displacement Ranges, One-Mode Model, Unbuckled Panel, s = 0, SPL =114 dB.

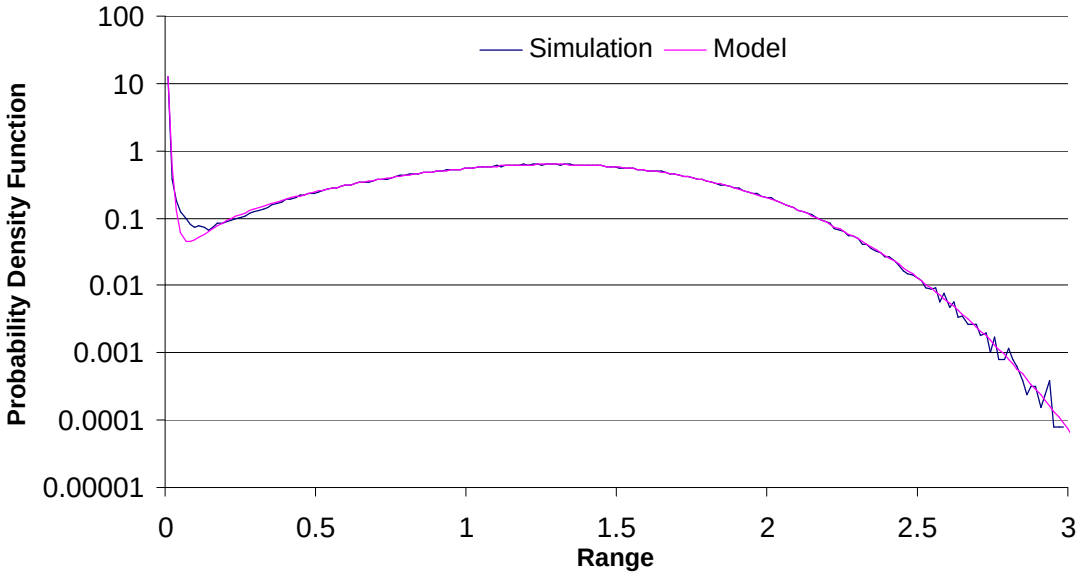

Figure 26. Comparison of Probability Density Functions of Displacement Ranges, One-Mode Model, Unbuckled Panel, s = 0, SPL =124 dB.

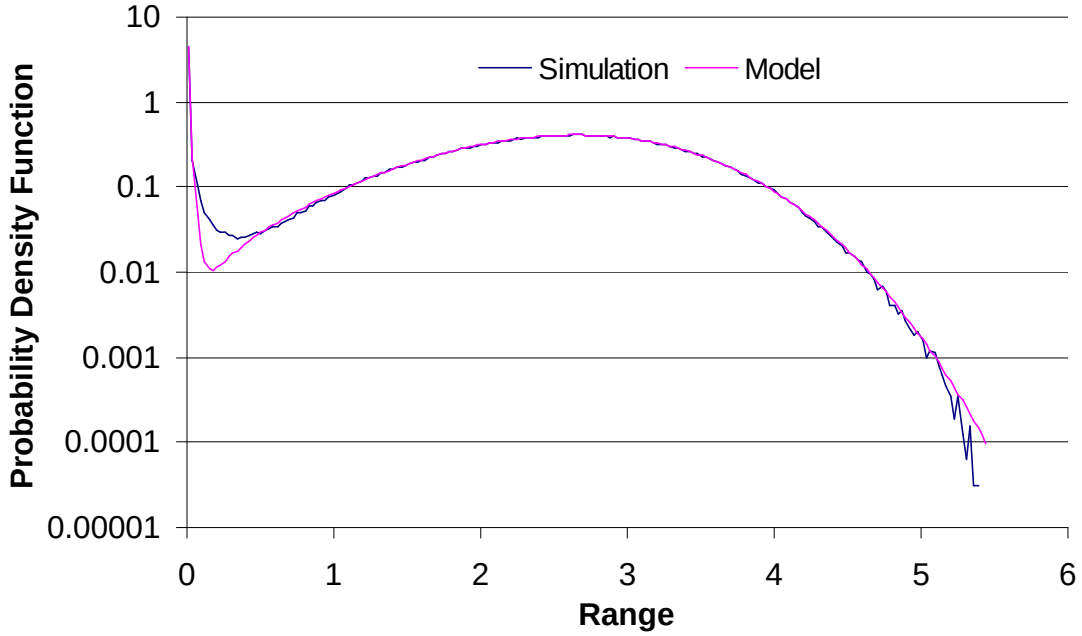

Figure 27. Comparison of Probability Density Functions of Displacement Ranges, One-Mode Model, Unbuckled Panel, s = 0, SPL =134 dB.

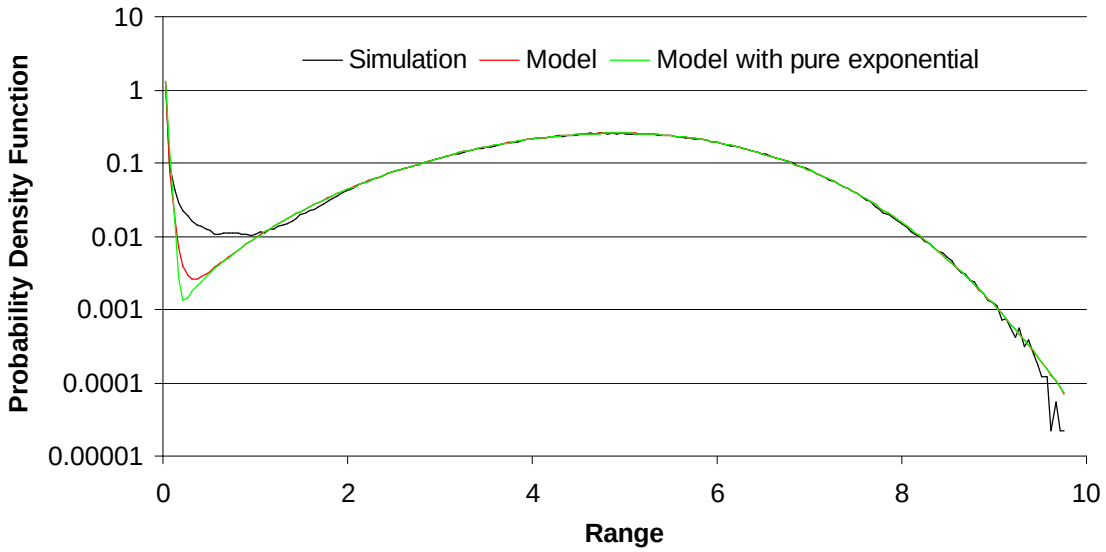

Figure 28. Comparison of Probability Density Functions of Displacement Ranges, One-Mode Model, Unbuckled Panel, s = 0, SPL =144 dB.

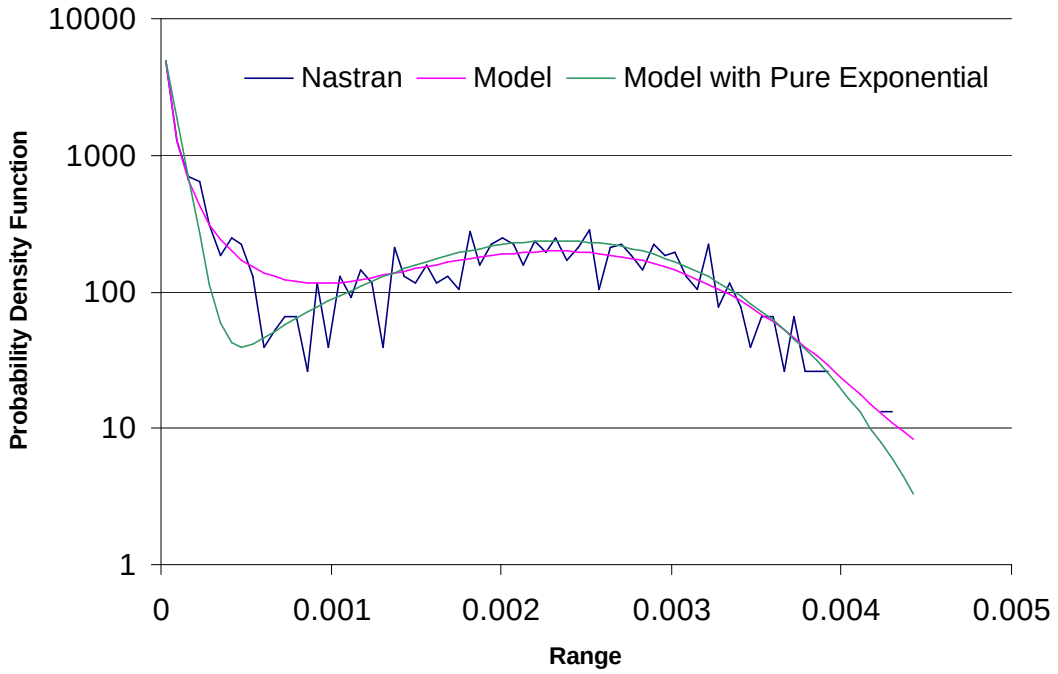

Figure 29. Comparison of Probability Density Functions of Displacement Ranges, Finite Element Data, Unbuckled Panel, *s* = 0, *SPL* =110 dB.

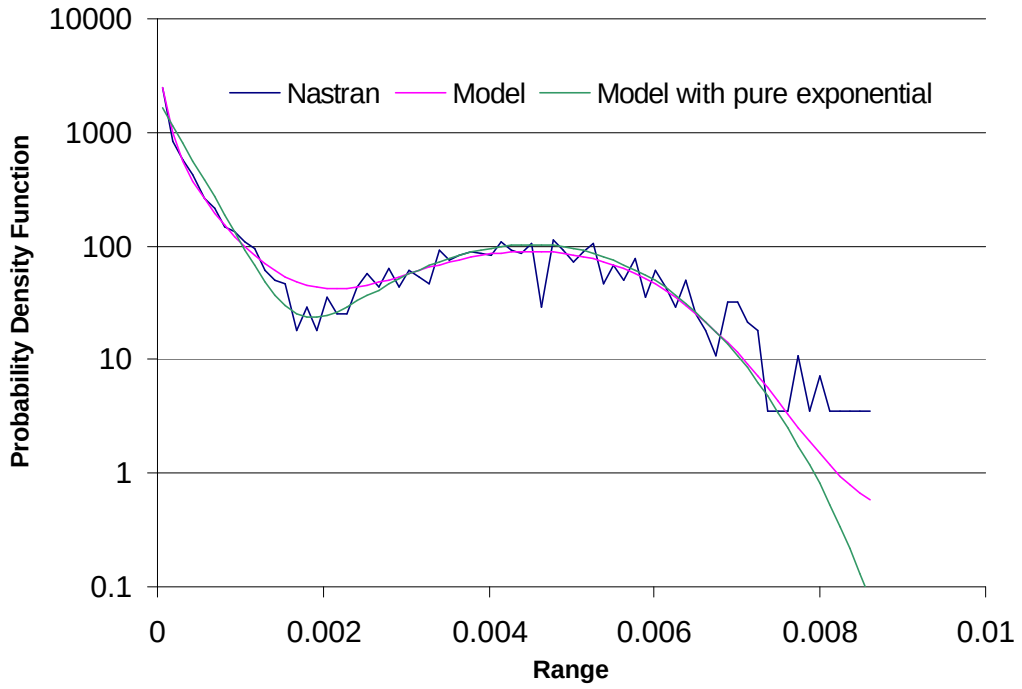

Figure 30. Comparison of Probability Density Functions of Displacement Ranges, Finite Element Data, Unbuckled Panel, *s* = 0, *SPL* =120 dB.

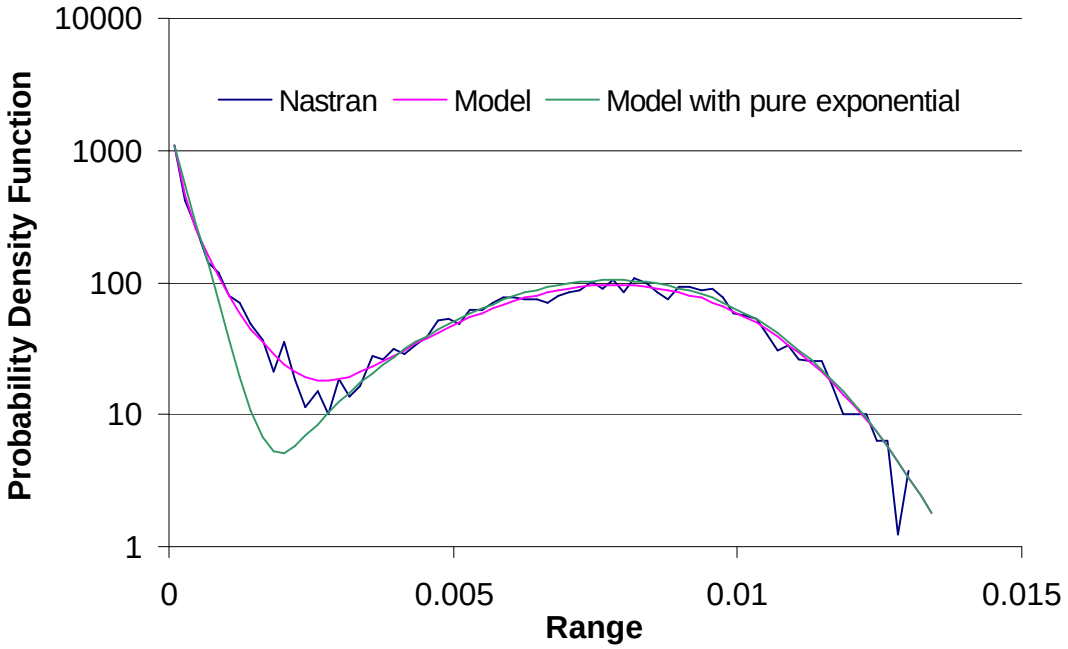

Figure 31. Comparison of Probability Density Functions of Displacement Ranges, Finite Element Data, Unbuckled Panel, s = 0, SPL =130 dB.

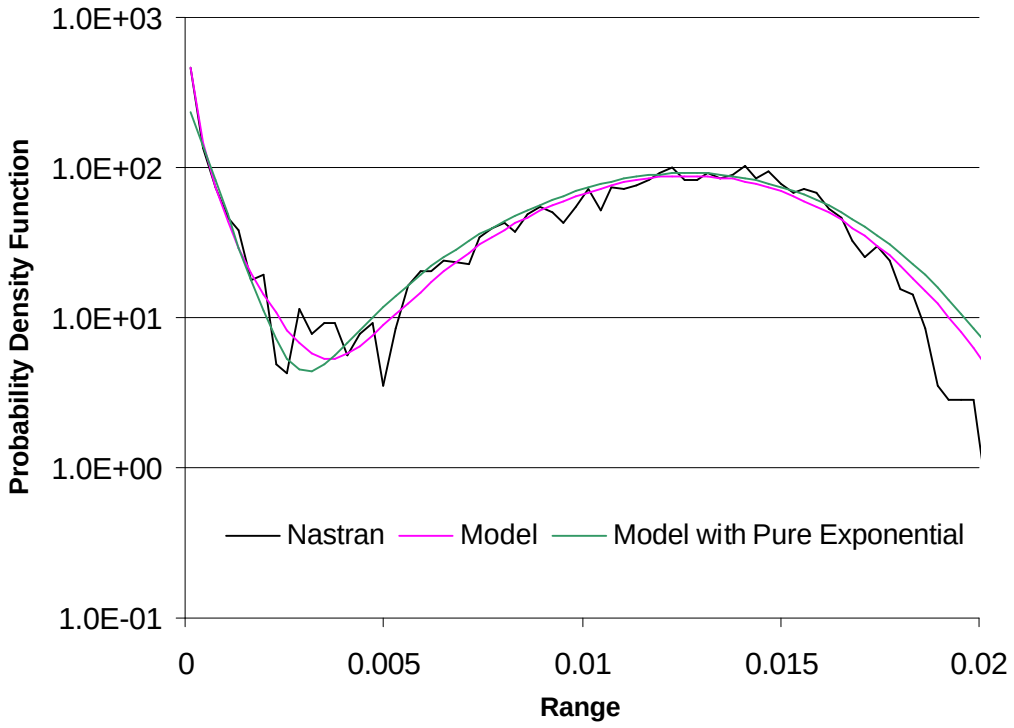

Figure 32. Comparison of Probability Density Functions of Displacement Ranges, Finite Element Data, Unbuckled Panel, s = 0, SPL =140 dB.

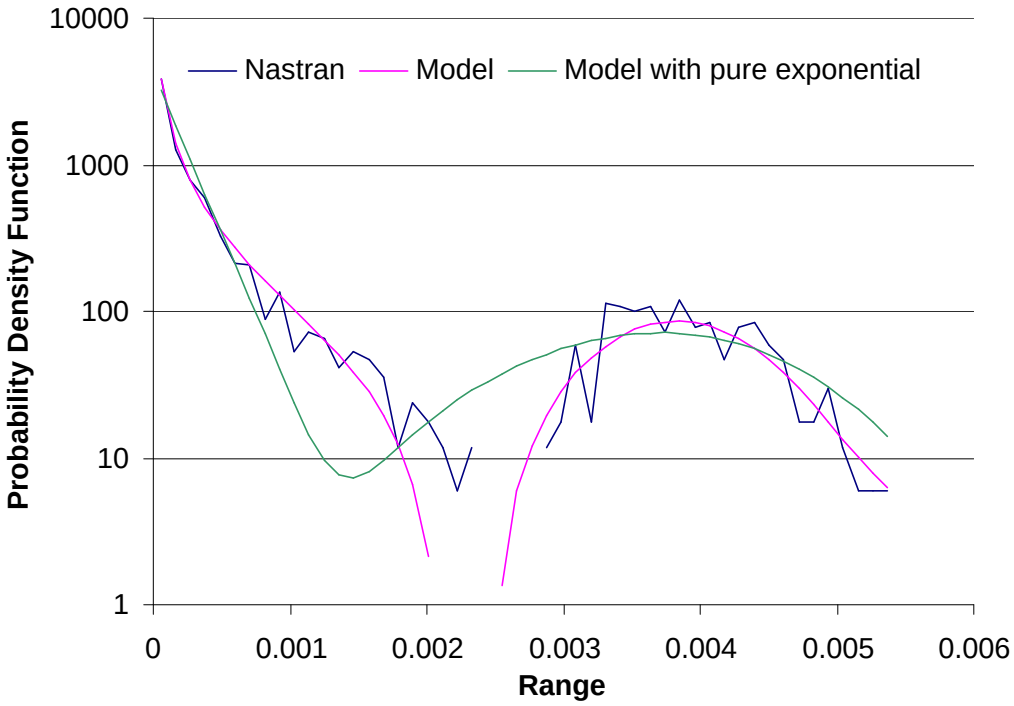

Figure 33. Comparison of Probability Density Functions of Displacement Ranges, Finite Element Data, Buckled Panel, s = 1.8, SPL =110 dB.

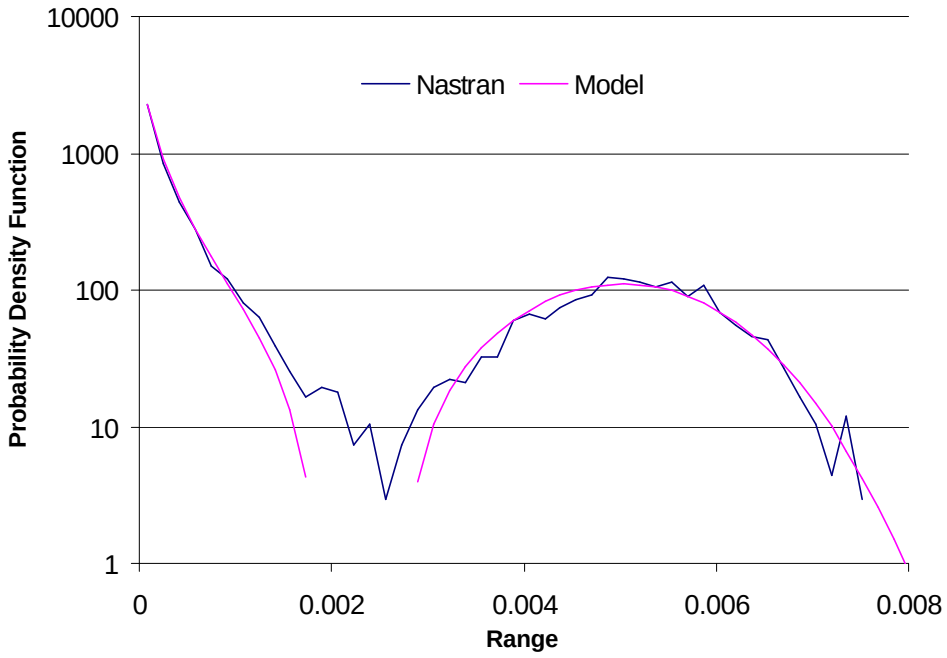

Figure 34. Comparison of Probability Density Functions of Displacement Ranges, Finite Element Data, Buckled Panel, s = 1.8, SPL =120 dB.

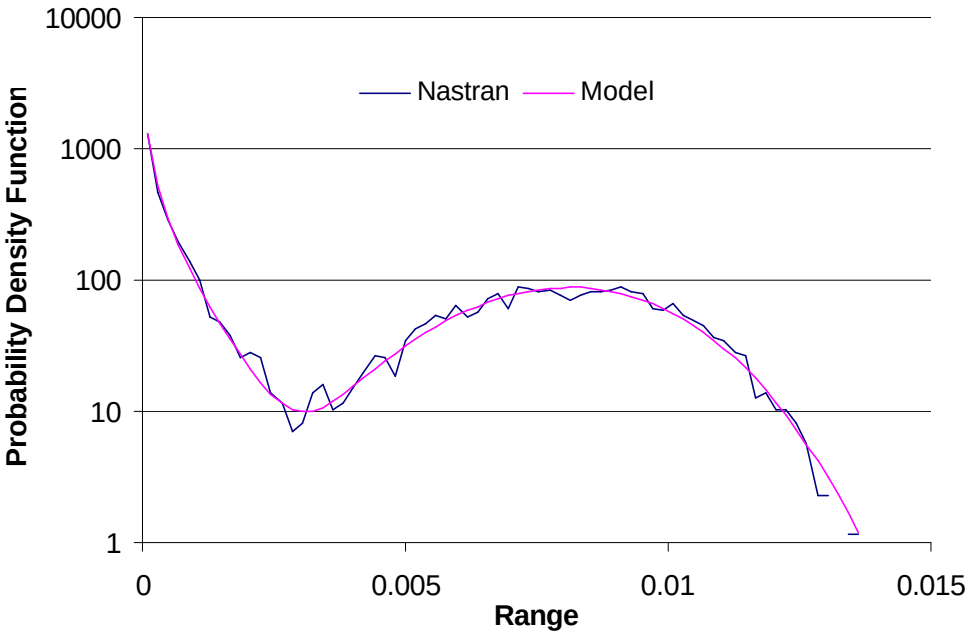

Figure 35. Comparison of Probability Density Functions of Displacement Ranges, Finite Element Data, Buckled Panel, s = 1.8, SPL =130 dB.

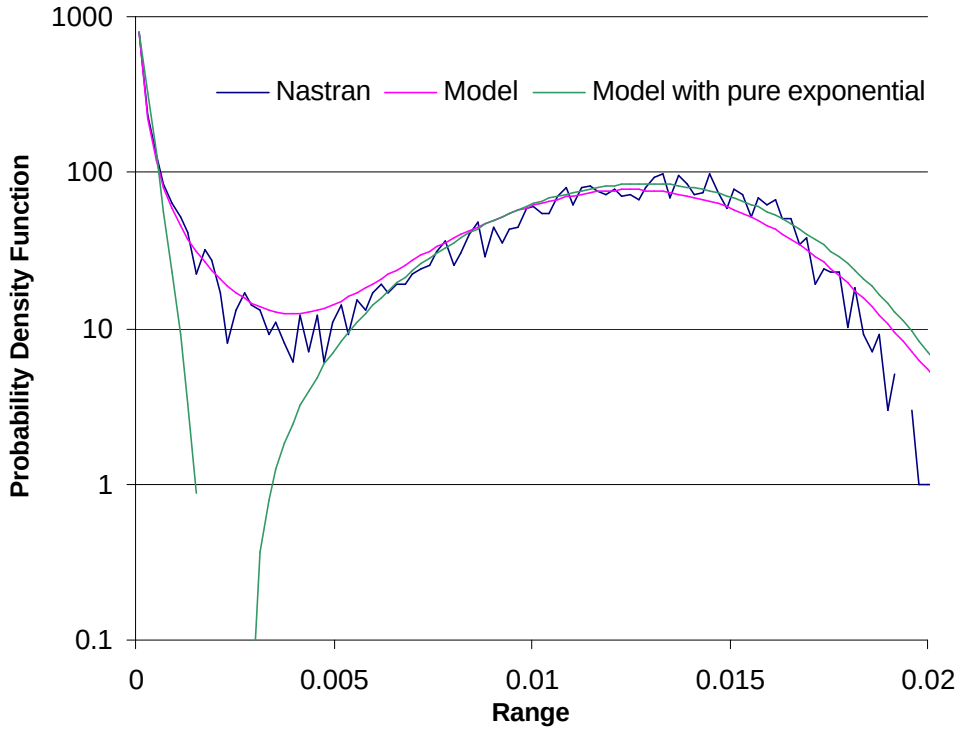

Figure 36. Comparison of Probability Density Functions of Displacement Ranges, Finite Element Data, Buckled Panel, s = 1.8, SPL =140 dB.

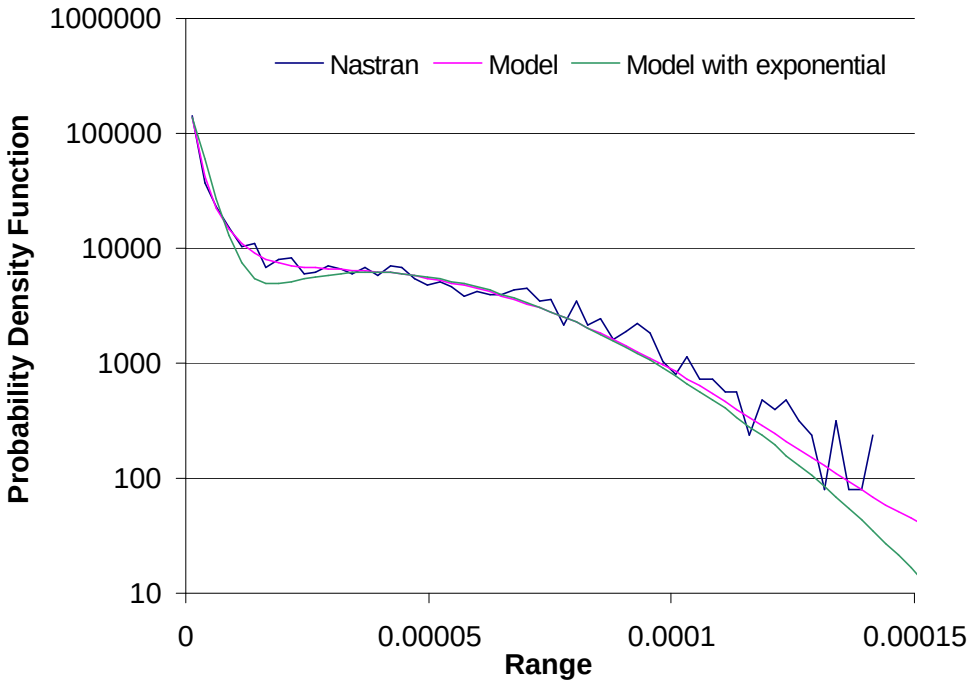

Figure 37. Comparison of Probability Density Functions of Stress Ranges, Finite Element Data, Unbuckled Panel, *s* = 0, *SPL* =110 dB.

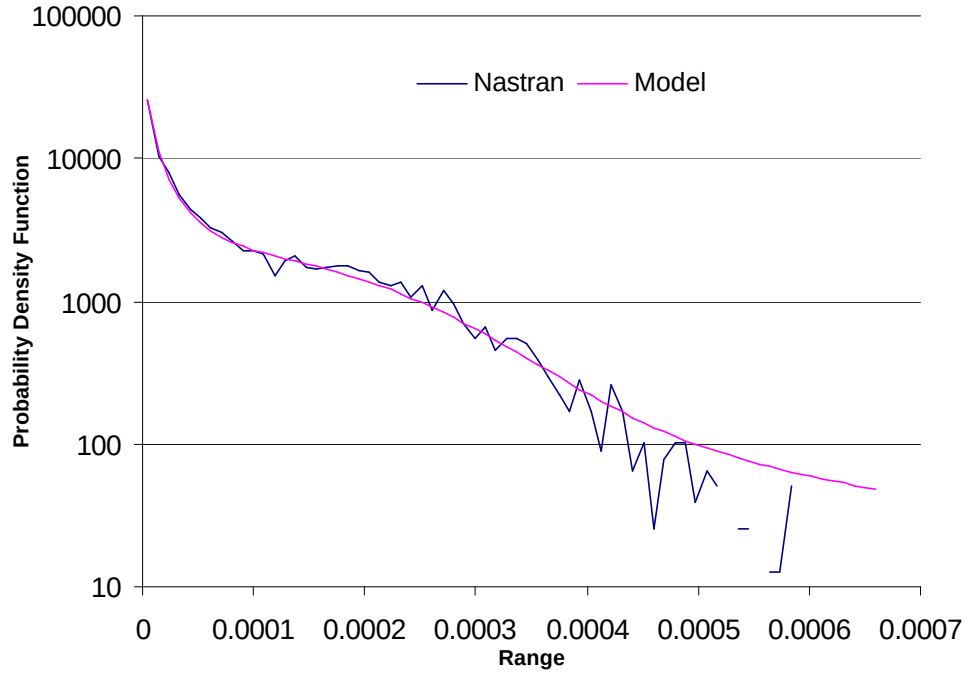

Figure 38. Comparison of Probability Density Functions of Stress Ranges, Finite Element Data, Unbuckled Panel, *s* = 0, *SPL* =120 dB.

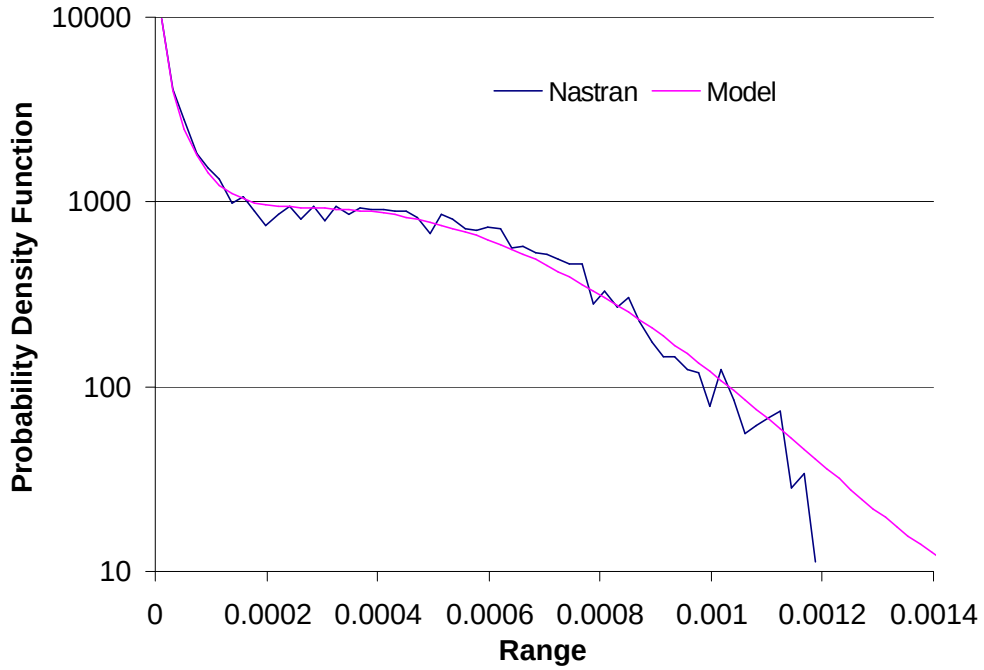

Figure 39. Comparison of Probability Density Functions of Stress Ranges, Finite Element Data, Unbuckled Panel, s = 0, SPL =130 dB.

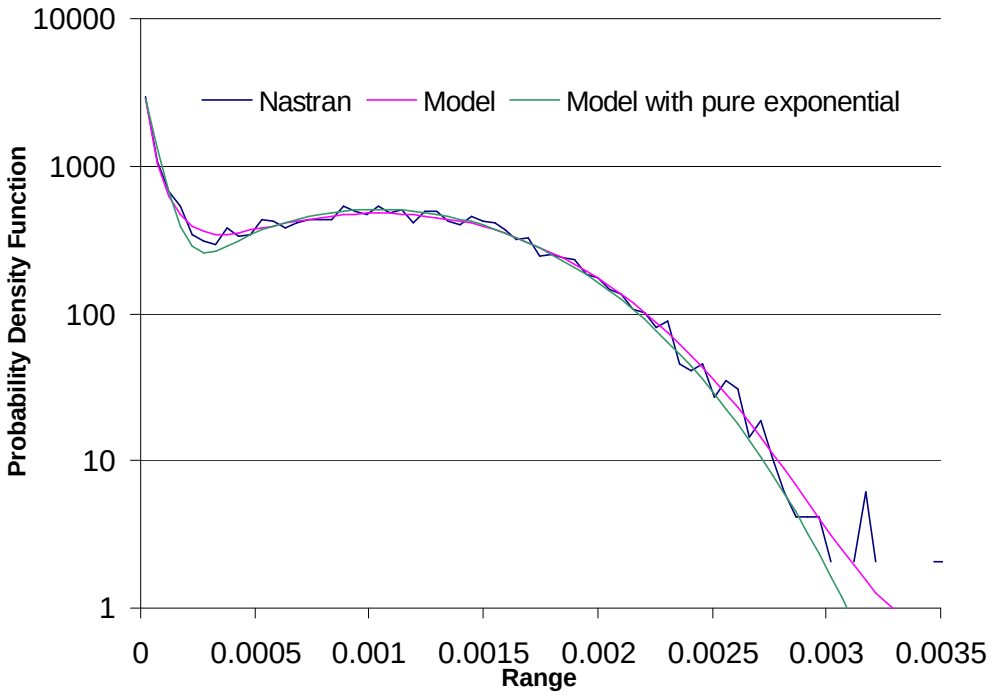

Figure 40. Comparison of Probability Density Functions of Stress Ranges, Finite Element Data, Unbuckled Panel, s = 0, SPL =140 dB.

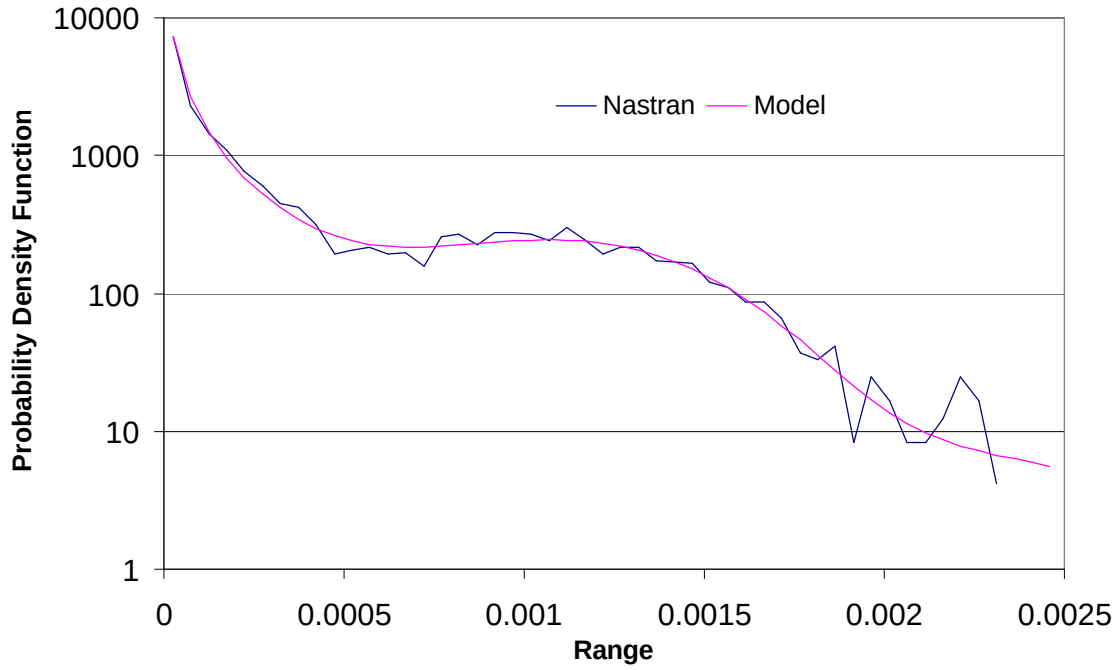

Figure 41. Comparison of Probability Density Functions of Stress Ranges, Finite Element Data, Buckled Panel, s = 1.8, SPL =110 dB.

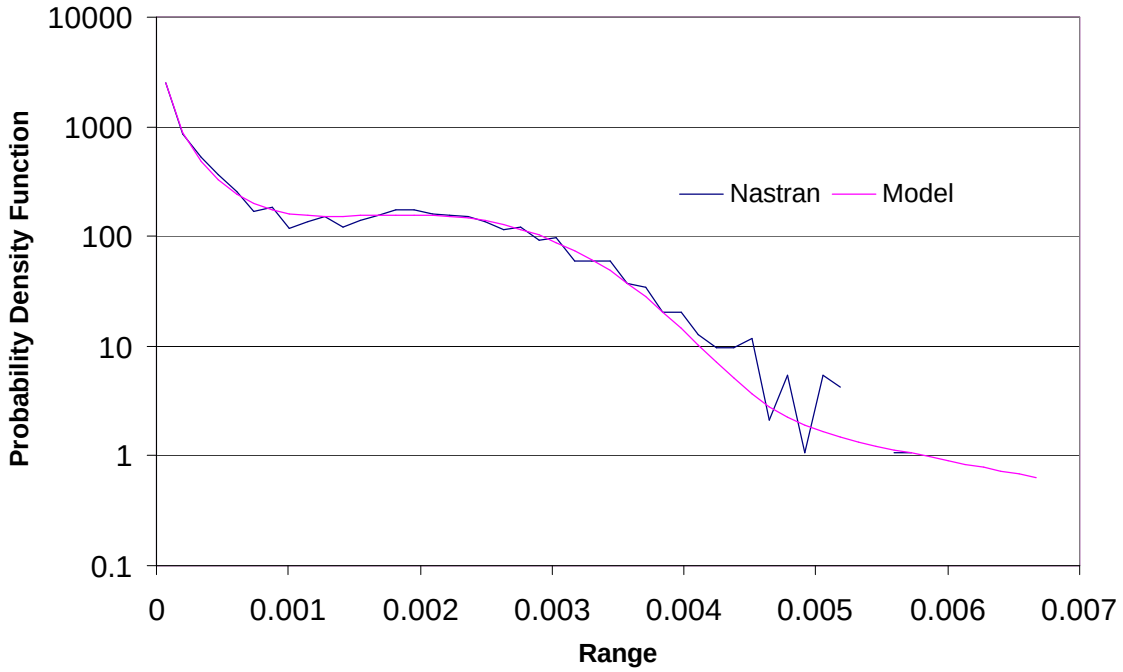

Figure 42. Comparison of Probability Density Functions of Stress Ranges, Finite Element Data, Buckled Panel, s = 1.8, SPL =120 dB.

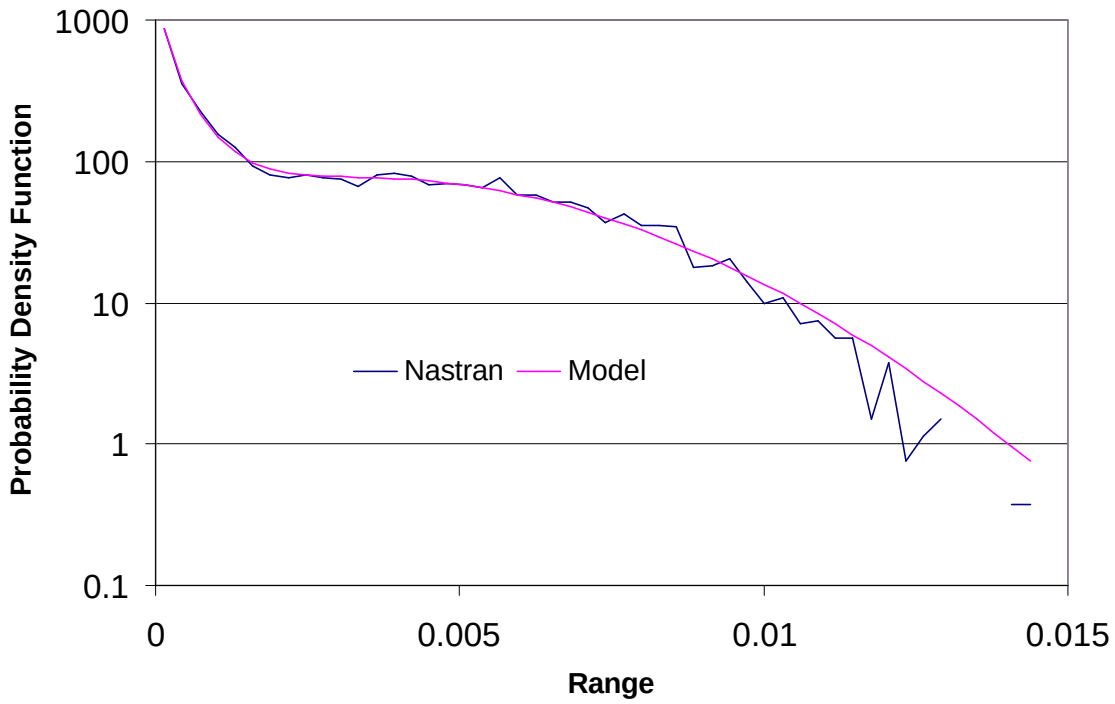

Figure 43. Comparison of Probability Density Functions of Stress Ranges, Finite Element Data, Buckled Panel, *s* = 1.8, *SPL* =130 dB.

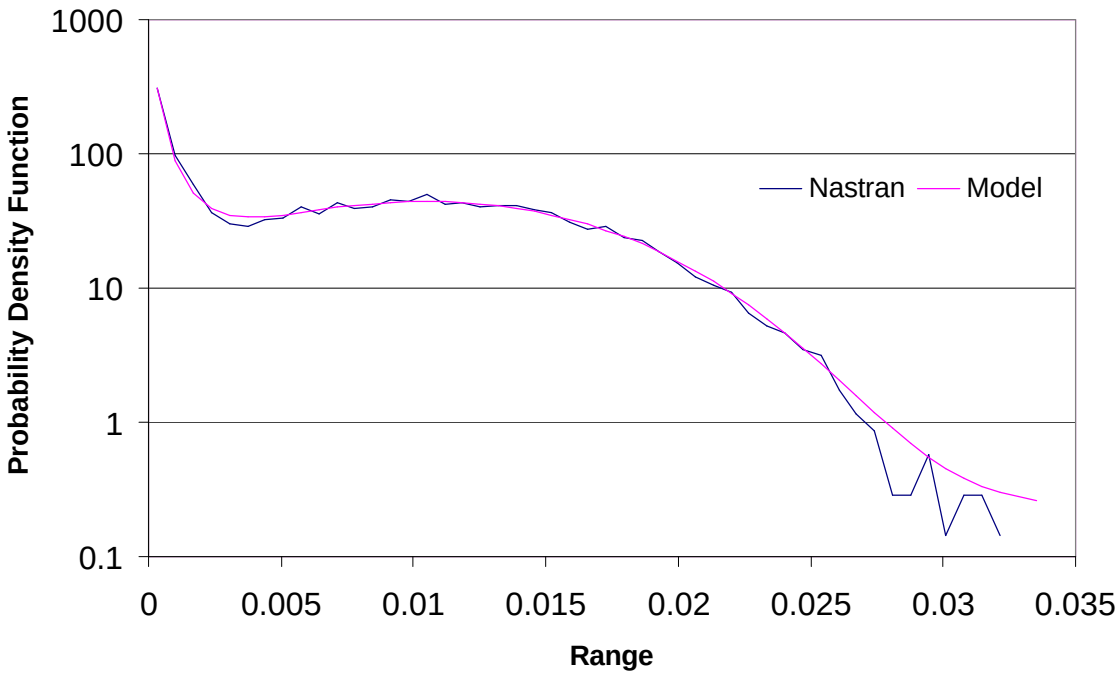

Figure 44. Comparison of Probability Density Functions of Stress Ranges, Finite Element Data, Buckled Panel, *s* = 1.8, *SPL* =140 dB.

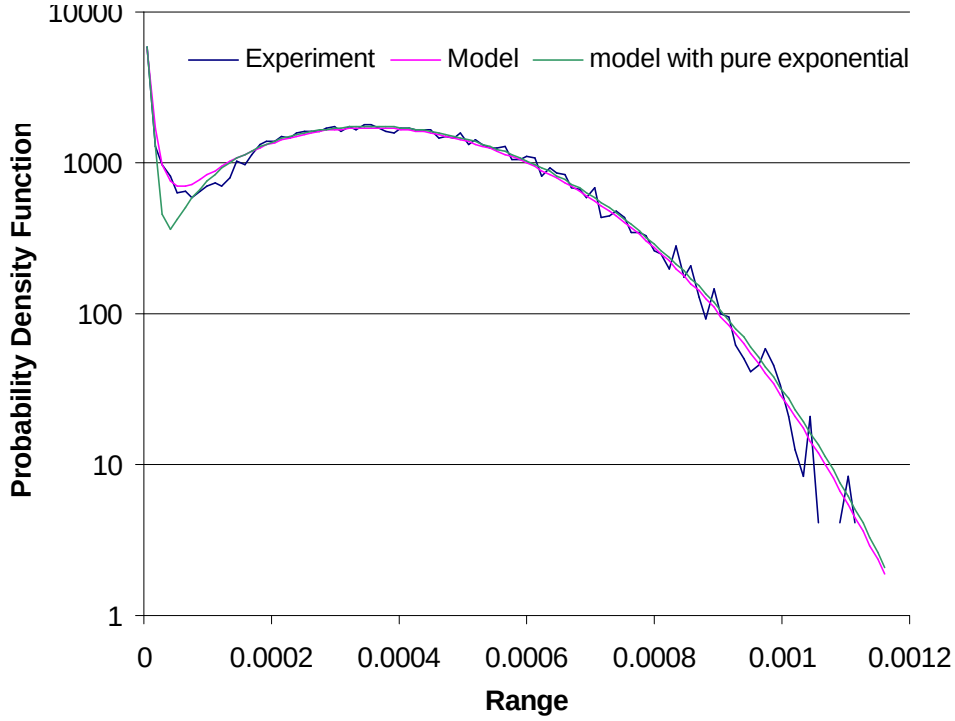

Figure 45. Comparison of Probability Density Functions of Strain Ranges Experimental Data, Unbuckled Panel, s = 0, SPL =152 dB.

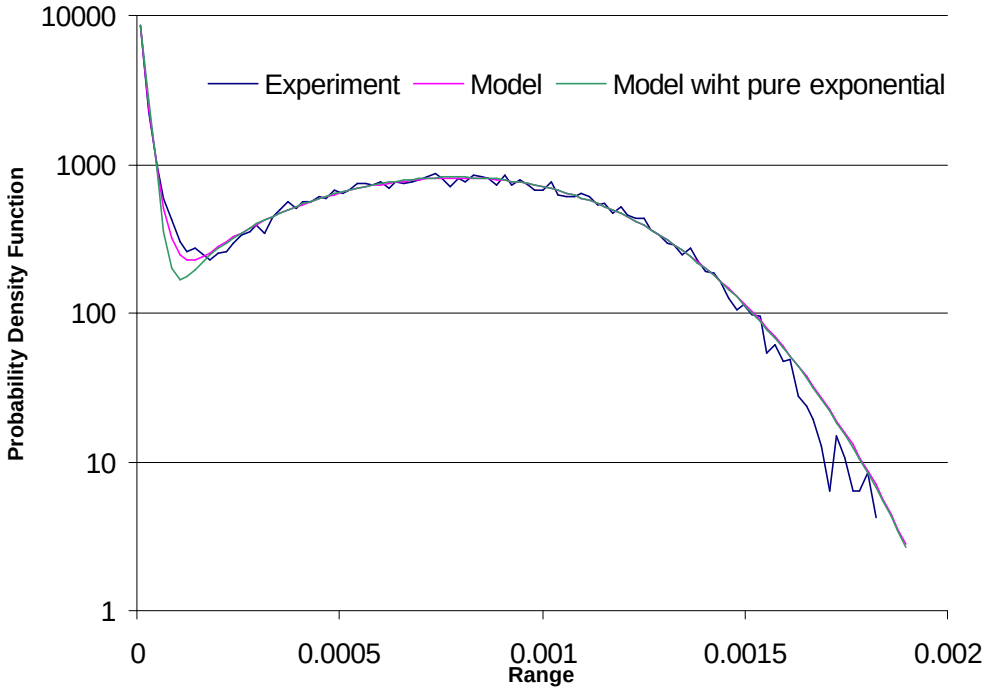

Figure 46. Comparison of Probability Density Functions of Strain Ranges Experimental Data, Unbuckled Panel, s = 0, SPL =158 dB.

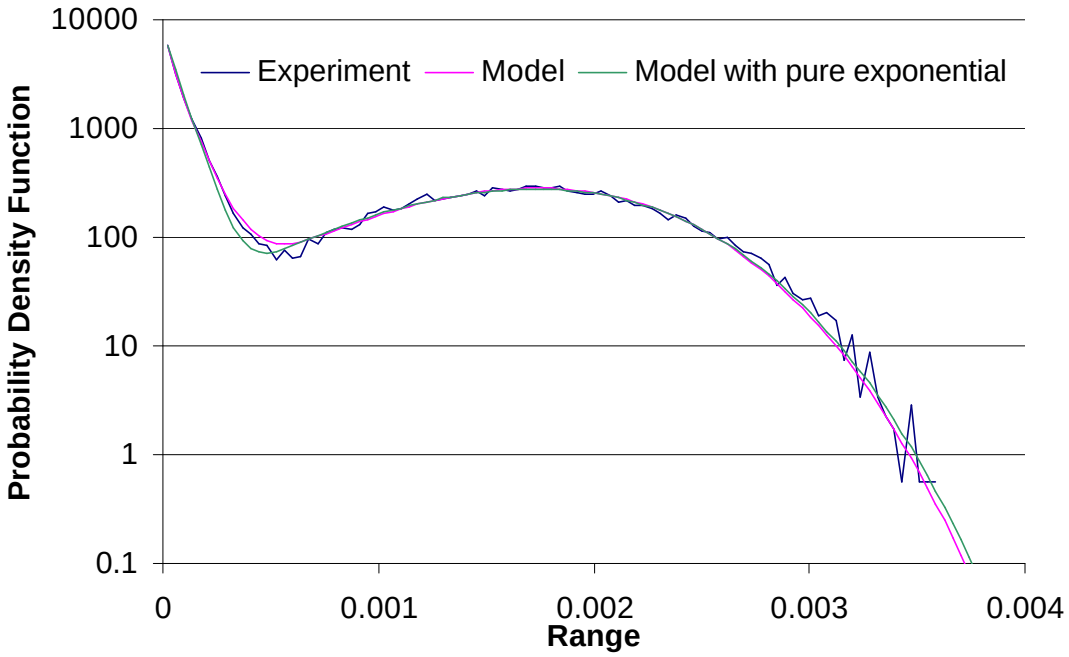

Figure 47. Comparison of Probability Density Functions of Strain Ranges Experimental Data, Unbuckled Panel, s = 0, SPL =167 dB.

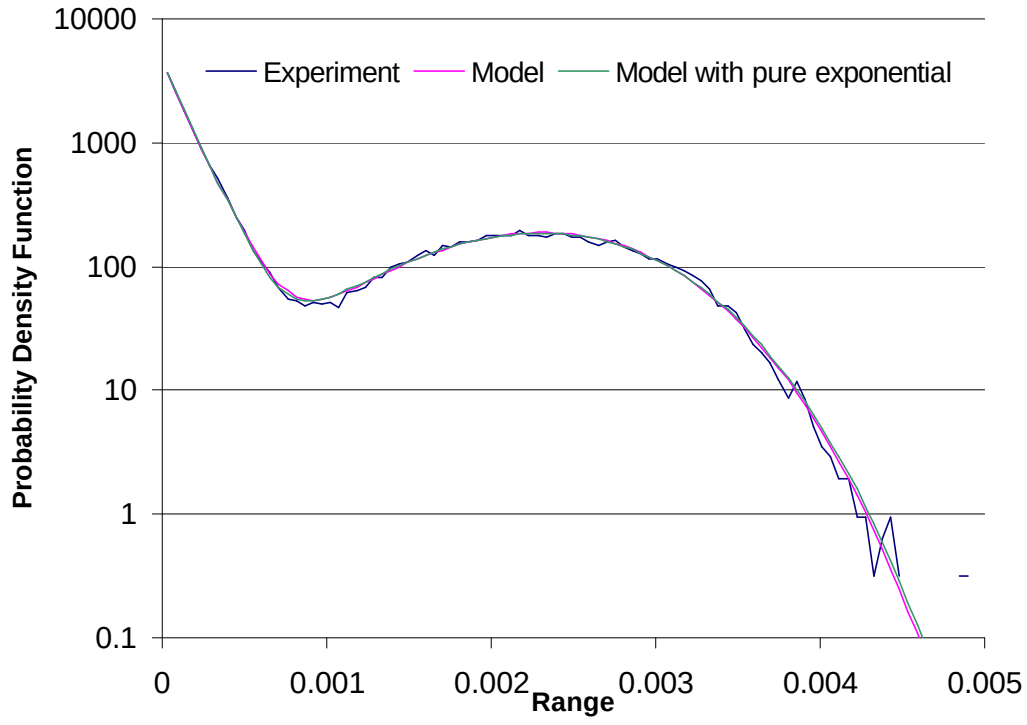

Figure 48. Comparison of Probability Density Functions of Strain Ranges Experimental Data, Unbuckled Panel, s = 0, SPL =172 dB.

3.0 MODEL VALIDATION

The work carried out in the previous section has motivated the selection of the mixture probability density function model given by Eq. (5), (9)-(11), and (15) and has demonstrated its validity in a series of cases. It is desired here to extend the validation of the model to a series of other situations.

The modeling of the displacement and stress ranges for buckled and unbuckled panels subjected to an acoustic excitation at a non-zero incidence will be considered first. The effect of a non-zero incidence angle is to produce a time shift between the excitation (pressure) exerted at different points of the panel. Then, even if the pressure field is assumed to vary in time as a white noise (as is the case here), a non-zero incidence angle will induce a combined time-space correlation between the samples of the panel loading. In that sense, a non-zero incident loading is reminiscent of a colored excitation process. The assessment of the model of Eq. (5), (9)-(11), and (15) on the non-zero incident case thus also provides its partial validation to the situation of a colored excitation process. The shorter the time required for the wave to pass over the panel, the shorter the time shift, and thus the more white the excitation will appear. In the present situation, it was assumed that the wave propagated along the long side of the panel (14 inches) at a 90 degree incidence (i.e. grazing or perfectly parallel to the panel surface) to provide the opposite limiting case to the zero incidence considered in earlier assessments. With a sampling time $\Delta t = 2.82\ 10^{-4}$ sec, it was found that the travel time over the panel is 4.2 Δt which was rounded of to 5 Δt. A white noise wave was thus propagated over the panel at the rate of 2.8 inches per Δt. The assessment of the model of Eq. (5), (9)-(11), and (15) was then performed, see Fig. 49-64, on the

range of displacements and stresses for both unbuckled and buckled panels. Again, the agreement is excellent in all cases.

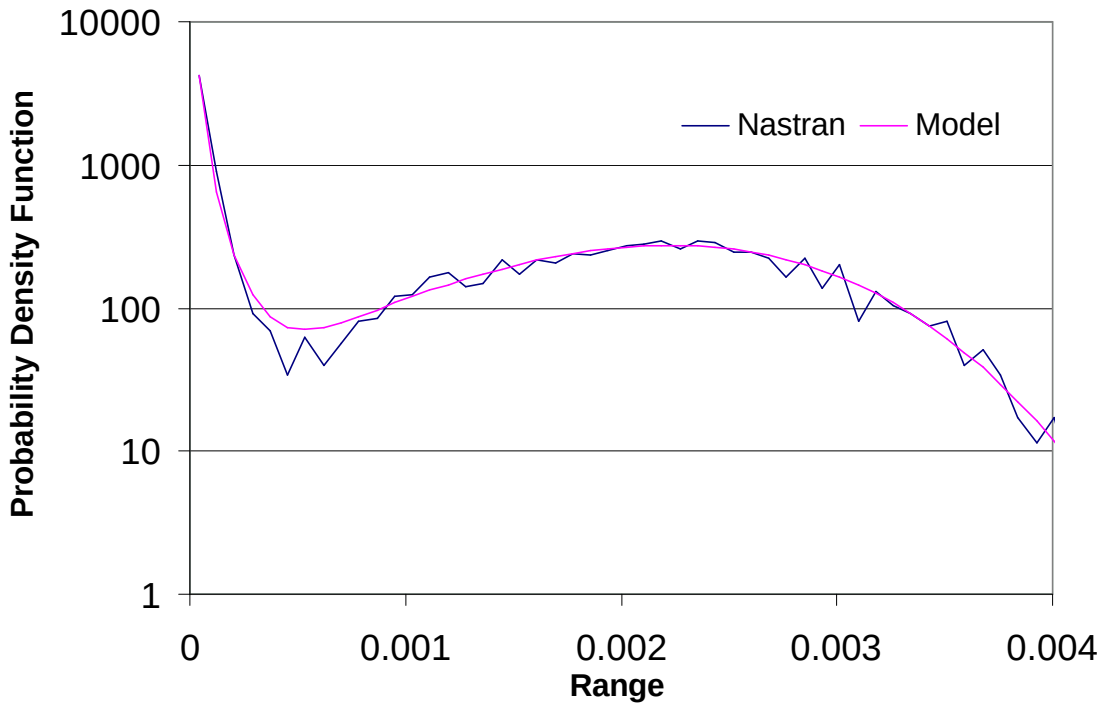

Figure 49. Comparison of Probability Density Functions of Displacement Ranges, Finite Element Data, Unbuckled Panel, Grazing Incidence, s = 0, SPL =110 dB.

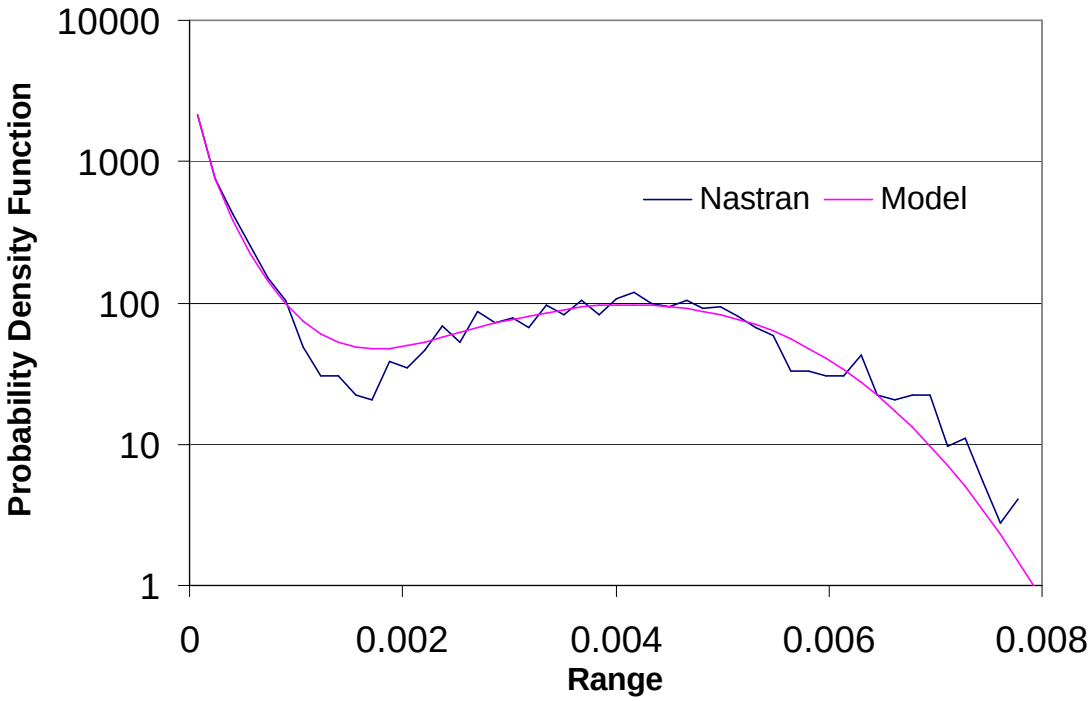

Figure 50. Comparison of Probability Density Functions of Displacement Ranges, Finite Element Data, Unbuckled Panel, Grazing Incidence, s = 0, SPL =120 dB.

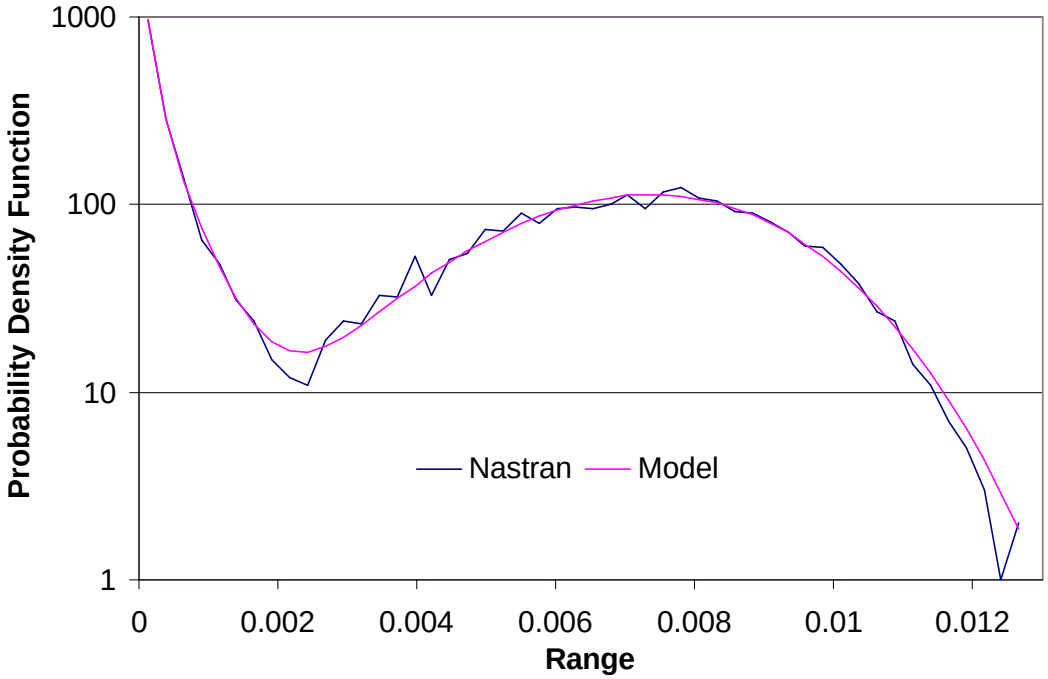

Figure 51. Comparison of Probability Density Functions of Displacement Ranges, Finite Element Data, Unbuckled Panel, Grazing Incidence, s = 0, SPL =130 dB.

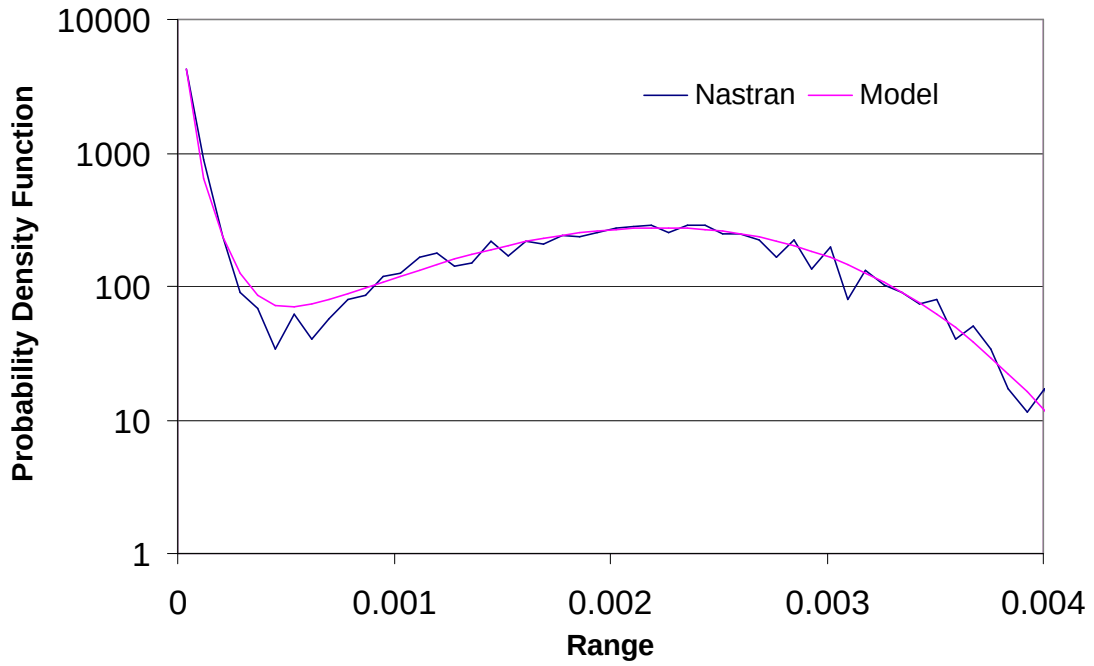

Figure 52. Comparison of Probability Density Functions of Displacement Ranges, Finite Element Data, Unbuckled Panel, Grazing Incidence, *s* = 0, *SPL* =140 dB.

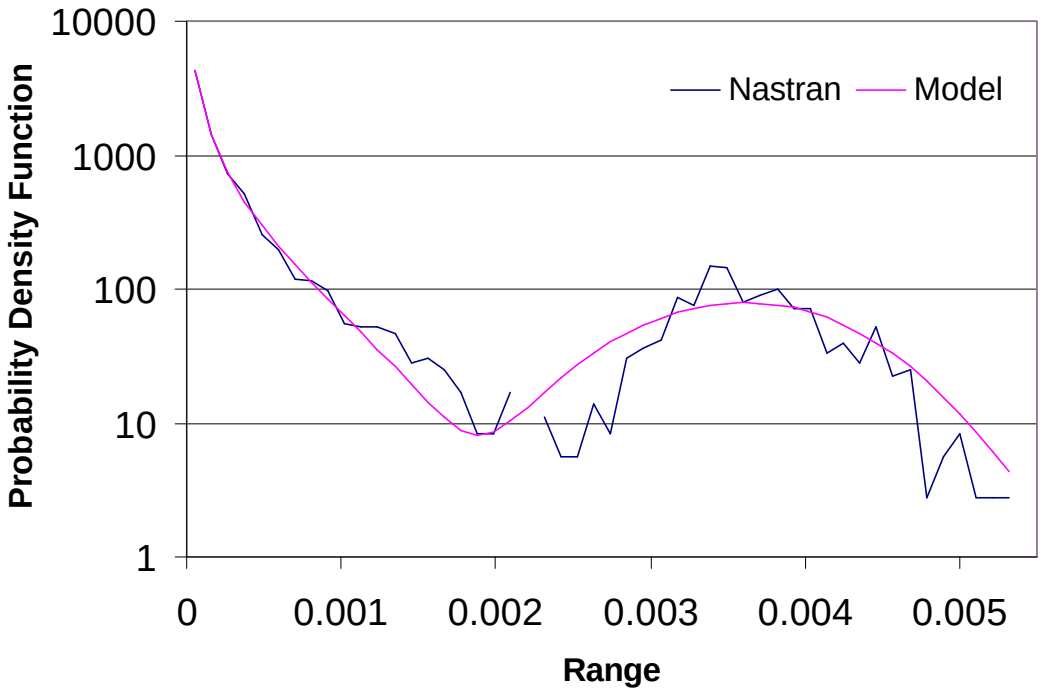

Figure 53. Comparison of Probability Density Functions of Displacement Ranges, Finite Element Data, Buckled Panel, Grazing Incidence, *s* = 1.8, *SPL* =110 dB.

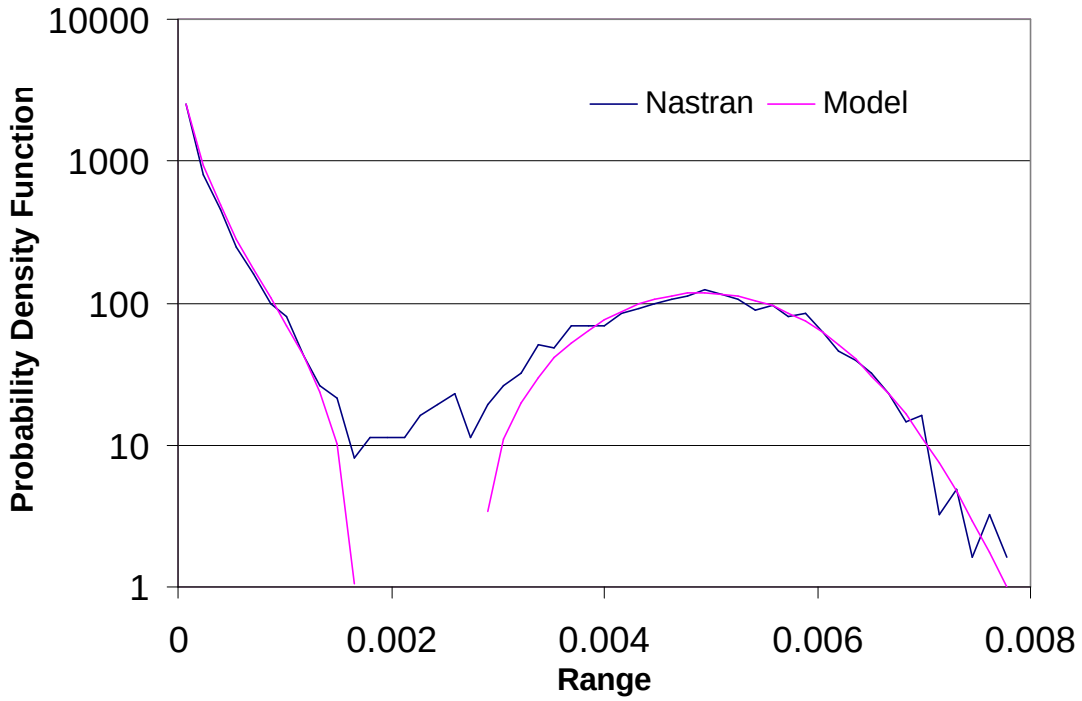

Figure 54. Comparison of Probability Density Functions of Displacement Ranges, Finite Element Data, Buckled Panel, Grazing Incidence, *s* = 1.8, *SPL* =120 dB.

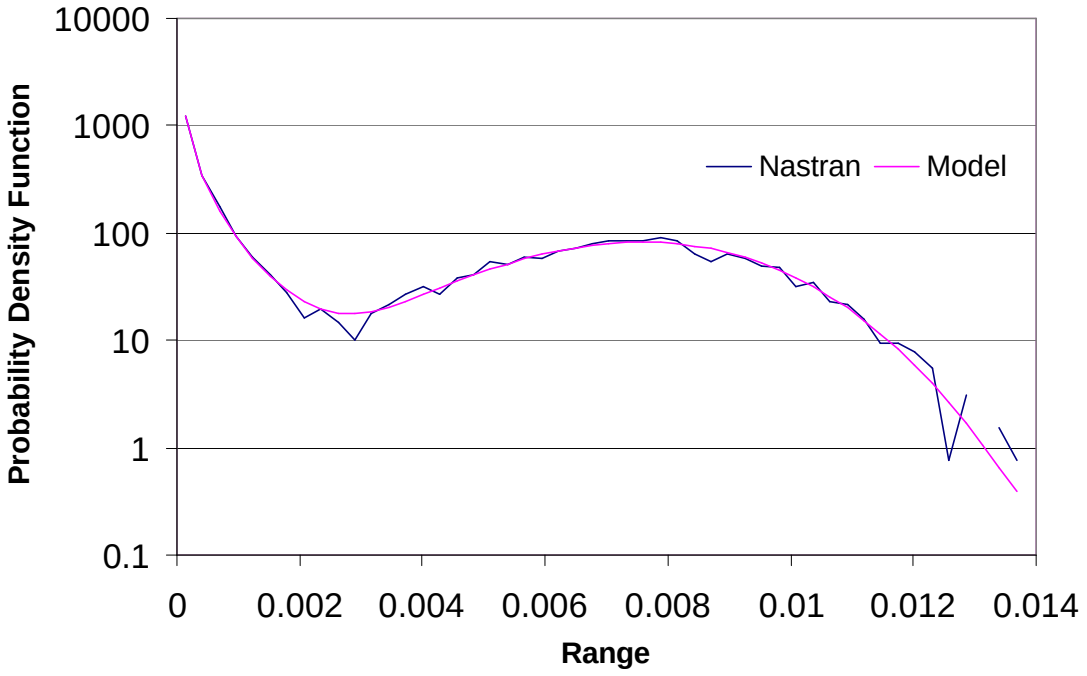

Figure 55. Comparison of Probability Density Functions of Displacement Ranges, Finite Element Data, Buckled Panel, Grazing Incidence, *s* = 1.8, *SPL* =130 dB.

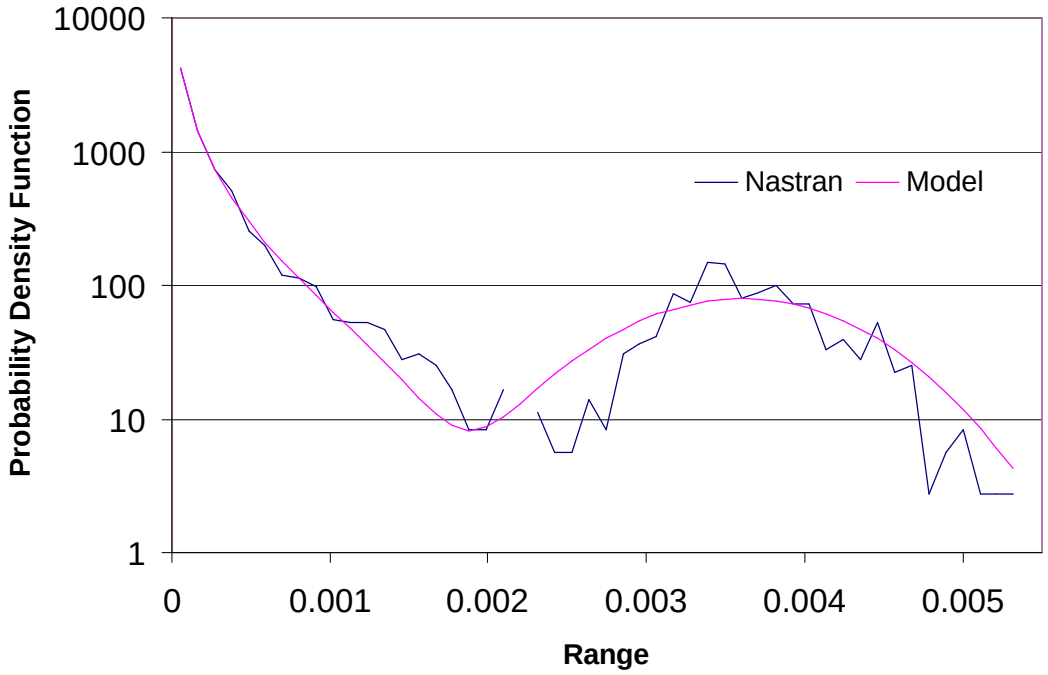

Figure 56. Comparison of Probability Density Functions of Displacement Ranges, Finite Element Data, Buckled Panel, Grazing Incidence, *s* = 1.8, *SPL* =140 dB.

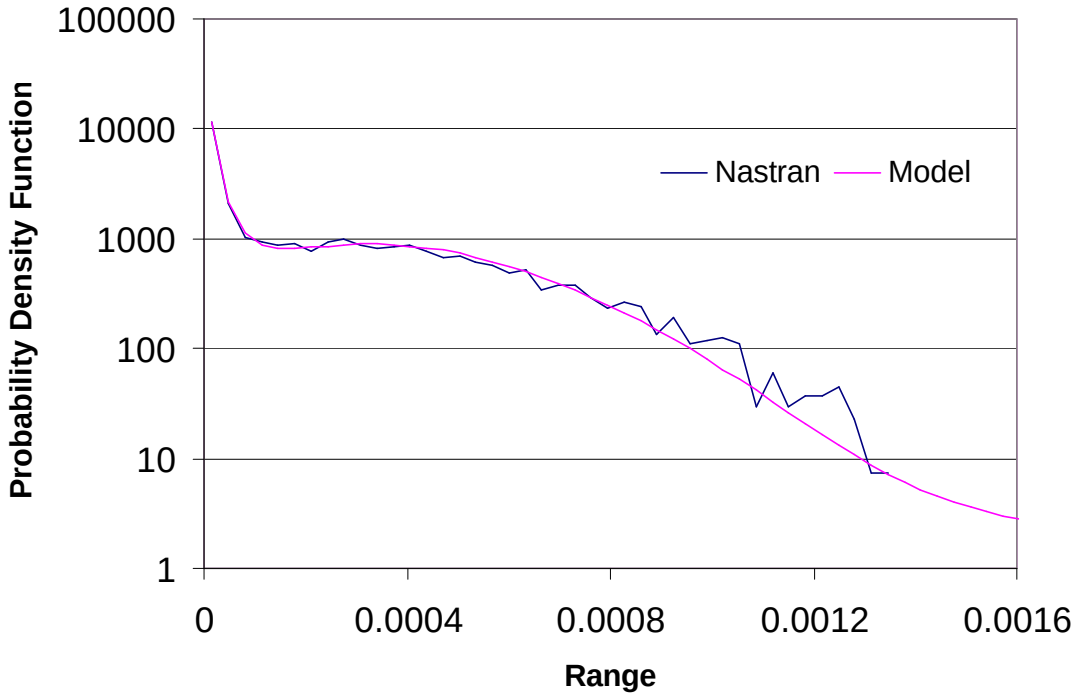

Figure 57. Comparison of Probability Density Functions of Stress Ranges, Finite Element Data, Unbuckled Panel, Grazing Incidence, *s* = 0, *SPL* =110 dB.

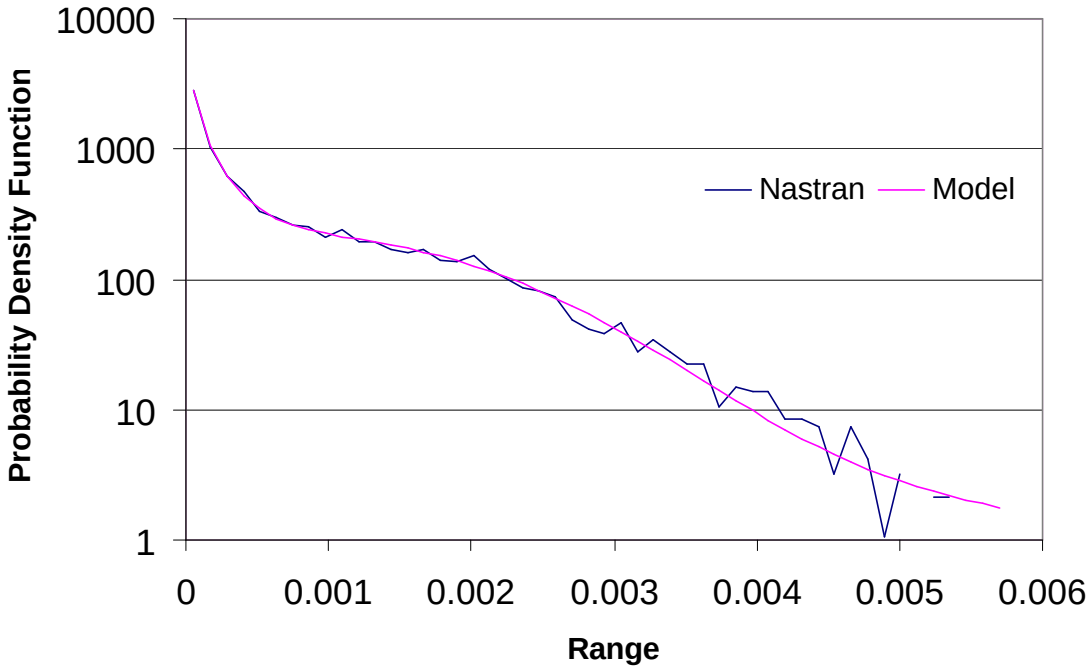

Figure 58. Comparison of Probability Density Functions of Stress Ranges, Finite Element Data, Unbuckled Panel, Grazing Incidence, *s* = 0, *SPL* =120 dB.

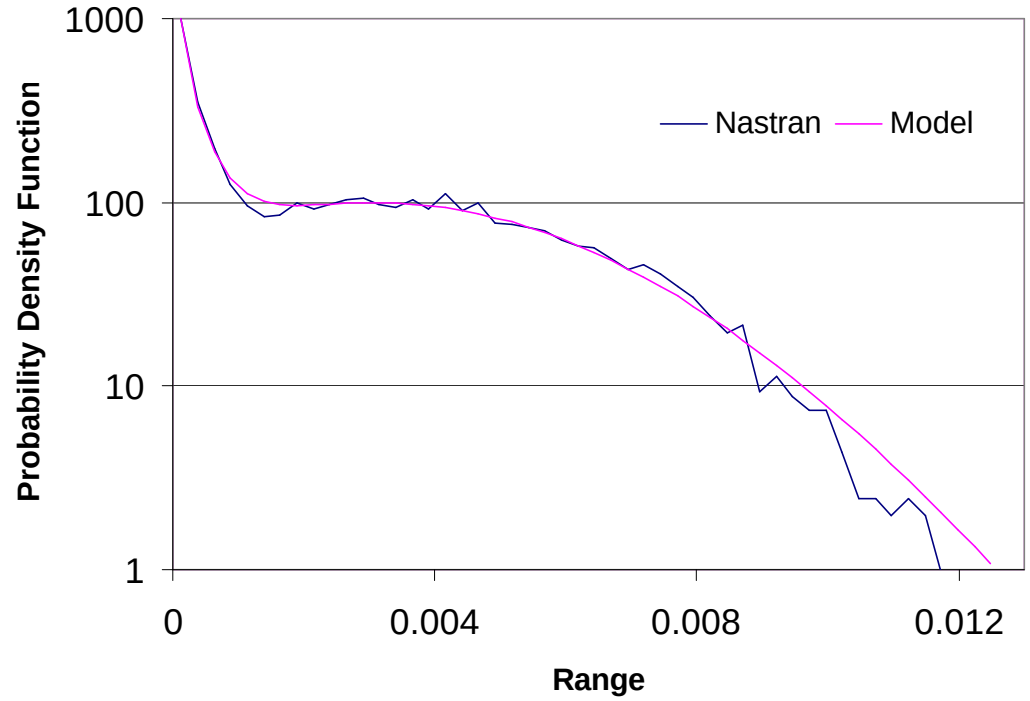

Figure 59. Comparison of Probability Density Functions of Stress Ranges, Finite Element Data, Unbuckled Panel, Grazing Incidence, *s* = 0, *SPL* =130 dB.

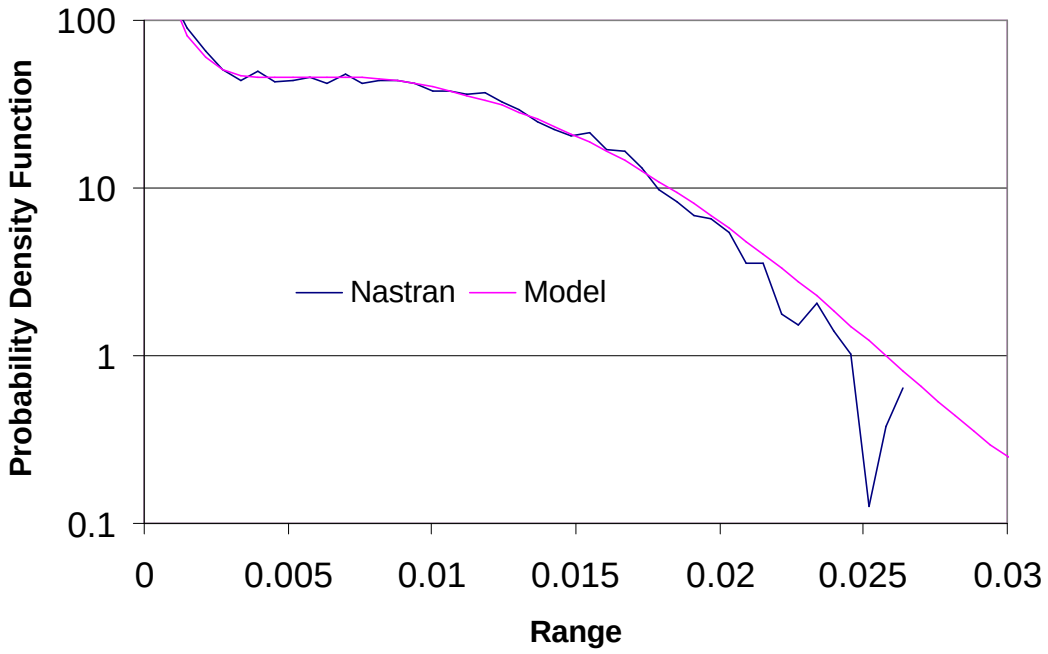

Figure 60. Comparison of Probability Density Functions of Stress Ranges, Finite Element Data, Unbuckled Panel, Grazing Incidence, s = 0, SPL =140 dB.

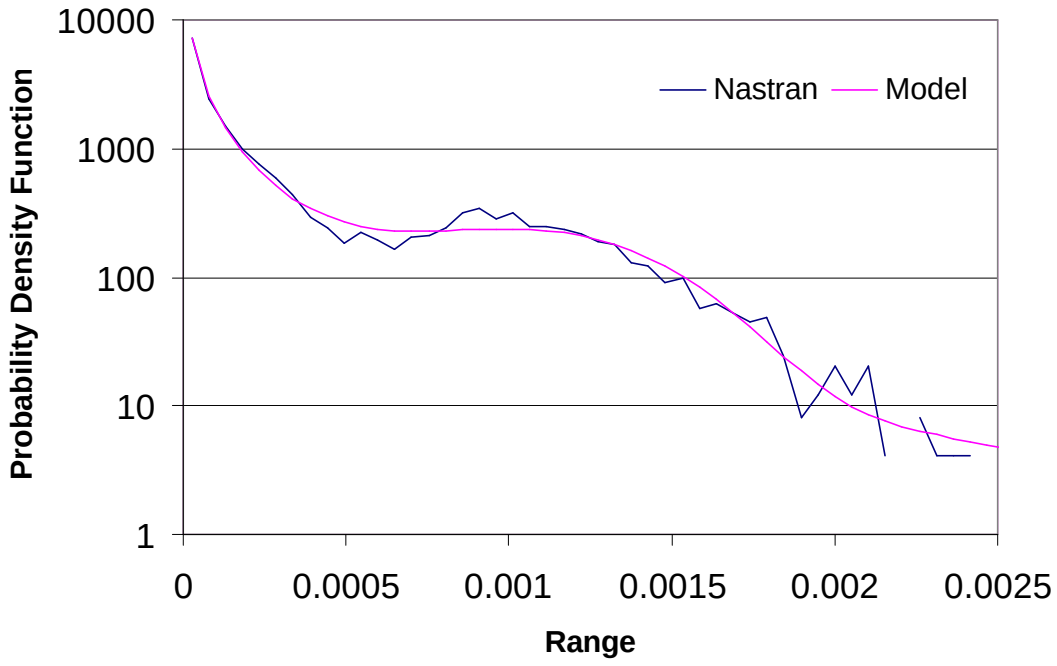

Figure 61. Comparison of Probability Density Functions of Stress Ranges, Finite Element Data, Buckled Panel, Grazing Incidence, s = 1.8, SPL =110 dB.

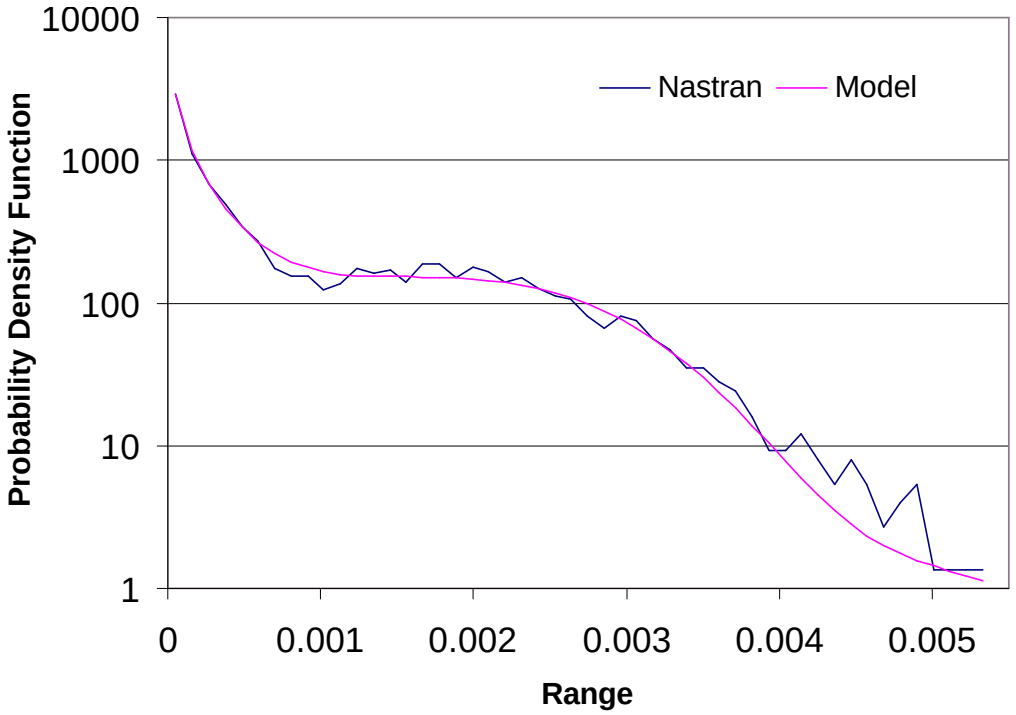

Figure 62. Comparison of Probability Density Functions of Stress Ranges, Finite Element Data, Buckled Panel, Grazing Incidence, *s* = 1.8, *SPL* =120 dB.

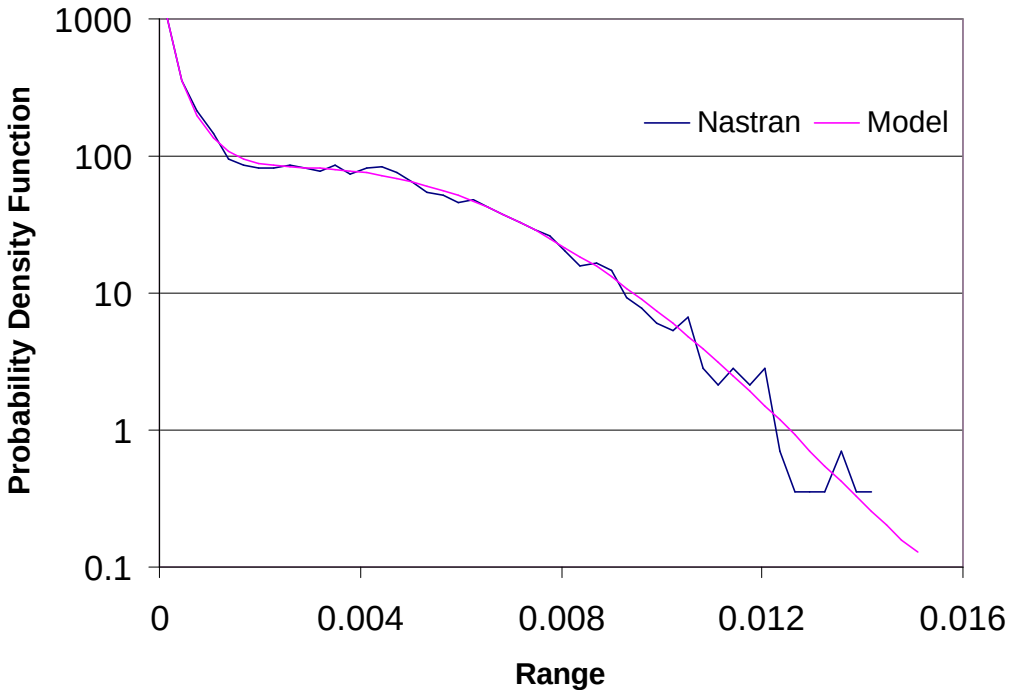

Figure 63. Comparison of Probability Density Functions of Stress Ranges, Finite Element Data, Buckled Panel, Grazing Incidence, *s* = 1.8, *SPL* =130 dB.

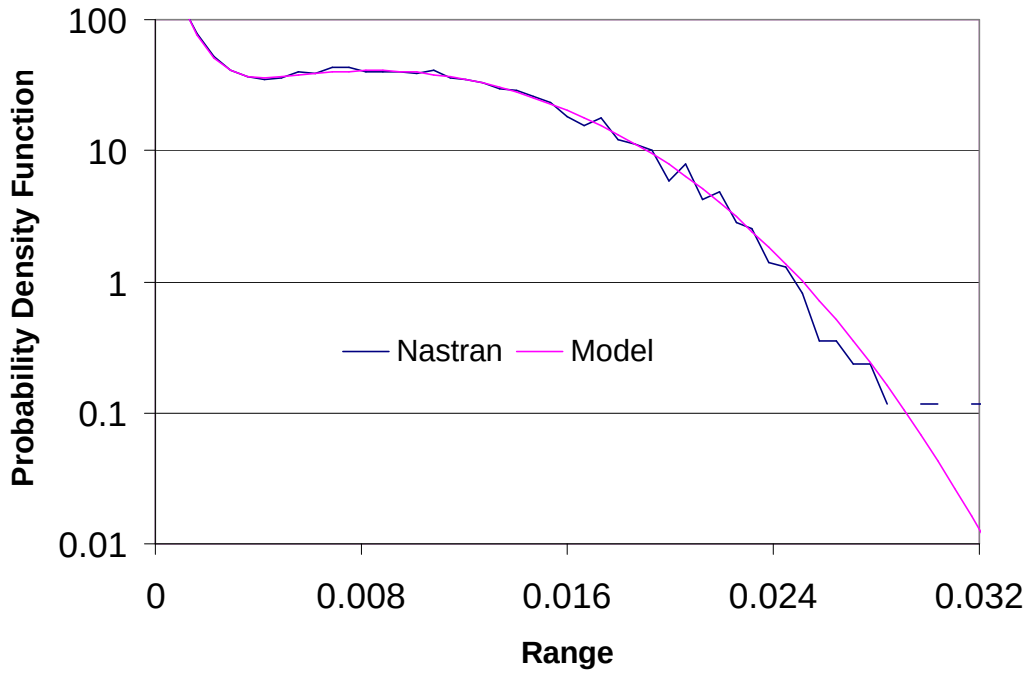

Figure 64. Comparison of Probability Density Functions of Stress Ranges, Finite Element Data, Buckled Panel, Grazing Incidence, s = 1.8, SPL =140 dB.

The work conducted so far focused on the behavior at the center of a panel of rather arbitrary dimensions, i.e. 10 in. x 14 in. x 0.04 in. The "arbitrariness" of the dimensions suggests that the excellent matching of the simulation and model probability density functions obtained above is a general property. However, the features of the response may be geometry dependent and it is thus necessary to consider other panel geometries to obtain a more complete perspective. The two essential characteristics of a rectangular panel are its thickness and its aspect ratio. Thus, two additional panels were considered:

(1) the first one had the same in-plane dimensions as the original panel but twice the thickness, i.e. its dimensions were 10 in. x 14 in. x 0.08 in. This panel was considered subjected to a

normally incident acoustic wave of sound pressure level of 140 dB and 150 dB. This panel will be referred to as panel 2 in the ensuing discussion.

(2) the second panel had the same thickness and a very similar area as the original one but had a different aspect ratio. Specifically, this second panel was chosen to be square with dimensions 12 in. x 12 in. x 0.04 in and was submitted to white noise excitations of *SPL* = 130 dB and 140 dB. This panel will be referred to as panel 3 in the ensuing discussion.

For simplicity, the original panel will be referred to as panel 1 in the remainder of this report.

As done with the original panel, the response (displacement and stress) at the center of the panel due to a white noise excitation was first computed for 32,000 time steps. The corresponding probability density function of the displacement and stress ranges was then obtained and was further fitted by the proposed model. Shown in Fig. 65-68 are the corresponding comparisons of the MSC.Nastran and model probability density functions of the stress ranges which again demonstrate the appropriateness of the proposed model.

The consideration of the center of the panel is, as the geometry of the panel, a restricting factor in the validation of the model. Accordingly, the analysis was broadened to include a more arbitrary point, e.g. node 40 on the panels 1 and 2 and node 35 on panel 3, see Fig. 69-70. As for the middle of the panels, the probability density functions of the ranges of the response of these new points were obtained and were fitted by the proposed five-parameter model. Shown in Fig. 71-75 are the comparisons between the MSC.Nastran distributions of ranges and the corresponding models. Note once more the excellent matching between the MSC.Nastran and model curves.

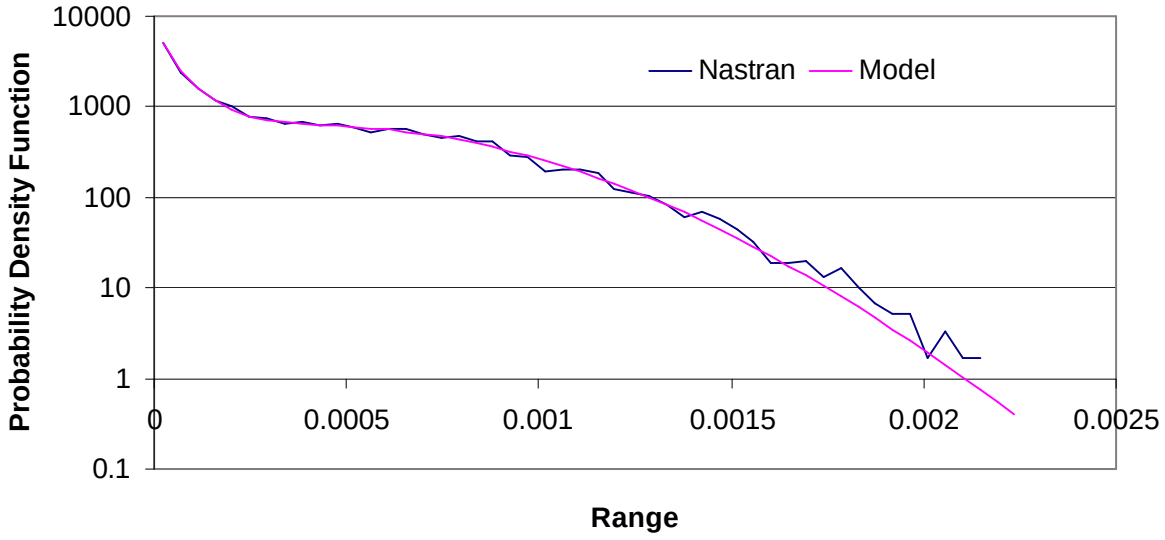

Figure 65. Comparison of Probability Density Functions of Stress Ranges, Finite Element Data, Unbuckled *double thickness* Panel, Zero Incidence, Center Point, *s* = 0, *SPL* =140 dB.

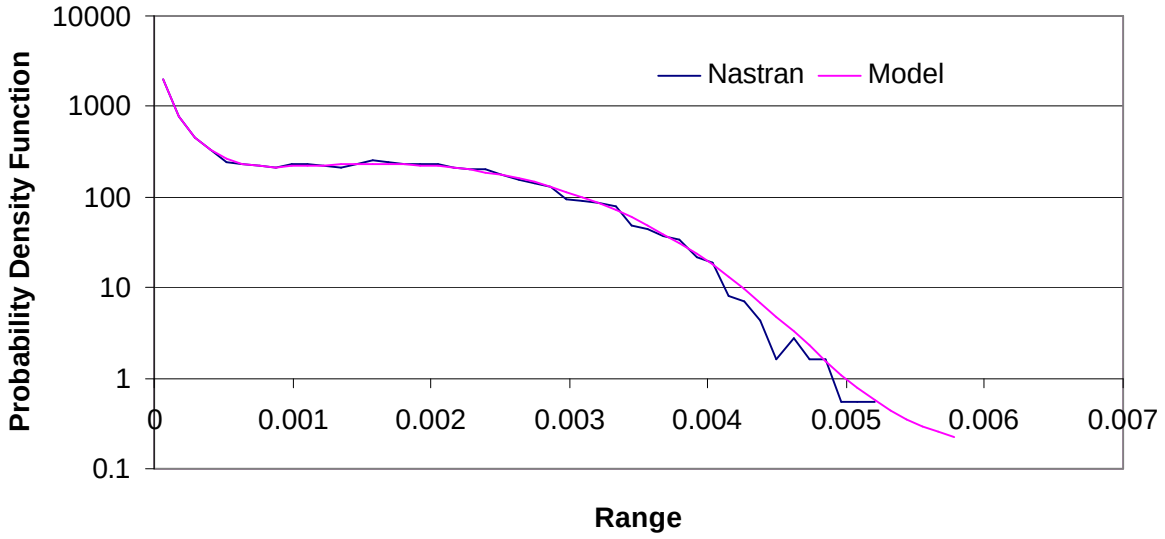

Figure 66. Comparison of Probability Density Functions of Stress Ranges, Finite Element Data, Unbuckled *double thickness* Panel, Zero Incidence, Center Point, *s* = 0, *SPL* =150 dB.

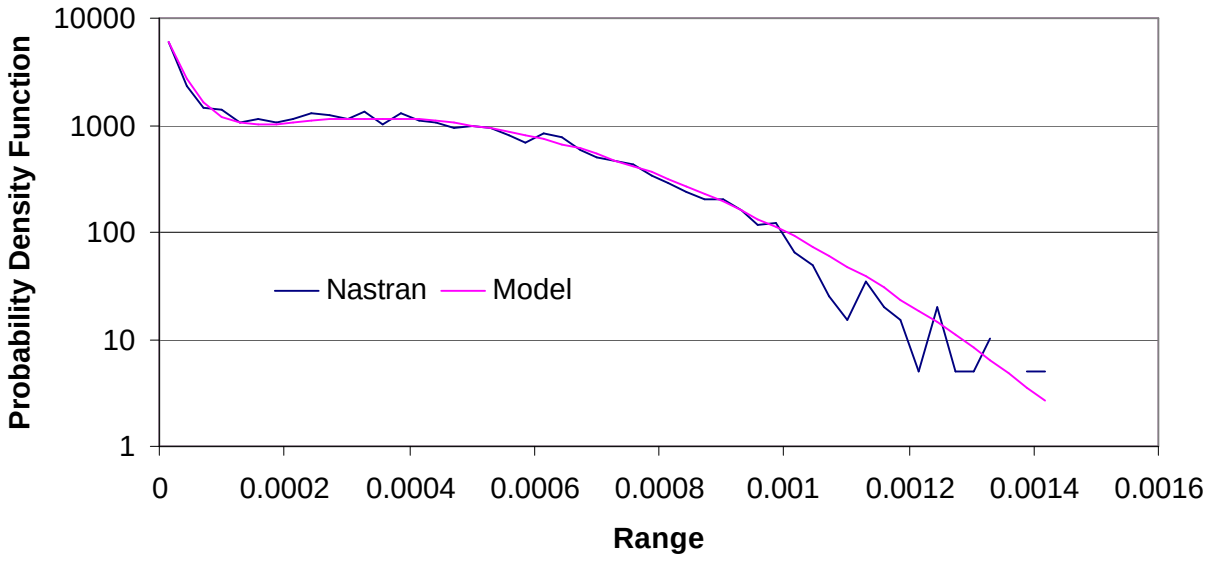

Figure 67. Comparison of Probability Density Functions of Stress Ranges, Finite Element Data, Unbuckled *square* Panel, Zero Incidence, Center Point, *s* = 0, *SPL* =130 dB.

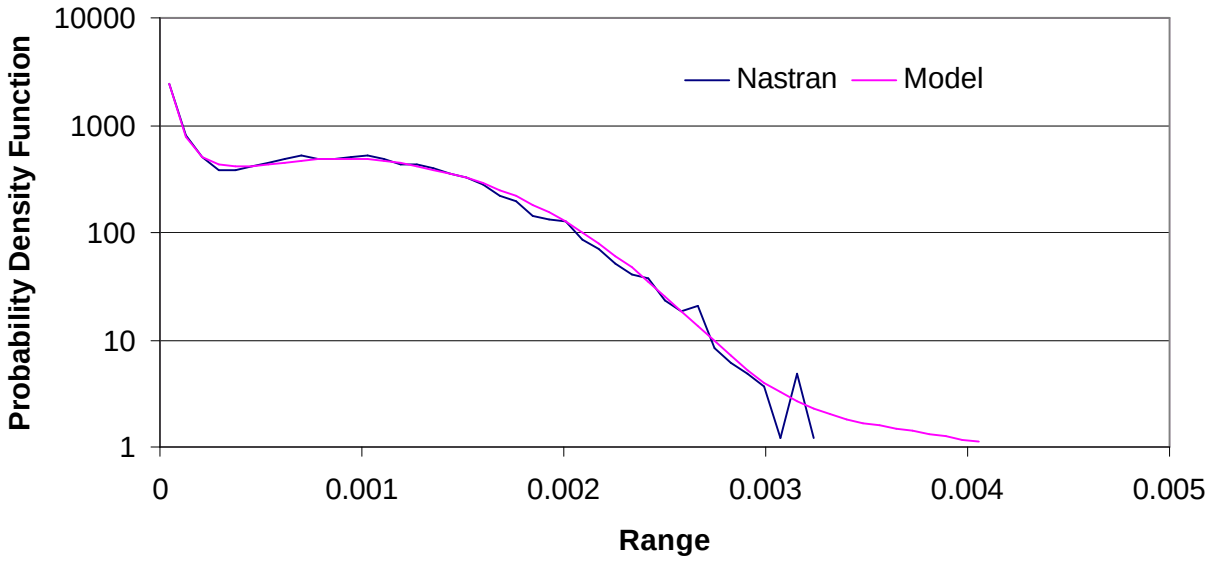

Figure 68. Comparison of Probability Density Functions of Stress Ranges, Finite Element Data, Unbuckled *square* Panel, Zero Incidence, Center Point, *s* = 0, *SPL* =140 dB.

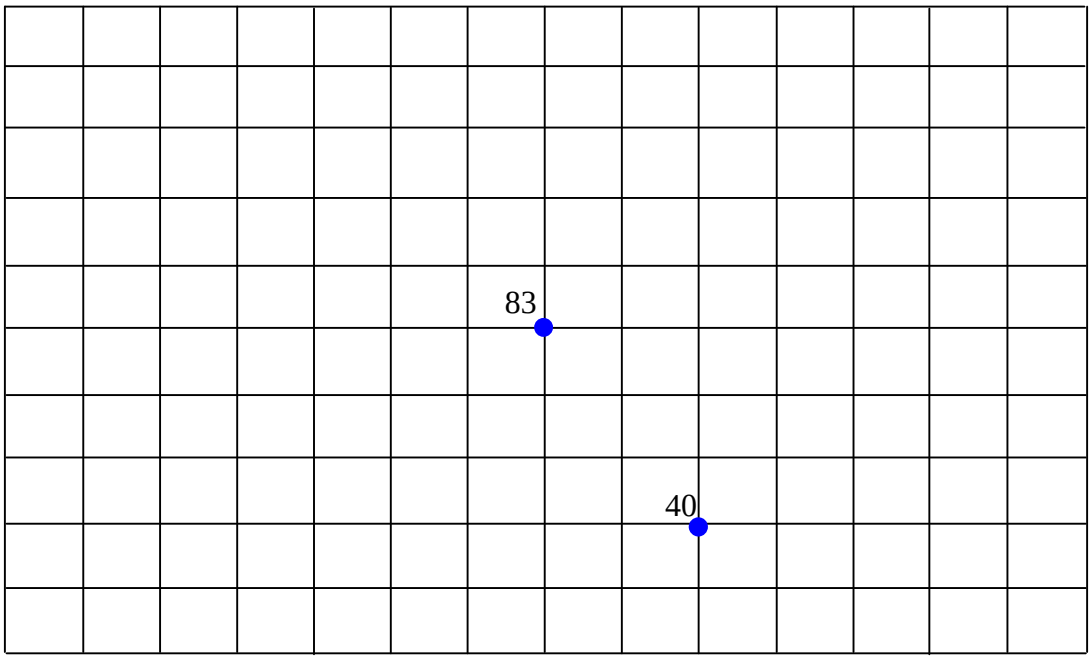

Figure 69. Finite Element Mesh of the Original Panel (Panel 1) Showing the Center Point (83) and the Off-Center Node (40).

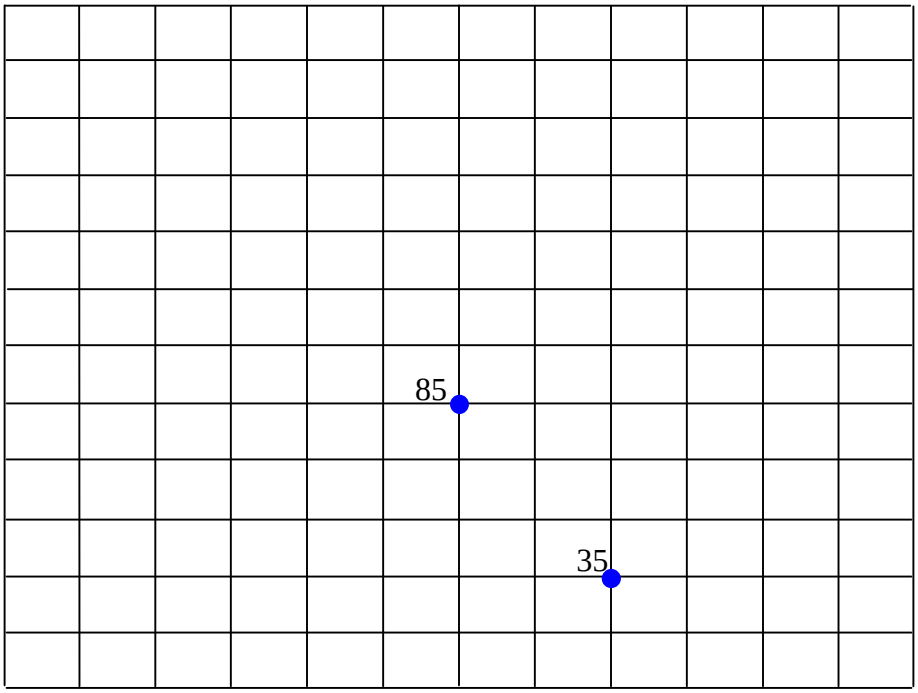

Figure 70. Finite Element Mesh of the Square Panel (Panel 3) Showing the Center Point (85) and the Off-Center Node (35).

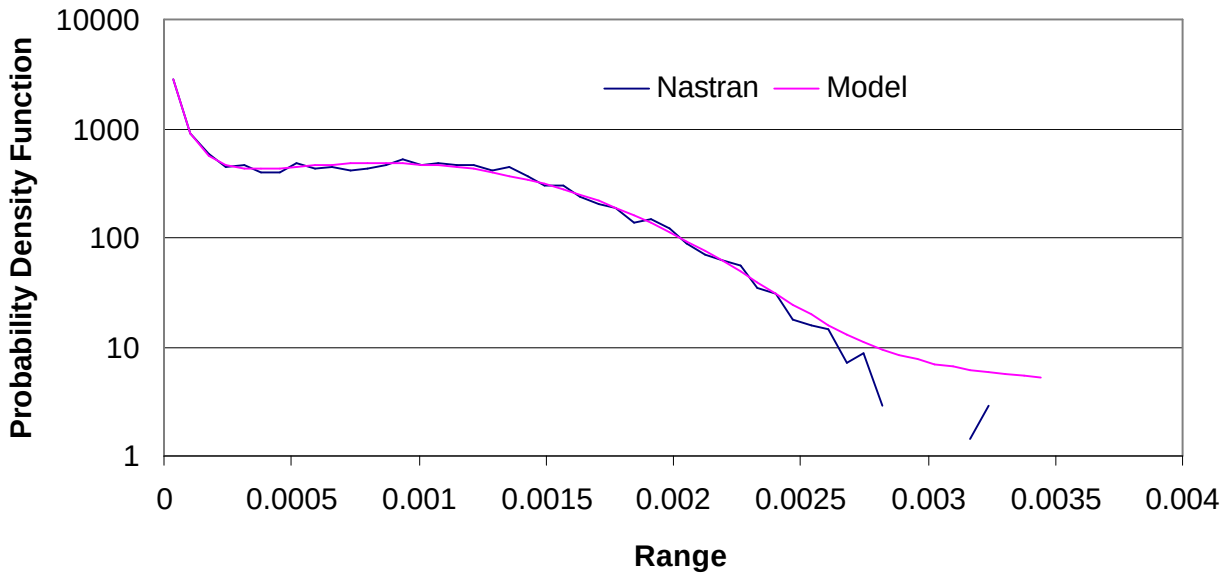

Figure 71. Comparison of Probability Density Functions of Stress Ranges, Finite Element Data, Unbuckled *original* Panel, Zero Incidence, Non-Center Point (#40), *s* = 0, *SPL* =140 dB.

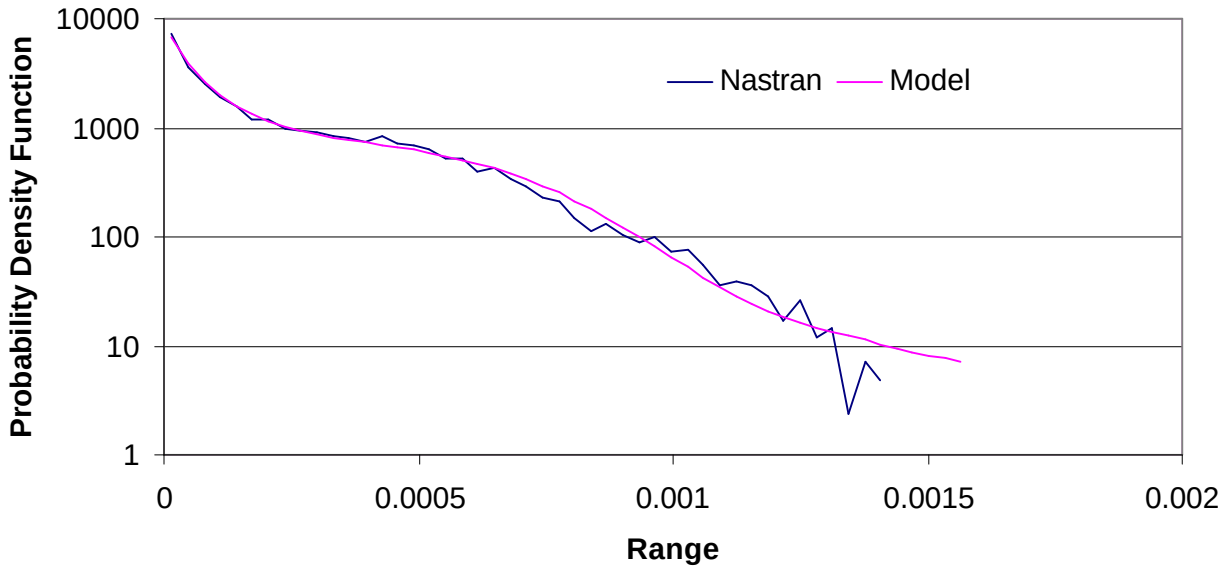

Figure 72. Comparison of Probability Density Functions of Stress Ranges, Finite Element Data, Unbuckled *double thickness* Panel, Zero Incidence, Non-Center Point (#40), *s* = 0, *SPL* = 140 dB.

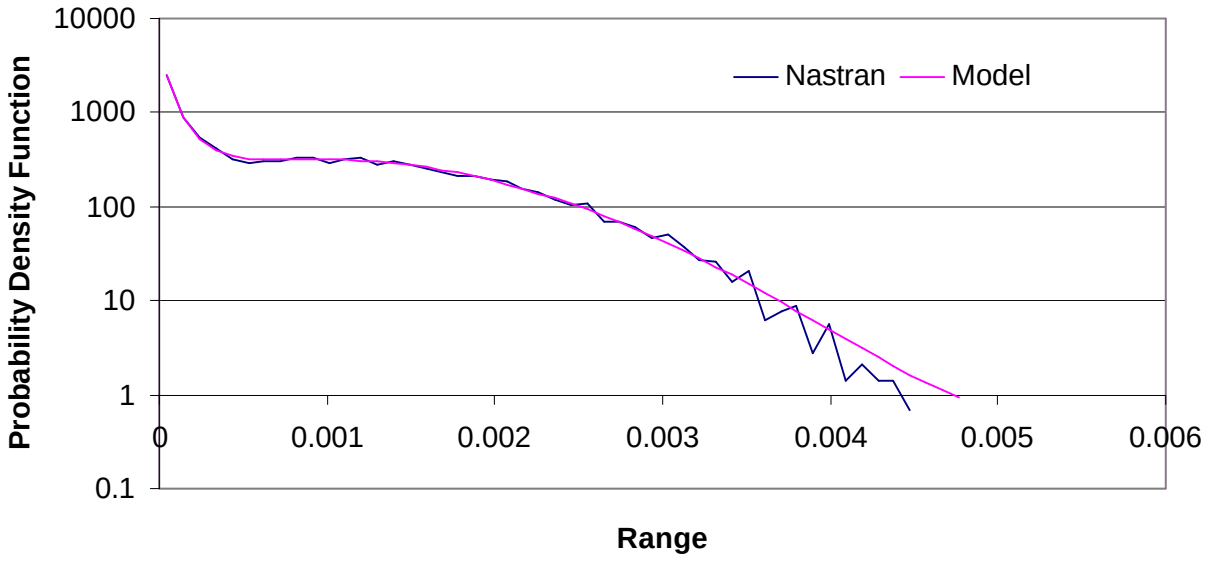

Figure 73. Comparison of Probability Density Functions of Stress Ranges, Finite Element Data, Unbuckled *double thickness* Panel, Zero Incidence, Non-Center Point (#40), s = 0, *SPL* = 150 dB.

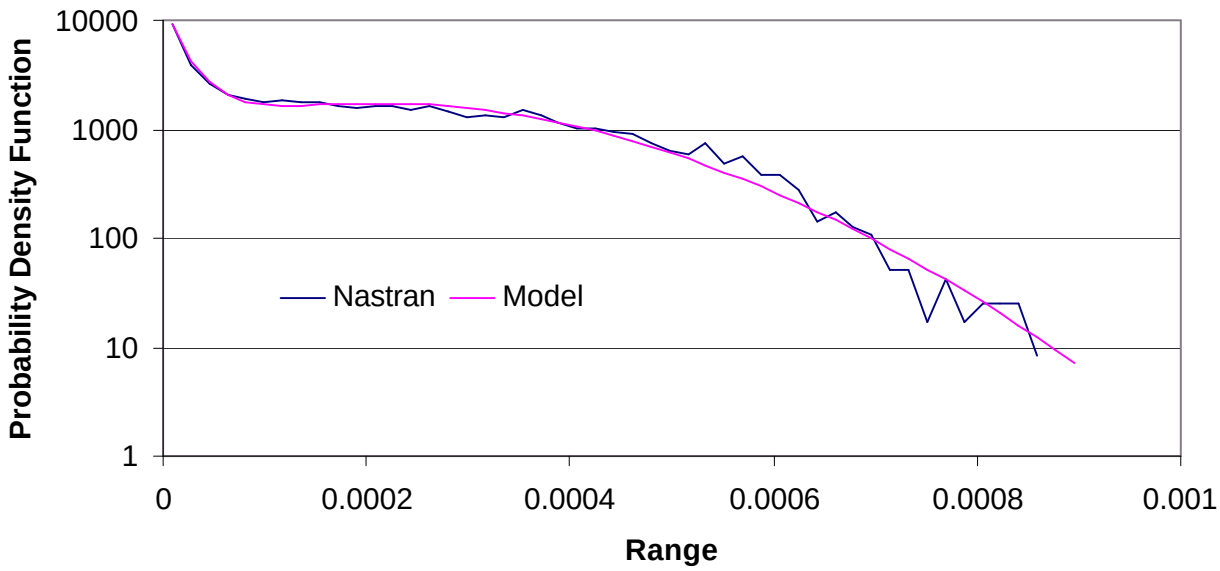

Figure 74. Comparison of Probability Density Functions of Stress Ranges, Finite Element Data, Unbuckled *square* Panel, Zero Incidence, Non-Center Point (#35), s = 0, *SPL* =130 dB.

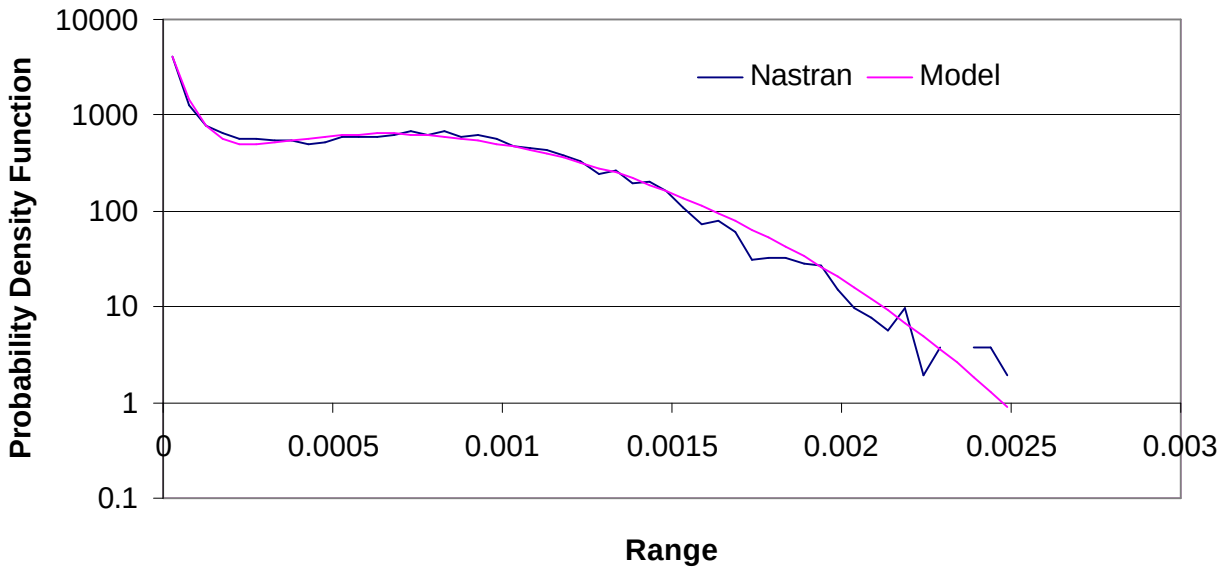

Figure 75. Comparison of Probability Density Functions of Stress Ranges, Finite Element Data, Unbuckled *square* Panel, Zero Incidence, Non-Center Point (#35), s = 0, *SPL* =140 dB.

4.0 SPECTRAL ESTIMATION

The results presented above provide a good assessment of the model of Eq. (5), (9)-(11), and (15) and motivate the formulation of an estimation technique of the parameters a, b, α, β, and B' that does not involve the fitting of simulation data. The characteristic of the response process that relates naturally to the fatigue life is the spectrum as both spectrum and damage are associated with the cycling aspects of the process. Accordingly, it was desired to establish a formal connection between the parameters a, b, α, β, and B' and the response spectrum, more specifically with the response spectral moments λ_p defined as

$$\lambda_p = \int_{-\infty}^{\infty} |\omega|^p \, S_{XX}(\omega)\, d\omega \tag{16}$$

where $S_{XX}(\omega)$ is the power spectral density of the specific stress or displacement the ranges of which are being modeled. The estimation of the spectral moments requires first the determination of the spectrum $S_{XX}(\omega)$.

Two classes of approaches are available to achieve this first task: nonparametric methods and parametric techniques. In nonparametric methods, typically FFT based techniques (e.g. Welch periodogram), the spectrum is evaluated at a series of discrete points, one point at a time and independently of the other points. Parametric approaches, e.g. autoregressive (AR) and autoregressive moving average (ARMA) methods, are based on the modeling of the process considered, most often as the response to white noise input of a linear system, by fine tuning a set of parameters (see Marple, 1987). The spectrum is then obtained from the model of the process.

Since nonparametric methods do not assume a specific connection between values of the spectrum at different points, they are particularly well suited when the spectrum does not exhibit "continuous" features, e.g. is zero in most of the domain and nonzero in only a few disjoint intervals. The major drawback of nonparametric techniques is the large number of samples needed to obtain a fairly smooth estimate of the spectrum.

This drawback of nonparametric methods is in fact the advantage of parametric techniques. Since parameters are first obtained and the estimate of the spectrum is derived from the specified model, it is generally smooth. Further, since there are typically much fewer model parameters to estimate than points at which the spectrum is desired, parametric methods generally require much fewer samples than nonparametric techniques for an accurate estimation. Parametric methods are particularly effective when the model they are based on is a natural basis for the process considered. In this regard, note that autoregressive models have been shown (e.g. Gersch and Yonemoto, 1977) under weak conditions to exactly represent the sampled response of multi-degree-of-freedom systems subjected to white noise. Accordingly, autoregressive (AR) models are a natural basis for the estimation of spectra of the response of vibrating systems.

An autoregressive (AR) process is defined through the recurrence relation (see Marple, 1987)

$$p_n = b_0\ w_n - a_1\ p_{n-1} - a_2\ p_{n-2} \ldots - a_m\ p_{n-m} \tag{17}$$

where $p_n = p(n\ \Delta t)$, n = 1, 2, 3... are the obtained sampled values of the response (AR) process considered, w_n are independent Gaussian random numbers forming a discrete white noise

process, and a_1, a_2, ..., a_m, b_0 are AR model coefficients. In an AR spectral estimation, the parameters of the AR model are first determined from available data, e.g. time histories of the process considered, and then the spectrum of the process considered is approximated by the AR spectrum.

Given the AR model order *m*, the determination of a_1, a_2, ..., a_m, b_0 is usually accomplished through a well defined linear system of equations (see Marple, 1987) so that only the order must carefully be selected. As *m* is increased, the spectral features of the process are better and better represented in the AR spectrum, as can be expected since every non-predictable stationary Gaussian process can be modeled as an AR model of infinite order. When considering finite data sets however, it is generally found that increasing the order past a certain threshold produces only marginal improvements in the spectrum modeling but may lead to the appearance of small fictitious peaks, peak splitting, etc. The selection of the AR order was achieved here in concert with the estimated spectral moments which are the quantities of primary interest. Specifically, the AR order model was selected as the smallest value for which the spectral moments of Eq. (16) with $p \in [0,3]$ were found to converge to their asymptotic values.

In the present context, generating a large number of samples for the single mode model requires only a small CPU time, i.e. of the order of minutes to an hour. A large number of samples are also available for the experimental data. For the MSC.Nastran data however, a large CPU time (up to 30 hours) is already required to obtain as few as 30,000 samples. Accordingly, it is very desirable to use parametric methods for the estimation of the spectrum of the response processes, especially for the MSC.Nastran cases. Given its natural basis, the autoregressive (AR) modeling

technique will be used here but a validation of its accuracy is nevertheless desirable. To this end, the spectra of the single mode displacement time histories and the experimental strain data were first obtained by the Welch periodogram method (nonparametric approach), see Fig. 76-78. Next, the AR modeling of this data was accomplished as described above by monitoring the convergence of the spectral moments λ_1 and λ_2 as a function of the AR order *m* for the 152 dB excitation case, see Fig. 79. Clearly, a good convergence is obtained for both moments. The comparison between AR and Welch power spectral densities shown in Fig. 80 confirms the reliability of the AR modeling approach to spectral estimation and warrants its use in connection with the MSC.Nastran data, see Fig. 81-90.

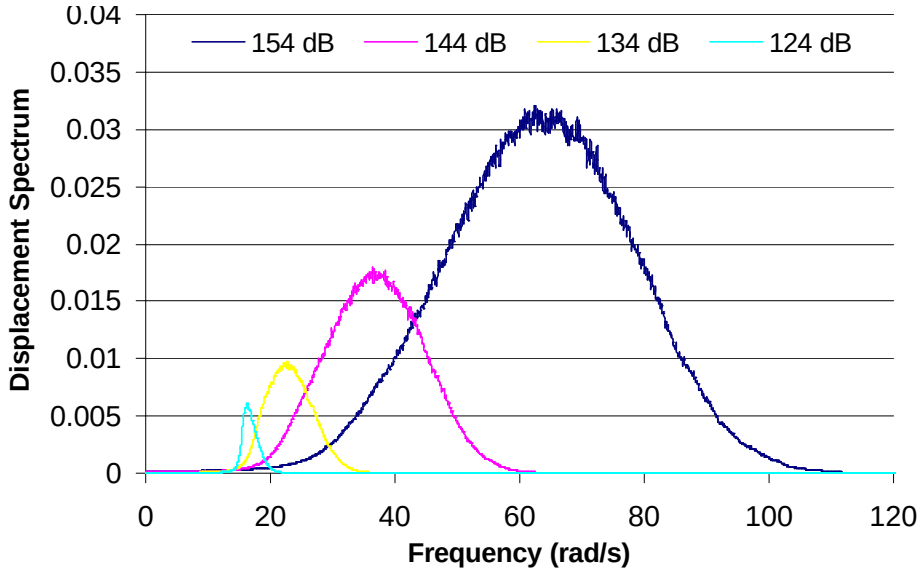

Figure 76. Power Spectral Density of the Displacement Process for Different *SPL*, One-Mode Model, Unbuckled Panel, *s* = 0, Nonparametric Estimation.

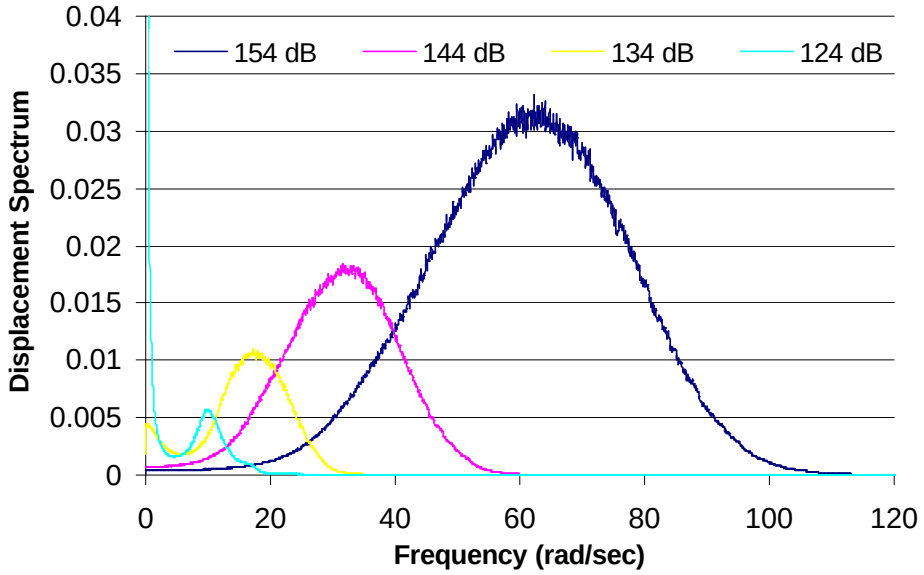

Figure 77. Power Spectral Density of the Displacement Process for Different *SPL*, One-Mode Model, Unbuckled Panel, *s* = 1.8, Nonparametric Estimation.

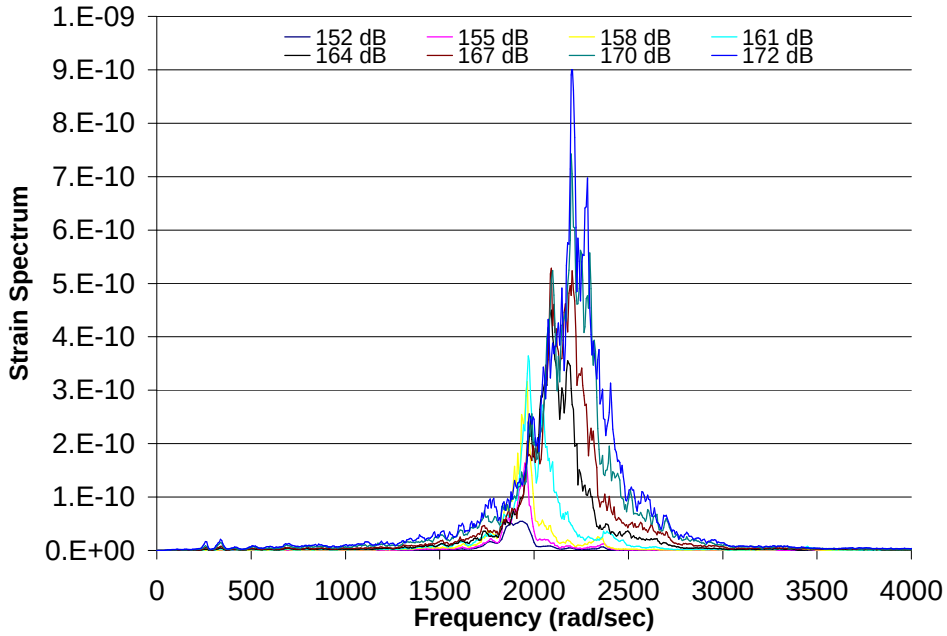

Figure 78. Power Spectral Density of the Strain Process for Different *SPL*, Experimental Data, Unbuckled Panel, *s* = 0, Nonparametric Estimation.

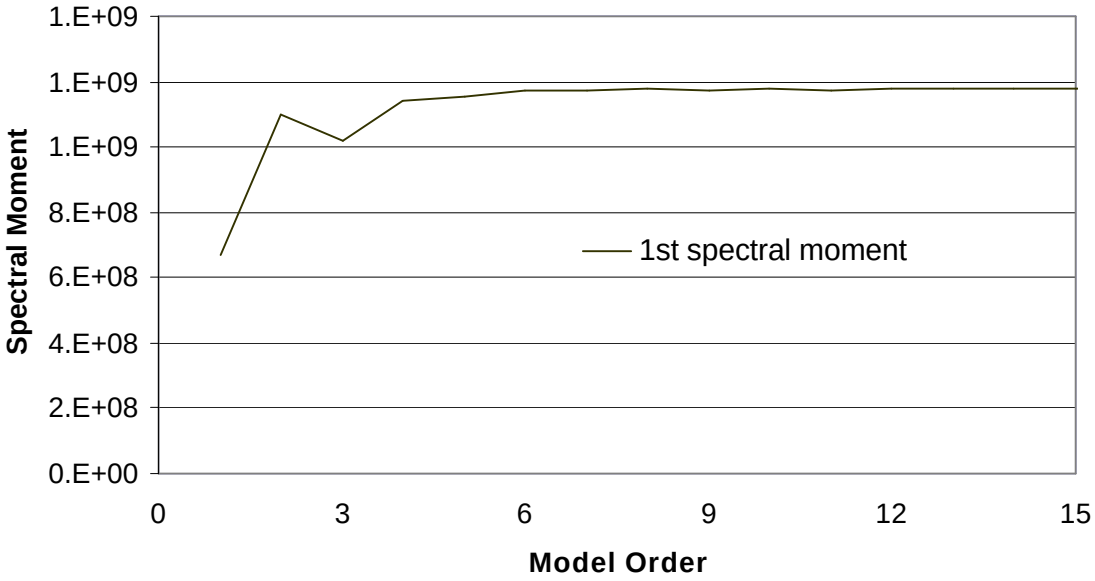

(a) 1st Spectral Moment

(b) 2nd Spectral Moment

Figure 79. Convergence of the Spectral Moments λ_1 and λ_2 as a Function of the AR Model Order, Experimental Data, *SPL* = 152 dB.

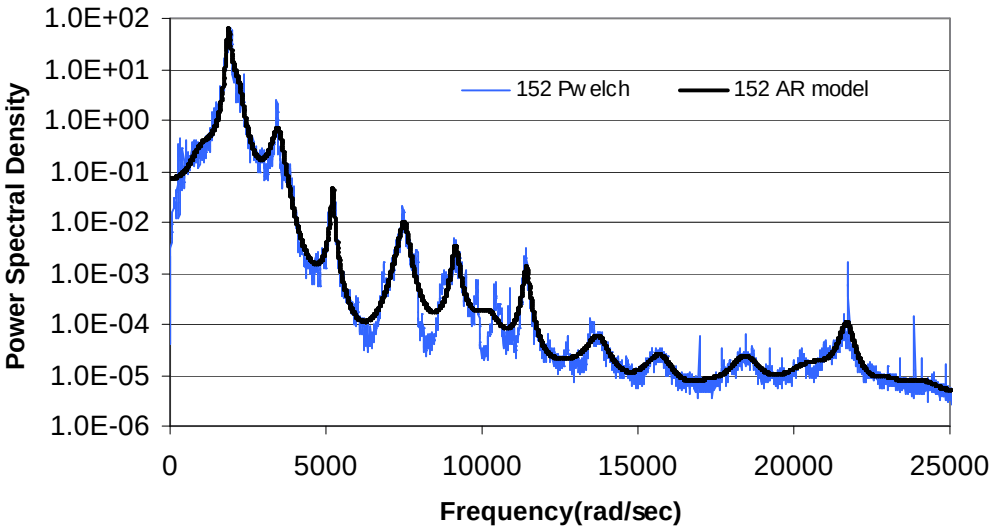

(a) *SPL*= 152 dB

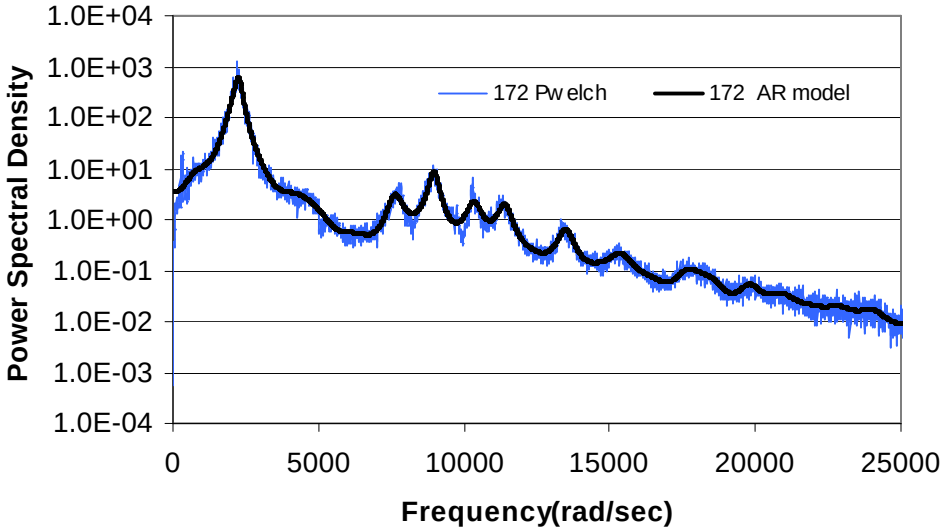

(b) *SPL* = 172 dB

Figure 80. Comparison of Welch and AR Estimates of the Power Spectral Density, Experimental Data, AR Model Order = 50, (a) *SPL*= 152 dB, (b) *SPL* = 172 dB.

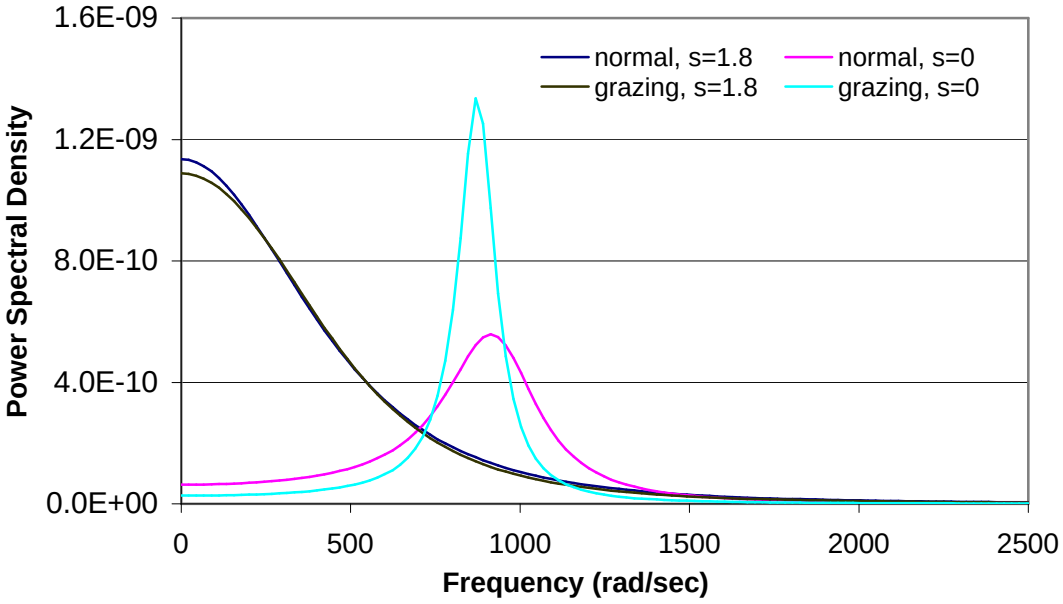

Figure 81. Power Spectral Density of Displacement, Finite Element Data, Original Panel, Center Point, *SPL* = 110 dB.

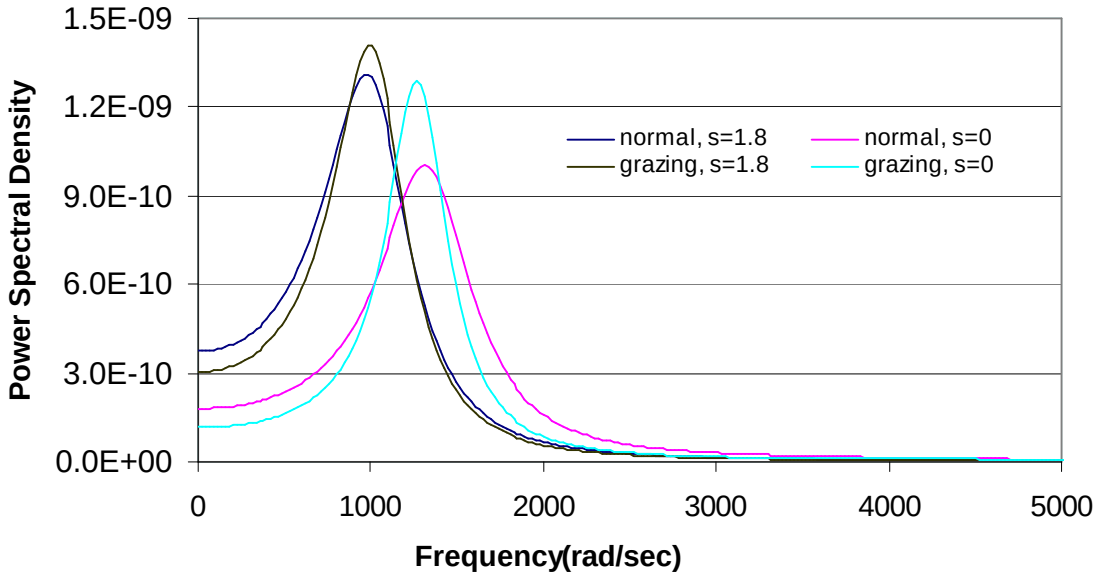

Figure 82. Power Spectral Density of Displacement, Finite Element Data, Original Panel, Center Point, *SPL* = 120 dB.

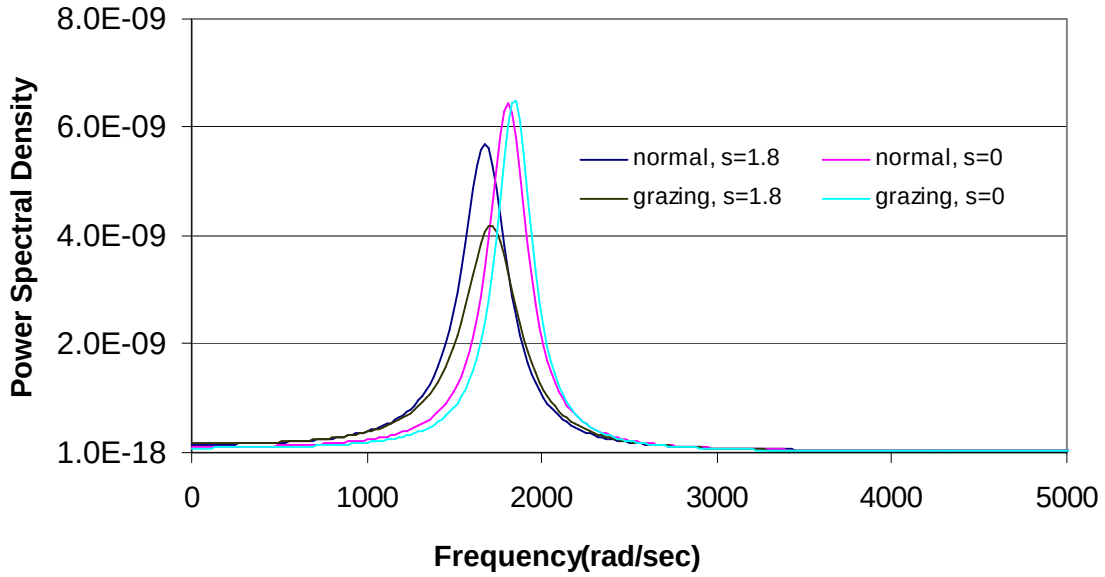

Figure 83. Power Spectral Density of Displacement, Finite Element Data, Original Panel, Center Point, *SPL* = 130 dB.

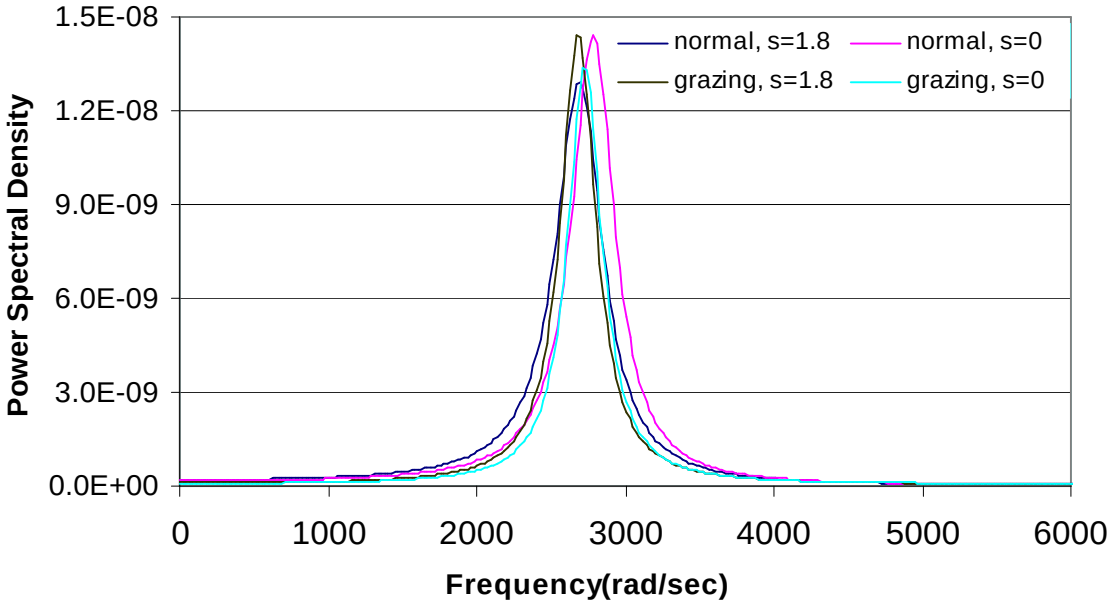

Figure 84. Power Spectral Density of Displacement, Finite Element Data, Original Panel, Center Point, *SPL* = 140 dB.

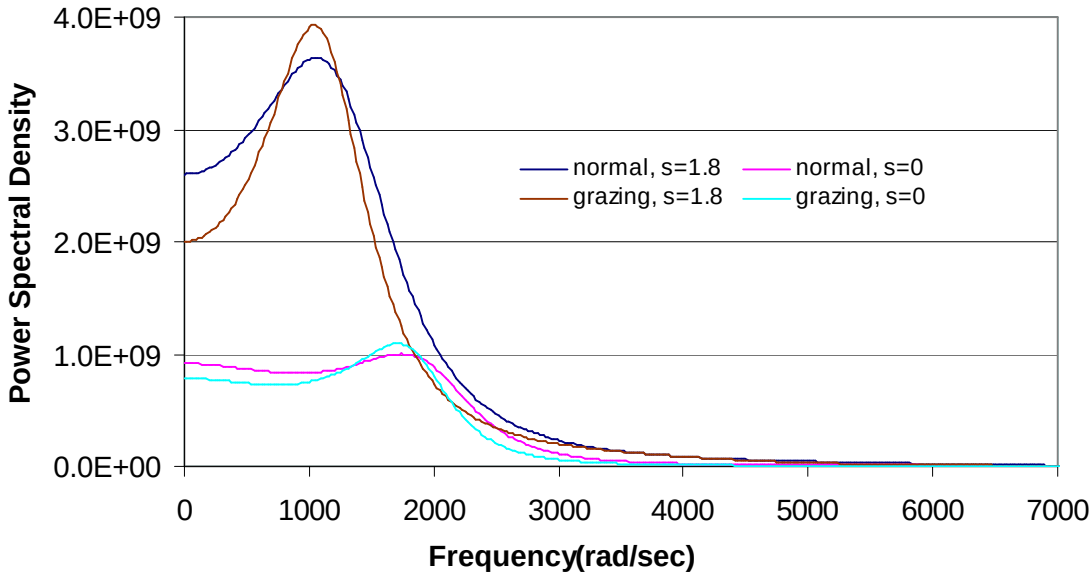

Figure 85. Power Spectral Density of Stress, Finite Element Data, Original Panel, Center Point, *SPL* = 110 dB.

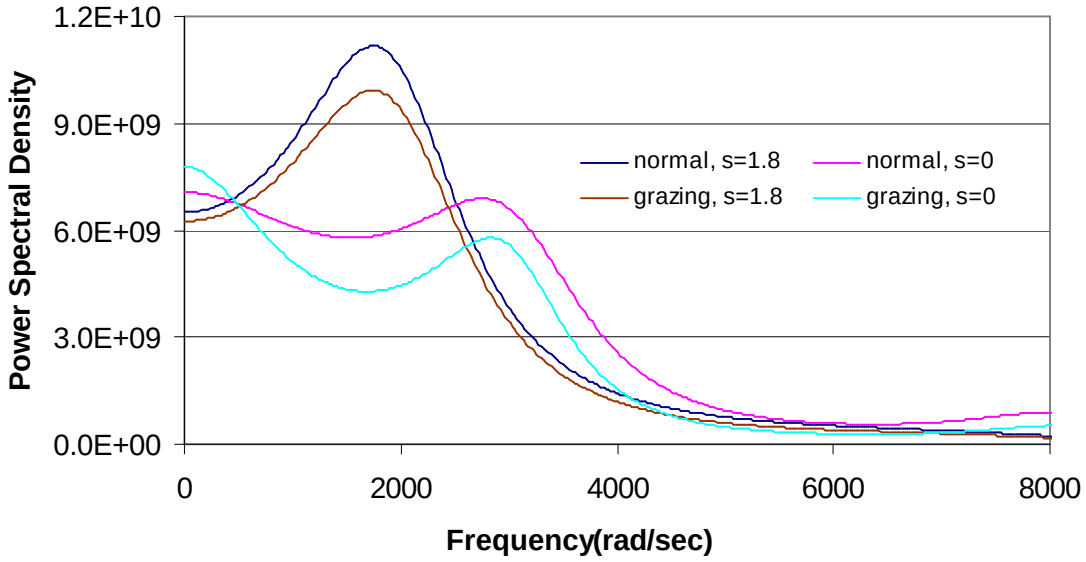

Figure 86. Power Spectral Density of Stress, Finite Element Data, Original Panel, Center Point, *SPL* = 120 dB.

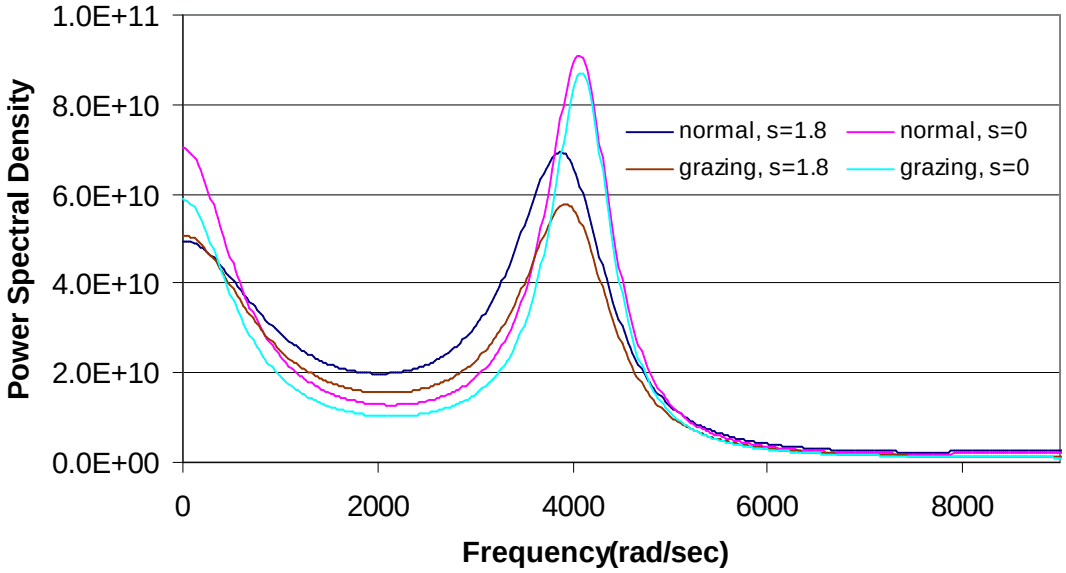

Figure 87. Power Spectral Density of Stress, Finite Element Data, Original Panel, Center Point, *SPL* = 130 dB.

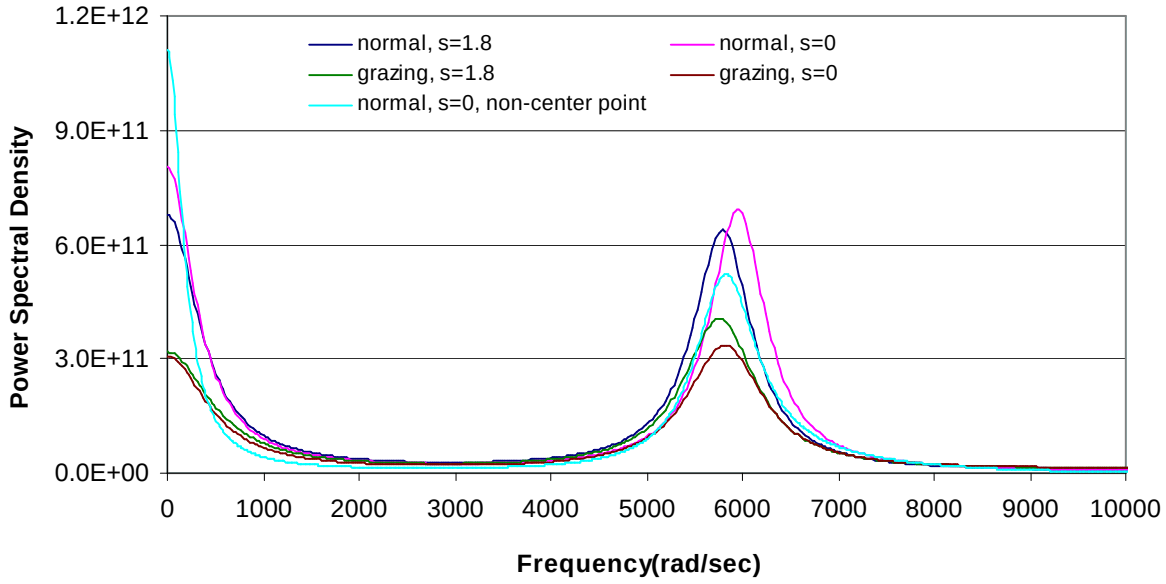

Figure 88. Power Spectral Density of Stress, Finite Element Data, Original Panel, Center Point, *SPL* = 140 dB.

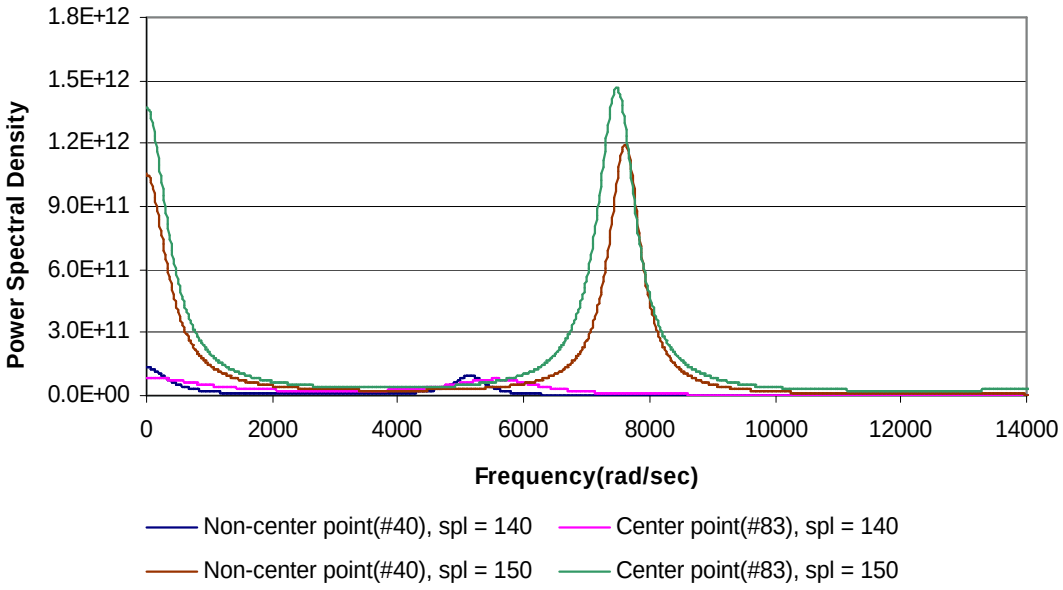

Figure 89. Power Spectral Density of Stress, Finite Element Data, Unbuckled *double thickness* Panel.

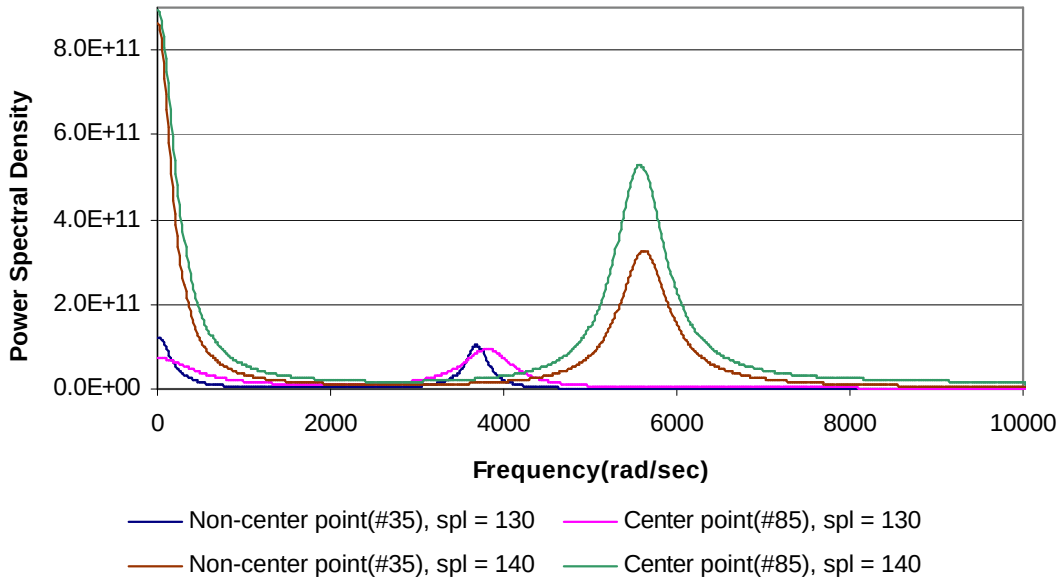

Figure 90. Power Spectral Density of Stress, Finite Element Data, Unbuckled *square* Panel.

5.0 RANGE MODEL PARAMETERS VS. SPECTRAL MOMENTS

The ensemble of results presented above allows one now to seek a relationship between the parameters of the proposed model of the probability density function of the stress ranges and the spectral moments of the stress process. To obtain the most useful correlation between the parameters *a*, *b*, α, β, B' and the spectral moments λ_p, a nondimensionalization of the model for the probability density function of the ranges, i.e.

$$p_R(r) = B\left\{B' \exp\left(-\alpha r^{\beta}\right) + \left(\frac{b}{2} r + \frac{a}{8} r^3\right) \exp\left[-\left(\frac{b}{8} r^2 + \frac{a}{64} r^4\right)\right]\right\} \tag{18}$$

was first performed. To this end, the ranges were scaled with respect to the standard deviation of the corresponding response, i.e. $\sqrt{\lambda_0}$ per Eq. (16). This process yielded the dimensionless parameters

$$\bar{a} = a\,\lambda_0^2 \qquad \bar{b} = b\lambda_0 \qquad \overline{B'} = B'\sqrt{\lambda_0} \qquad \bar{\alpha} = \alpha\,\lambda_0^{\beta/2} \tag{19}$$

Finally, the dimensionless spectral moments α_p were introduced as

$$\alpha_p = \frac{\lambda_p}{\sqrt{\lambda_0\,\lambda_{2p}}}. \tag{20}$$

Shown in Fig. 91-96 are the parameters $\bar{a}$, $\bar{b}$, *B*, $\overline{B'}$, $\bar{\alpha}$, and β corresponding to the stress range model as functions of the parameters α_p, for p =0.5. Note that similar plots could be obtained with other values of $p \in [0, 1.5]$. These results indicate that there exists a definite correlation between the spectral moments λ_p and the parameters of the model of Eq. (19), at least $\bar{a}$, $\bar{b}$, and *B*. Although, even for these parameters, a definite scatter can be observed which suggests that another stress process characteristic must be considered in the modeling effort. To this end,

note that the stresses do exhibit mean values and that these quantities are independent of the spectrum and spectral moment which are obtained by substracting it first. Shown in Fig. 97-102 are the parameters $\bar{a}$, $\bar{b}$, B, $\overline{B'}$, $\bar{\alpha}$, and β plotted vs. the mean value of the stress process.

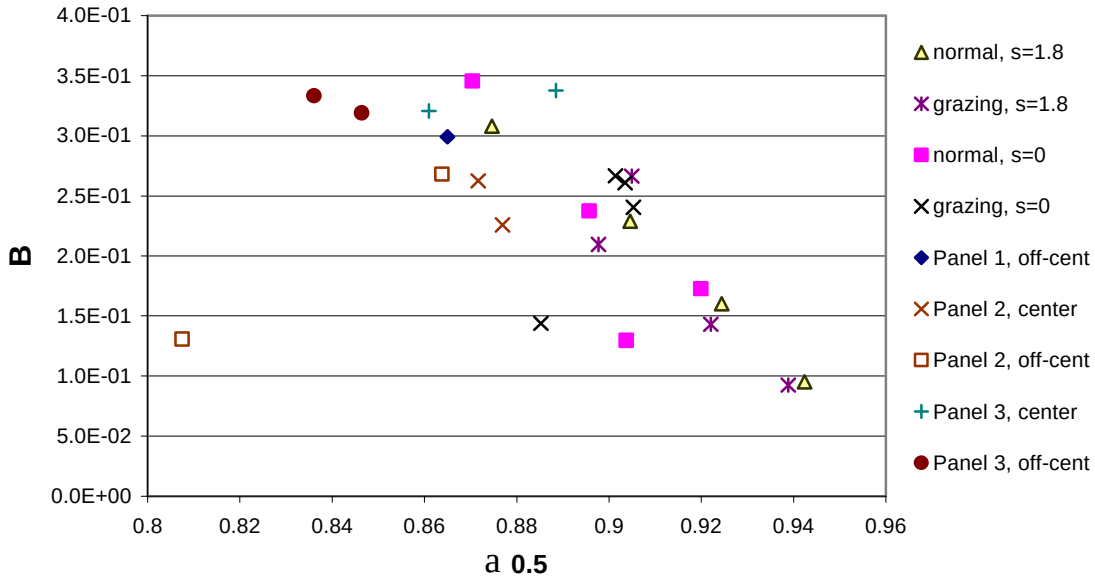

Figure 91. Dimensionless Coefficient *B* as a Function of $\alpha_{0.5}$, All Stress Data.

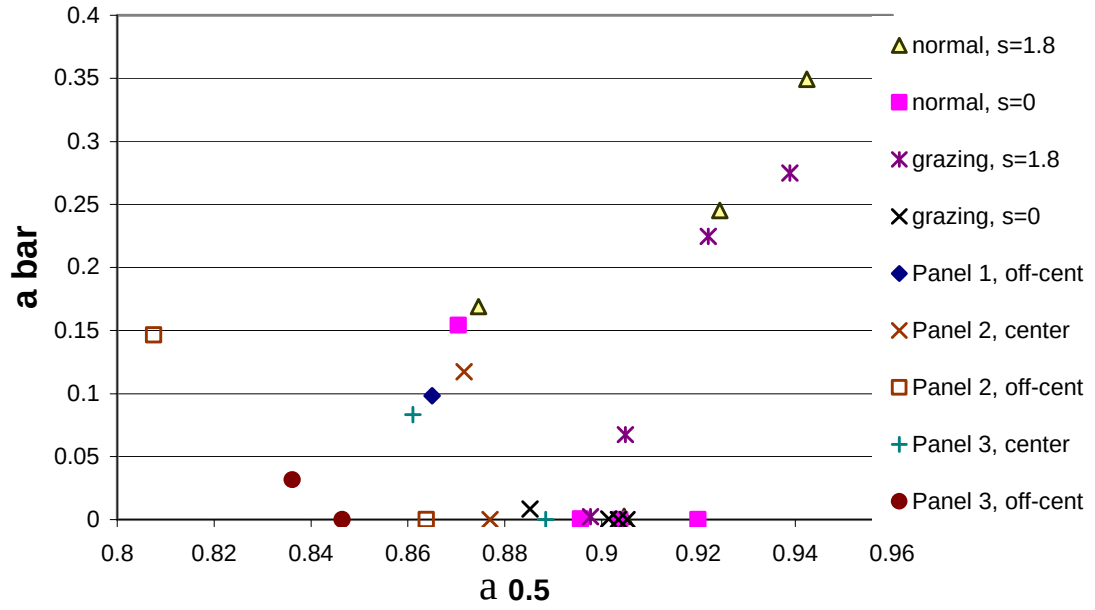

Figure 92. Dimensionless Coefficient $\bar{a}$ as a Function of $\alpha_{0.5}$, All Stress Data.

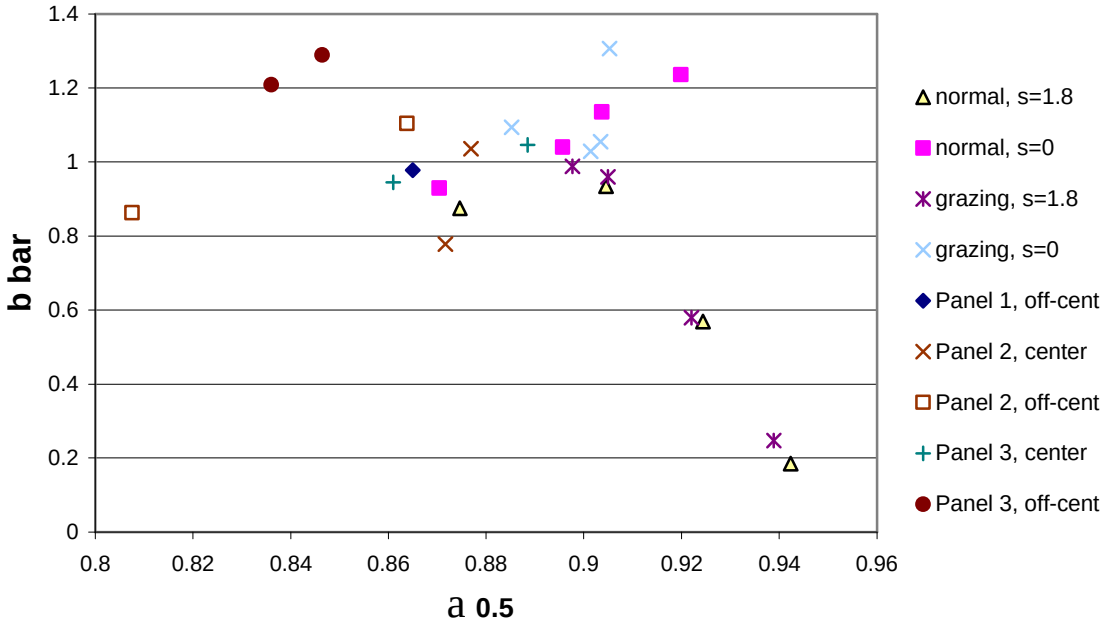

Figure 93. Dimensionless Coefficient $\bar{b}$ as a Function of $\alpha_{0.5}$, All Stress Data.

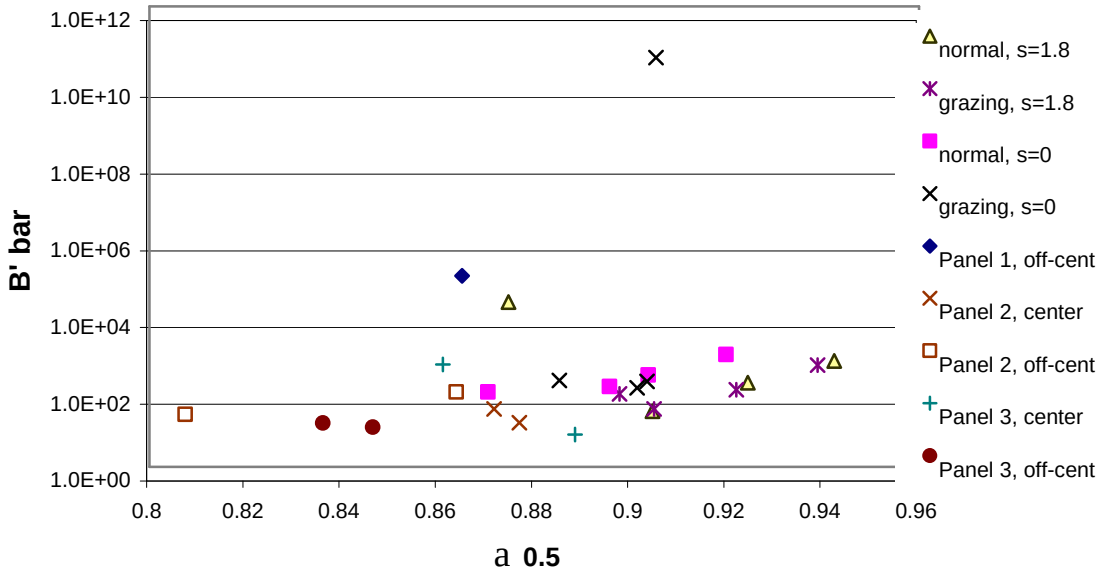

Figure 94. Dimensionless Coefficient $\overline{B'}$ as a Function of $\alpha_{0.5}$, All Stress Data.

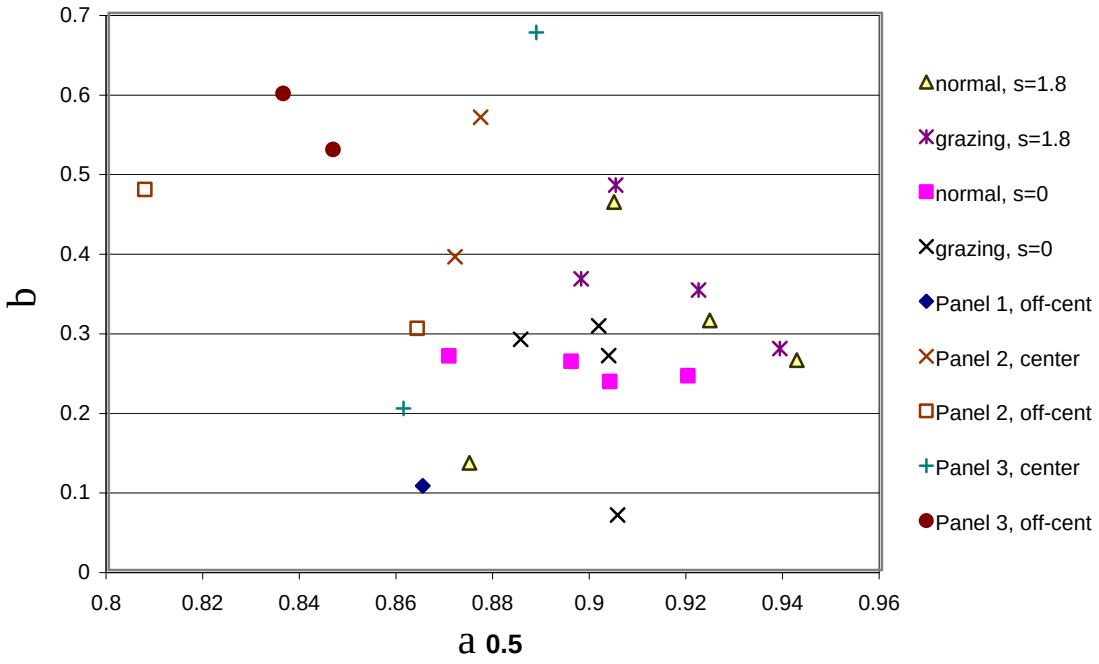

Figure 95. Dimensionless Coefficient β as a Function of $\alpha_{0.5}$, All Stress Data.

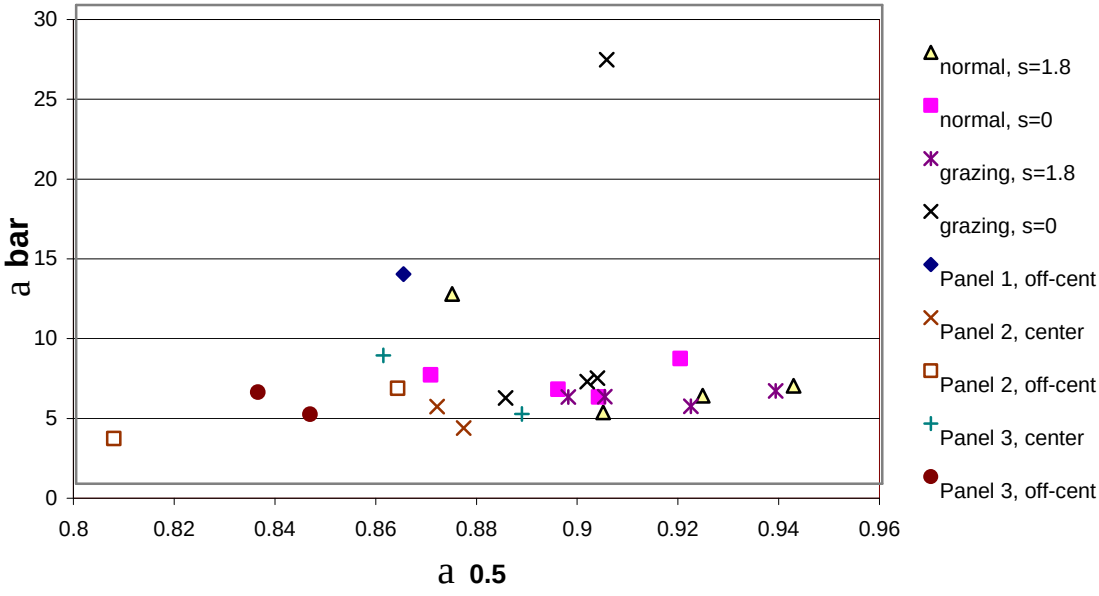

Figure 96. Dimensionless Coefficient $\bar{\alpha}$ as a Function of $\alpha_{0.5}$, All Stress Data.

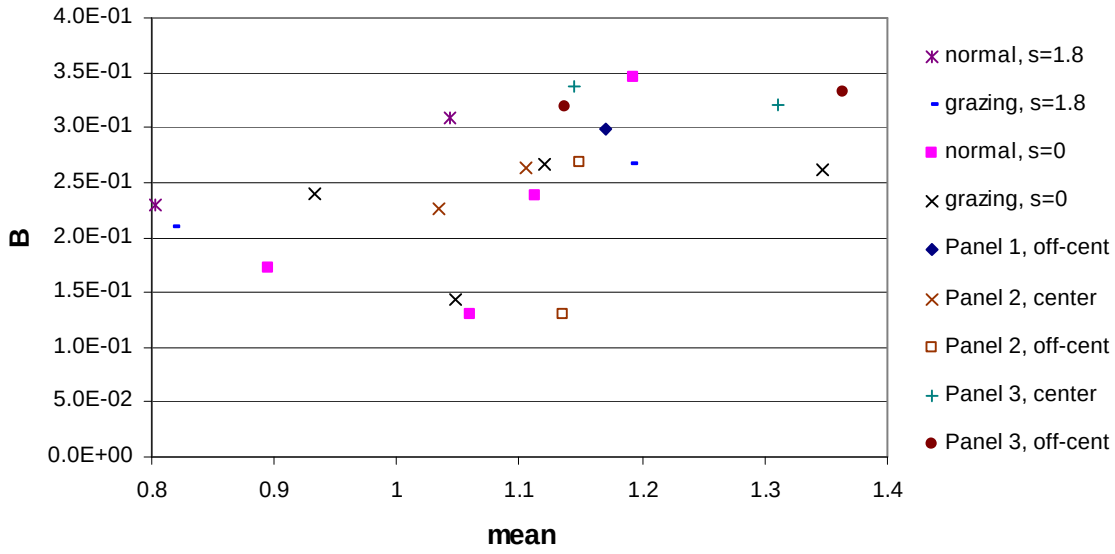

Figure 97. Dimensionless Coefficient *B* as a Function of the Mean Value, All Stress Data.

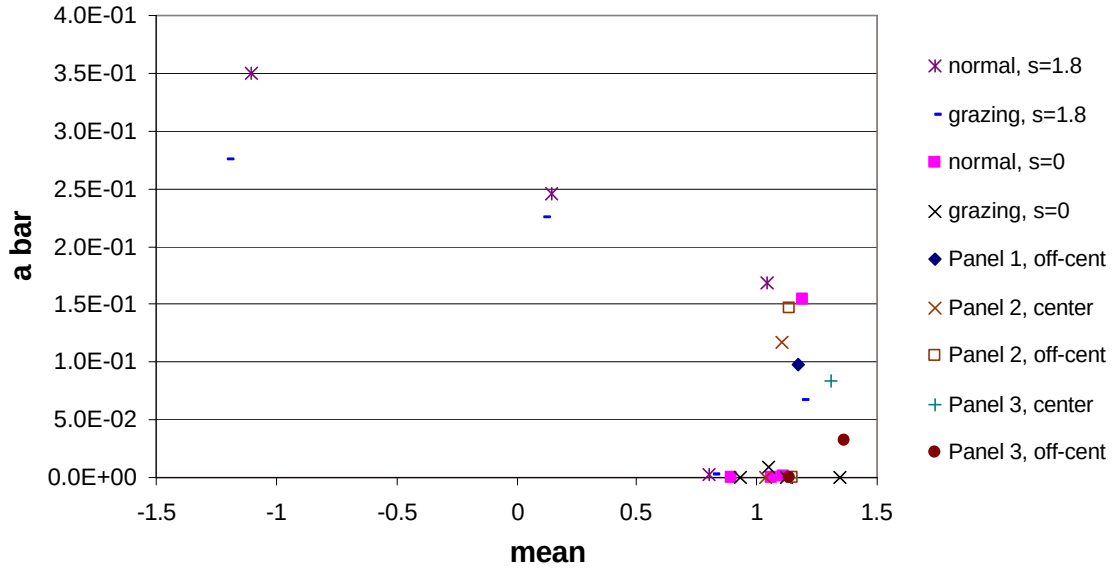

Figure 98. Dimensionless Coefficient $\bar{a}$ as a Function of the Mean Value, All Stress Data.

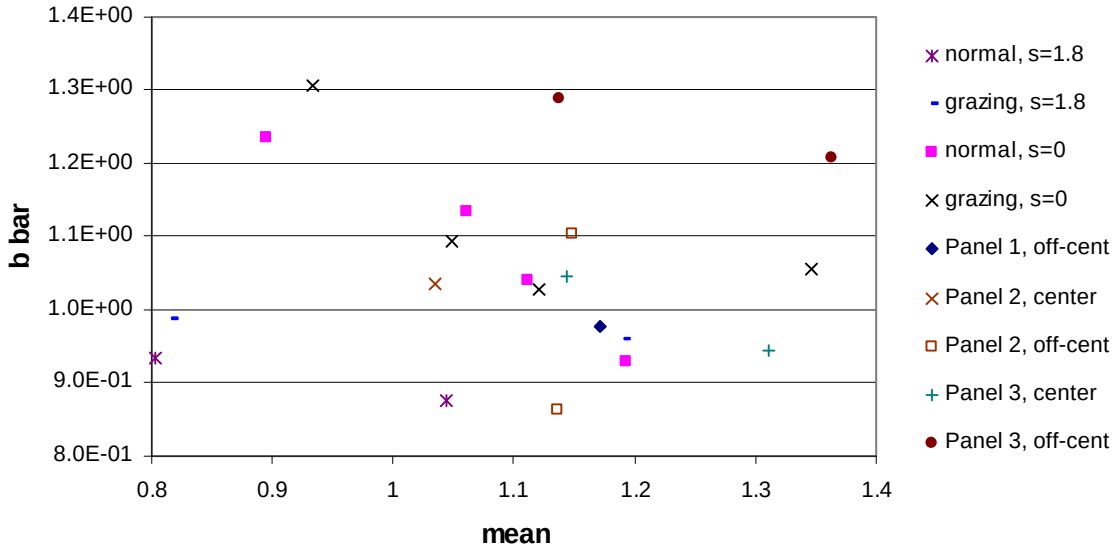

Figure 99. Dimensionless Coefficient $\bar{b}$ as a Function of the Mean Value, All Stress Data.

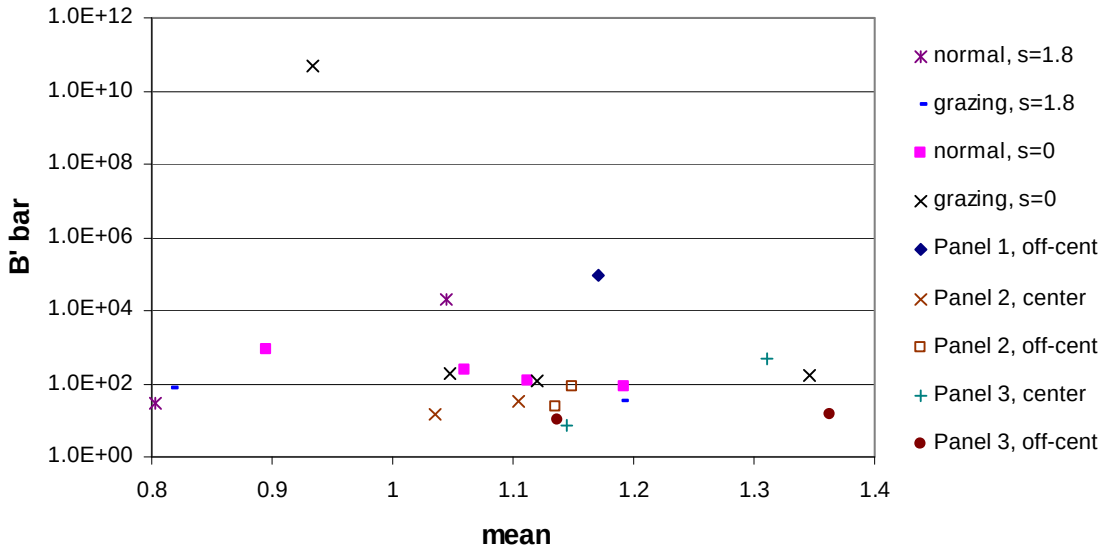

Figure 100. Dimensionless Coefficient $\overline{B'}$ as a Function of the Mean Value, All Stress Data.

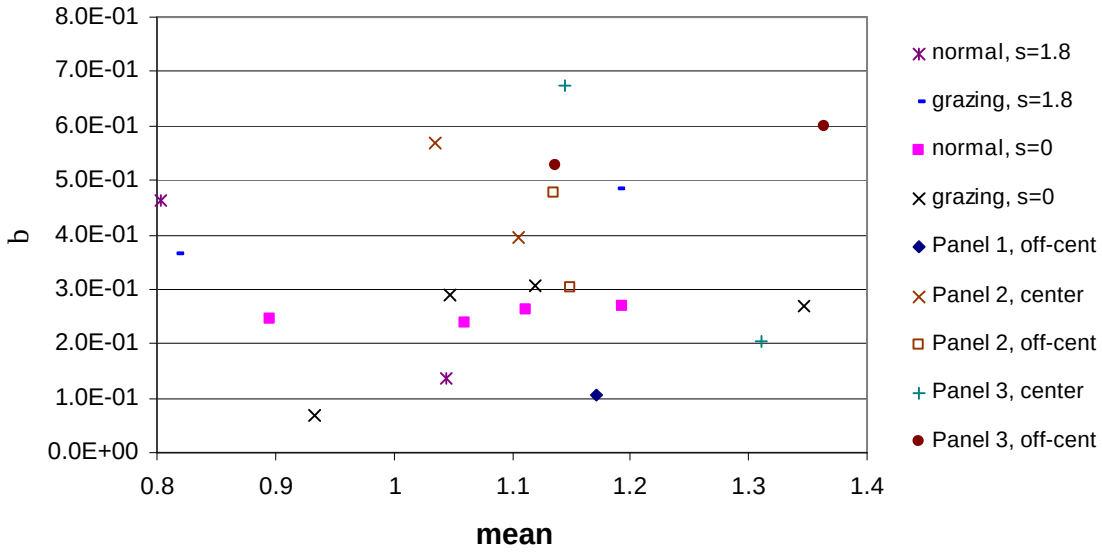

Figure 101. Dimensionless Coefficient β as a Function of the Mean Value, All Stress Data.

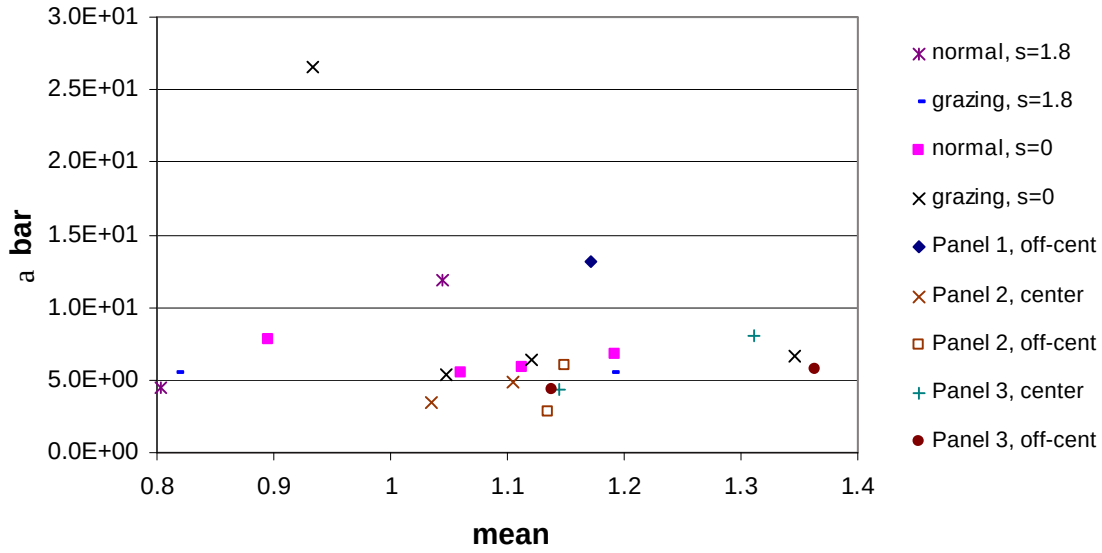

Figure 102. Dimensionless Coefficient $\bar{\alpha}$ as a Function of the Mean Value, All Stress Data.

It is seen from this last series of figures, as already observed in connection with $\alpha_{0.5}$ (see Fig. 91-96), that (i) a scatter is present in all parameters and (ii) the scatter is larger for the parameters

associated with the low-range part of the model than with those associated with its large-range component. Accordingly, an approximation of the latter parameters ($\bar{a}$, $\bar{b}$, and B) was sought first in terms of both $\alpha_{0.5}$ and the mean of the stress process. Proceeding with least squares, it was found that

$$\bar{a} \approx 10^{-1.5181}\,(1.4-\mu)^{0.1466} - 0.0364\,\mu^2 - 0.0798\,\mu + 0.2291 \tag{21}$$

$$\bar{b} \approx -62742\,a_{0.5}^4 + 220277\,a_{0.5}^3 - 289740\,a_{0.5}^2 + 169221\,a_{0.5} - 37027 \tag{22}$$

$$B \approx -47.795\,a_{0.5}{}^2 + 82.409\,a_{0.5} - 35.219 + 619.08\,\mu^5 - 3445.2\,\mu^4 + 7613\,\mu^3 - 8347.9\,\mu^2 + 4541.6376\,\mu - 980.6931 \tag{23}$$

where μ denotes the mean value. The matching between the approximate values given by Eq. (21)-(23) and their exact counterparts is shown in Fig. 103-105. While not perfect, the agreement is generally good to very good in all cases considered.

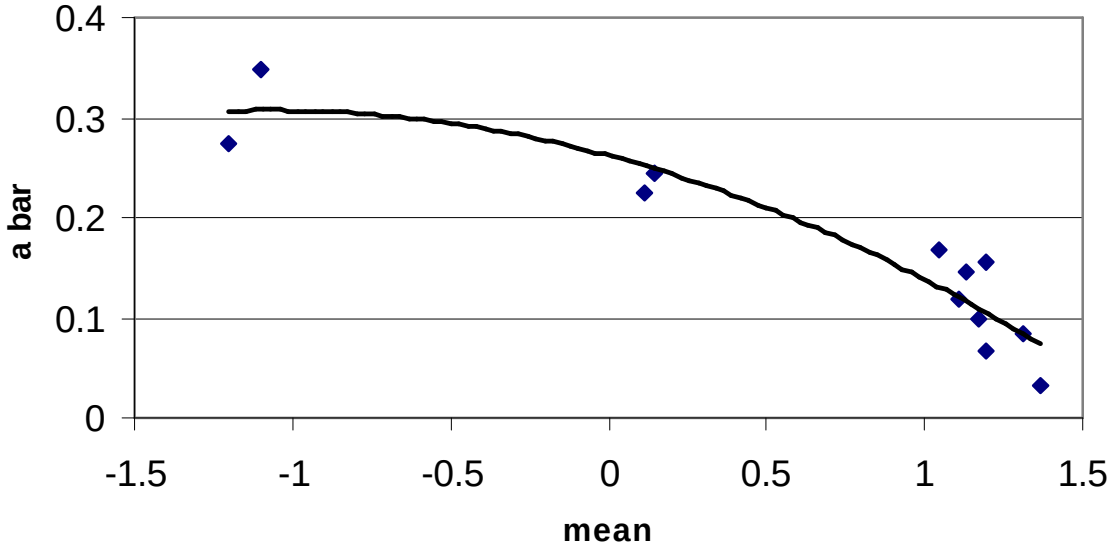

Figure 103. Comparison of the Values of the Parameter $\bar{a}$, From the Modeling of the Distribution of Ranges (dots) and From Eq. (21) (line). Note that the near zero branch of $\bar{a}$ is not shown.

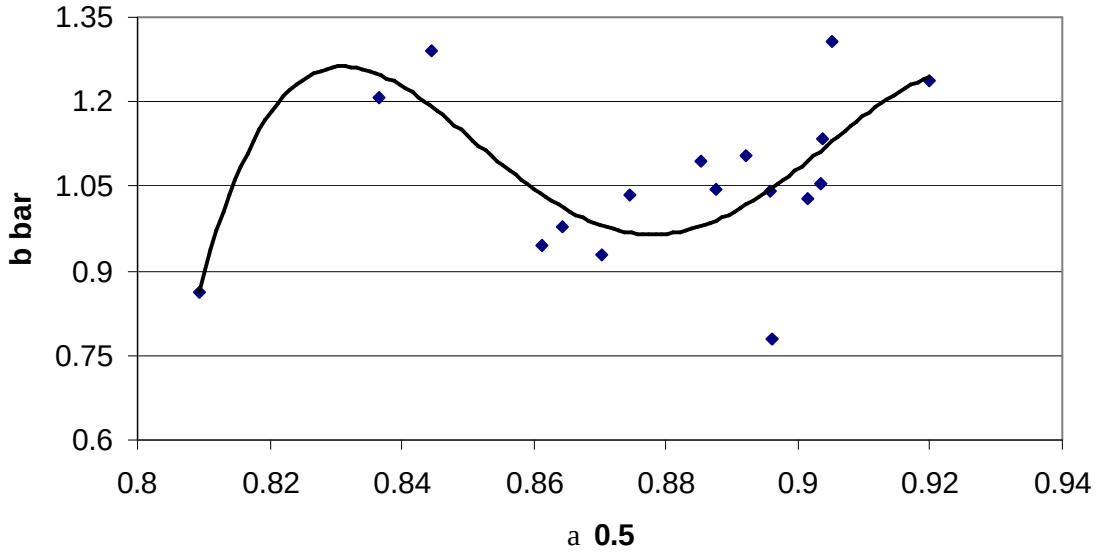

Figure 104. Comparison of the Values of the Parameter $\bar{b}$, From the Modeling of the Distribution of Ranges (dots) and From Eq. (22) (line).

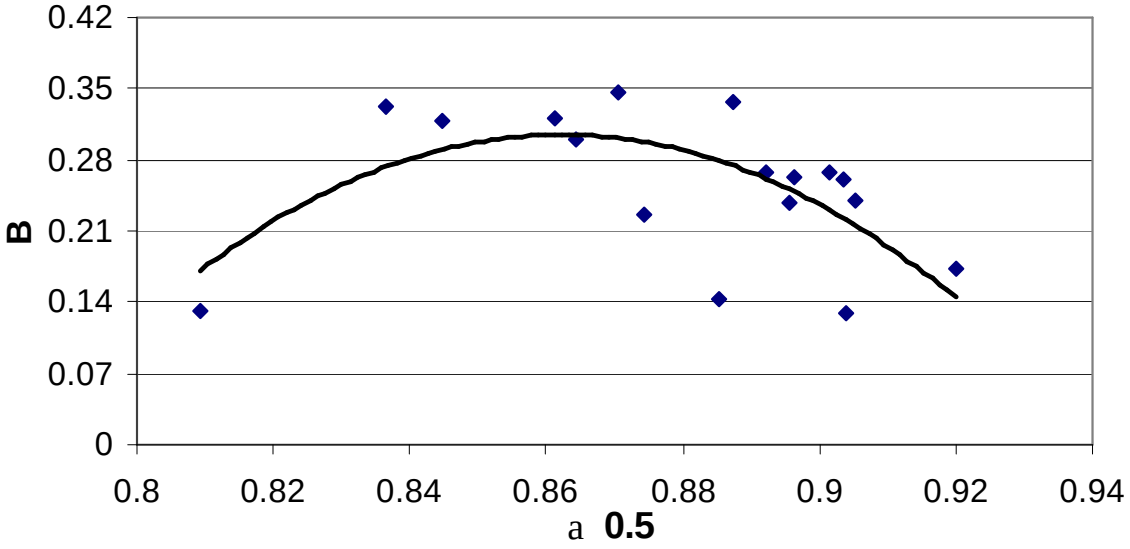

Figure 105. Comparison of the Values of the Parameter *B*, From the Modeling of the Distribution of Ranges (dots) and From Eq. (23) (line).

Note that not all stress results are shown in Fig. 103-105. In regards to $\bar{a}$, it should be noted that both Fig. 92 and 98 exhibit a two-branch behavior, i.e. there exists a series of cases where $\bar{a}$ is zero or equals a very small value and another group of situations in which this parameter is definitely non-zero. In fact, the zero/near zero values of $\bar{a}$ occur at very low sound pressure levels and for the unbuckled panel. For these situations, the panel behaves almost linearly so that a Rayleigh distribution of the peaks is expected and is indeed achieved (it corresponds to $a = 0$ in Eq. (18)). Only the nonzero values of $\bar{a}$ were used in obtaining the approximation of Eq. (21). Moreover, the approximation of $\bar{b}$ given by Eq. (22) is only valid for non-buckled panels (see Fig. 104) as the values of this parameter exhibit a different trend (especially at low sound pressure level) in the buckled cases, see Fig. 93 and 99.

How good are the approximations given by Eq. (21)-(23) and how significant is the scatter around the fitted curves? To answer this question, approximate probability density functions of the ranges were obtained by using the previously estimated values (see Fig. 97-102) for 4 of the 5 model parameters $\bar{a}$, $\bar{b}$, B, $\bar{\alpha}$, and β and either Eq. (21), (22), or (23) for the fifth one. In all cases, the constant $\overline{B'}$ was determined so that the total probability equals one. Shown in Fig. 106-108 are the comparisons between these approximate probability density functions (referred to as Model') with those obtained directly from the model (with all five parameters extracted from Fig. 97-102) and from the MSC.Nastran data for some cases yielding large differences between the data points and the regression curves of Fig. 103-105. While the differences in the values of the parameters are significant (typically of the order of 30%) for the cases of Fig. 106-108, it is seen that the probability density functions obtained from the curve fit equations (21)-(23) still represent fairly well the MSC.Nastran data.

Similarly positive results could not be obtained with the parameters $\bar{\alpha}$ and β as might be expected from Fig. 95, 96, 101, and 102. It was thus suggested that these coefficients may be dependent on a different characteristic of the stress process than the mean and spectral moments. Accordingly, potential correlations with the coefficients of skewness and kurtosis were investigated, e.g. see Fig. 109-114. However, a definite scatter was again observed on all parameters but especially on $\bar{\alpha}$, β, and $\bar{B}'$ rendering elusive the modeling of these coefficients as functions of the stress process characteristics.

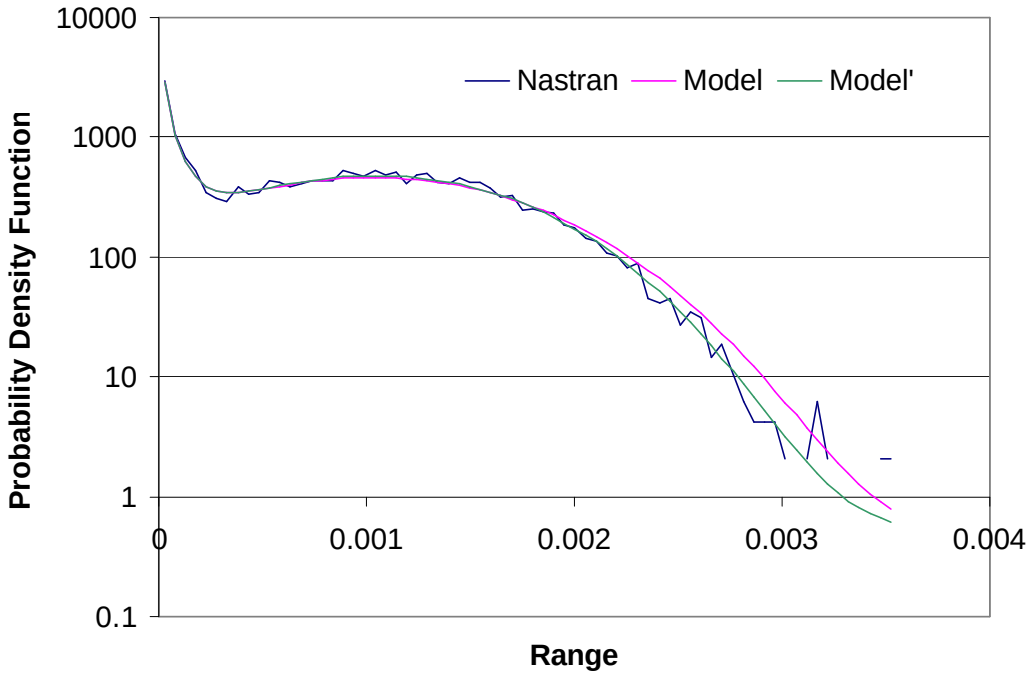

Figure 106. Comparison of Probability Density Functions of Stress Ranges, Finite Element Data, Unbuckled Panel, *s* = 0, *SPL* =140 dB. Model: all five parameters from Fig. 97-102. Model': same as Model but $\bar{a}$ from Eq. (21), ($\bar{a}$ = 0.106 vs. 0.154 from Fig. 98)

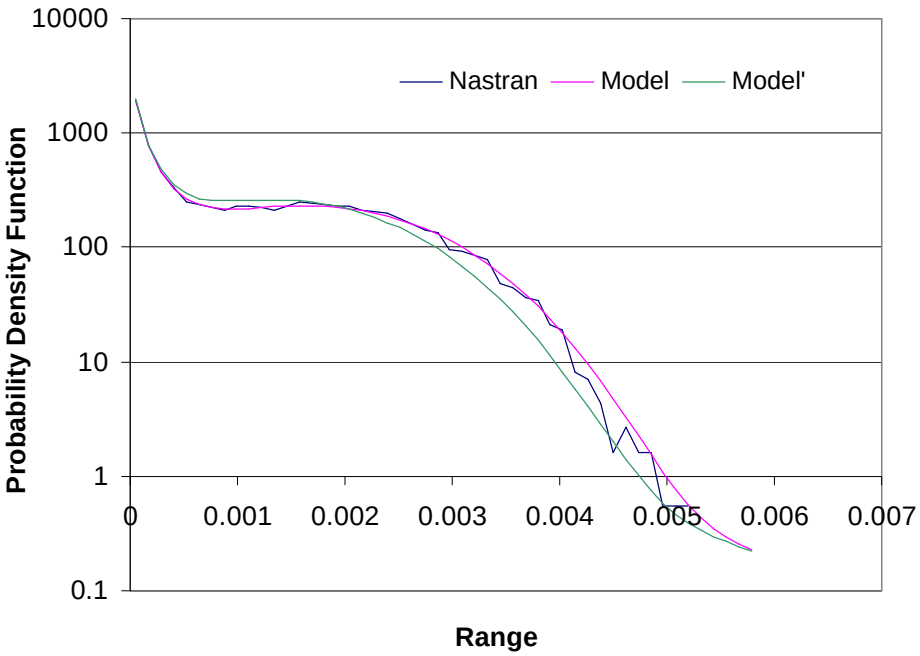

Figure 107. Comparison of Probability Density Functions of Stress Ranges, Finite Element Data, Unbuckled *double thickness* Panel, Zero incidence, Center Point, s = 0, *SPL* =150 dB.

Model: all five parameters from Fig. 97-102. Model': same as Model but $\bar{b}$ from Eq. (22)

($\bar{b}$ = 1.043 vs. 0.778 from Fig. 99)

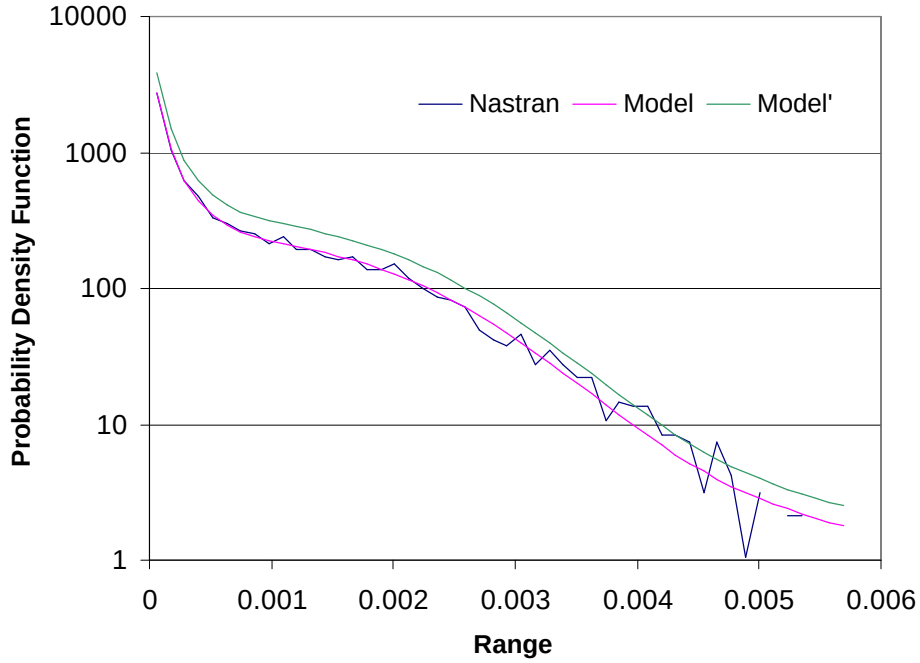

Figure 108. Comparison of Probability Density Functions of Stress Ranges, Finite Element Data, Unbuckled Panel, Grazing Incidence, s = 0, *SPL* =120 dB.

Model: all five parameters from Fig. 97-102. Model': same as Model but *B* from Eq. (23),
(*B* = 0.201 vs. 0.144 from Fig. 97)

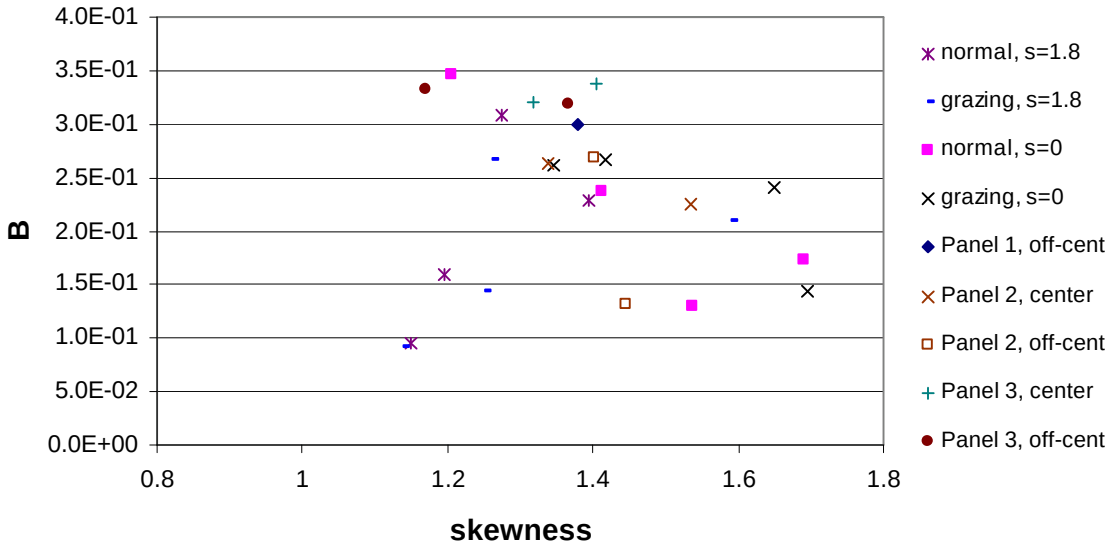

Figure 109. Dimensionless Coefficient *B* as a Function of the Coefficient of Skewness, All Stress Data.

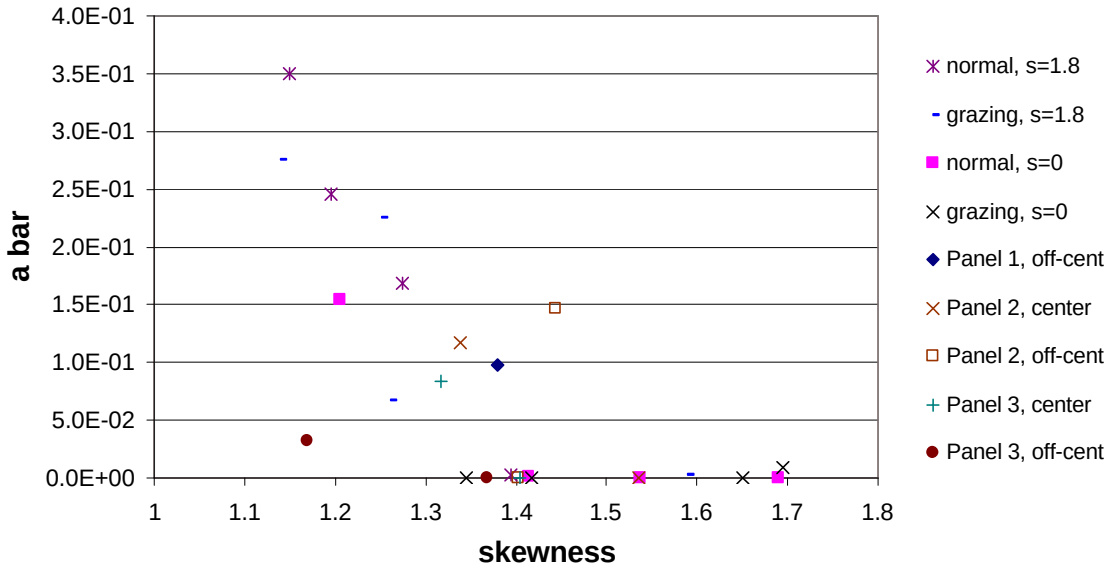

Figure 110. Dimensionless Coefficient $\bar{a}$ as a Function of the Coefficient of Skewness, All Stress Data.

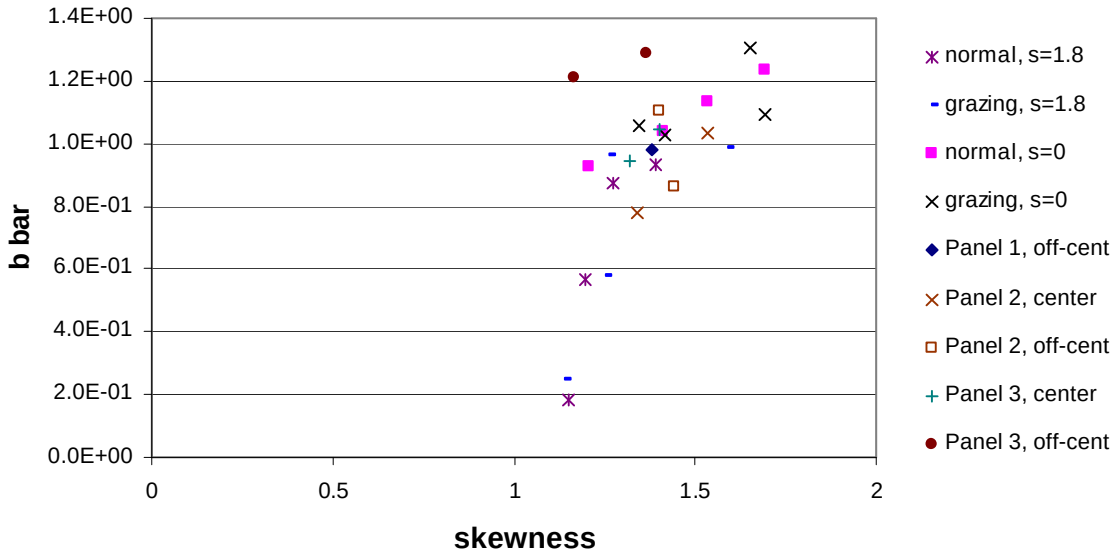

Figure 111. Dimensionless Coefficient $\bar{b}$ as a Function of the Coefficient of Skewness, All Stress Data.

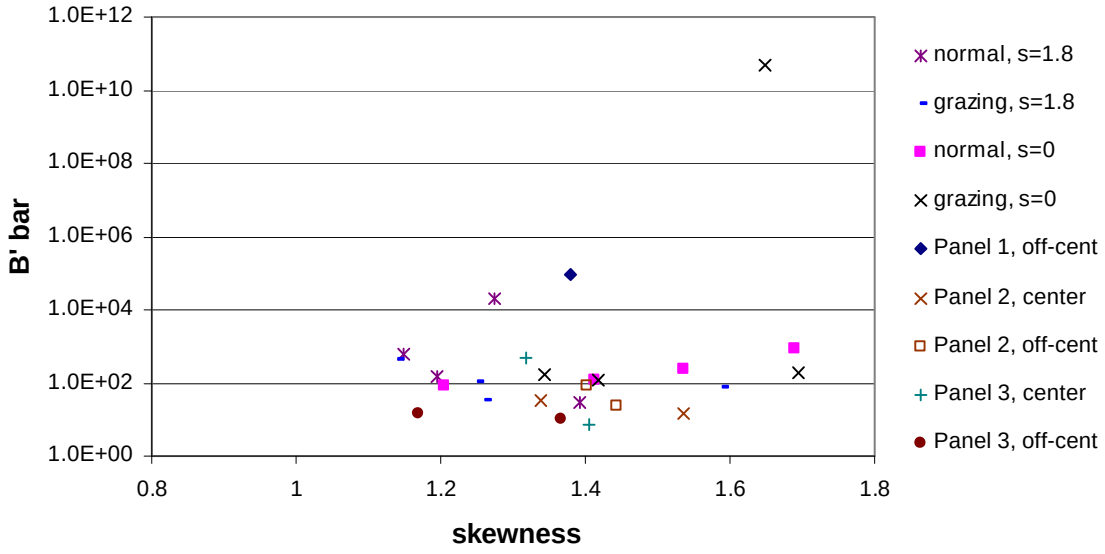

Figure 112. Dimensionless Coefficient $\overline{B'}$ as a Function of the Coefficient of Skewness, All Stress Data.

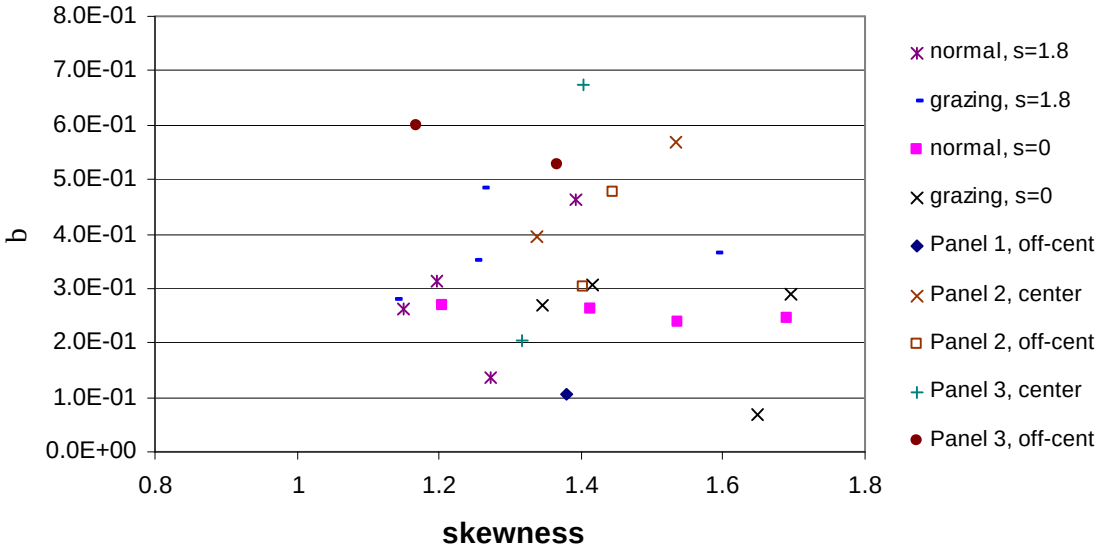

Figure 113. Dimensionless Coefficient β as a Function of the Coefficient of Skewness, All Stress Data.

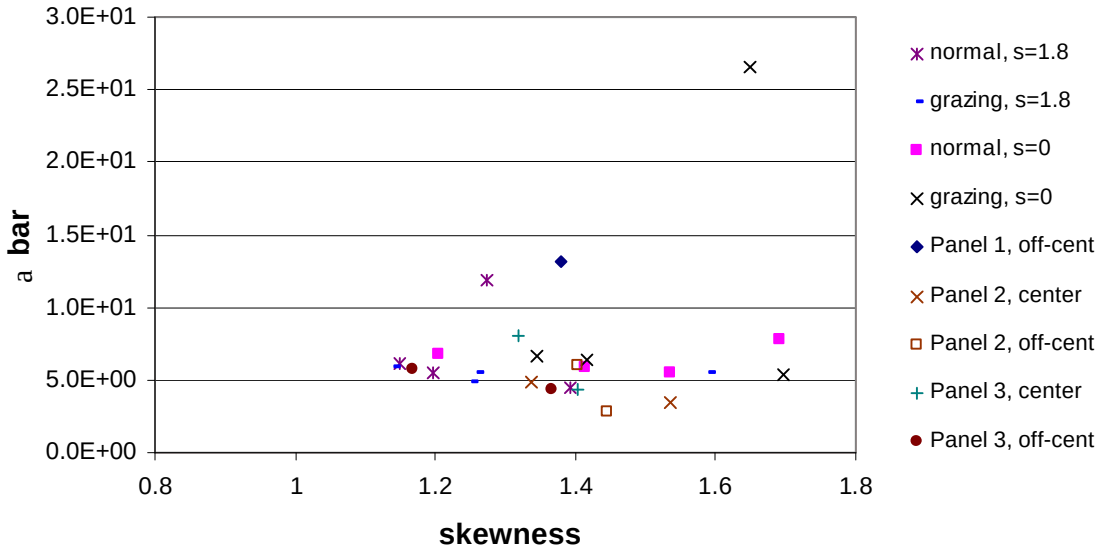

Figure 114. Dimensionless Coefficient $\bar{\alpha}$ as a Function of the Coefficient of Skewness, All Stress Data.

6.0 SUMMARY

The work carried out in this Phase I contract focused on the formulation and first assessment of a model for the probability density function of stress and displacement ranges that is specially tuned to the vibration of panels subjected to a severe acoustic excitation and steady thermal effects. The model was developed as a mixture of two components (see Eq. (5)): a high-range model that was physically derived from an analysis of the Duffing equation (i.e. Eq. (9)-(11)) and a low-range part that is postulated as a generalized exponential, see Eq. (15). Extensive validation on single mode data, strain measurements obtained at the A.F.R.L., and a series of finite element results (MSC.Nastran) has demonstrated the worth of the proposed model in accurately representing the probability density function over the entire domain of ranges of both displacements and stresses.

The second phase of the effort focused on the representation of the 5 parameters of the stress model as functions of the characteristics of the stress process, primarily its spectral moments, mean, skewness, and kurtosis. The evaluation of the power spectral density and spectral moments was carried out by both the Welch periodogram (FFT based nonparametric approach) and the autoregressive modeling method (parametric technique). The latter approach was found to be particularly well suited for the short length of the finite element response histories. The behavior of the 5 parameters (i.e. of their dimensionless forms, Eq. (19)) as function of the dimensionless spectral moment $\alpha_{0.5}$ (see Eq. (20)) was first analyzed and revealed that the 3 parameters associated with the high-range component of the model exhibit a fairly clean (albeit the presence of a small scatter) dependency on $\alpha_{0.5}$. A much higher level of scatter was however observed in connection with the coefficients characterizing the low-range component of

the model. The consideration of the mean and/or coefficients of skewness and kurtosis of the stress process has not provided a more focused representations of these low-range parameters but, in accord with $\alpha_{0.5}$, permits good regression formulas to be derived for the high-range parameters, see Eq. (21)-(23) and Fig. 106-108.

The objectives of the proposed effort were essentially accomplished. The only task that deserves further attention is the determination of a reliable representation of the low-range component expressible in terms of the spectral moments and/or mean of the stress process. The model introduced, i.e. Eq. (15), does provide an accurate representation of the probability density function but its parameters do not appear to be easily expressible in terms of the characteristics of the process, in contrast with the high-range component of the model. It is suggested that this difficulty may be associated with the lack of a physical justification of Eq. (15) (as opposed to Eq. (9)-(11) for the high-range part of the distribution). It is recommended that further effort be devoted to clarifying the low-range part of the probability density function on physical grounds and repeating the search for a correlation between model parameters and spectral moments and/or mean of the stress process.

7.0 REFERENCES

1. Bouyssy, V., Naboishikov, S.M., and Rackwitz, R., 1993, "Comparison of Analytical Counting Methods for Gaussian Processes," *Structural Safety*, Vol. 12, pp. 35-57.
2. Gersch, W., and Yonemoto, J., "Synthesis of Multivariate Random Vibration Systems: A Two-Stage Least Squares AR-MA Model Approach," *Journal of Sound and Vibration*, Vol. 52, No. 4, 1977, pp. 553-565.
3. Marple, S.L., *Digital Spectral Analysis with Applications*, Prentice Hall, 1987.
4. Yang, B., Mignolet, M.P., and S.M. Spottswood, "Modeling of Damage Accumulation for Duffing Oscillator-Type Systems Under Severe Random Excitations," *Presented at the 4th Computational Stochastic Mechanics Conference*, Corfu, Greece, Jun. 9-12, 2002.
5. ZONA, 2002, Interim Report #2, Phase II SBIR contract number F33615-01-C-3111.